Discrete Tire Modeling for Anti-lock Braking System Simulations

Srikanth Veppathur Sivaramakrishnan

Thesis submitted to the Faculty of the
Virginia Polytechnic Institute and State University
in partial fulfillment of the requirements for the degree of

Master of Science
in
Mechanical Engineering

Saied Taheri, Chair
Mehdi Ahmadian
Robert L. West

July 01, 2013
Blacksburg, Virginia

Keywords: Tire Modeling, ABS, Rigid Ring, Enveloping

Discrete Tire Modeling for Anti-lock Braking System Simulations

Srikanth Veppathur Sivaramakrishnan

(ABSTRACT)

Tires play an extremely important role in the operation of a vehicle as they transmit forces between the ground and the vehicle. Consistent efforts have been made over the years towards modeling and simulation of tires and more recently, there has been an increasing need to understand the transient response of tires to various high-frequency events such as anti-lock braking and short-wavelength disturbances from the road. Major thrust has been provided by the tire industry to develop simulation models that accurately predict the dynamic response of tires without the use of computationally intensive tools such as FEA.

The objective of this research is to explain the development, implementation and validation of a simulation tool based on a dynamic tire model that would assist in the analysis of the effect of tire belt vibrations on the braking performance of a vehicle. A rigid ring tire model, tandem elliptical cam enveloping model and a rule-based ABS model have been developed for this purpose. These were combined together in a quarter vehicle model and implemented in Matlab-Simulink®. These models were developed for adaptation with CarSim® to provide a simulation tool that can be utilized in both tire and vehicle design processes. In addition to model implementation, a parameterization procedure was developed to estimate the parameters of the rigid ring tire and enveloping model based on experimental data for a given tire. Validation studies have also been performed to ensure the accuracy and validity of the tire model. Following this, the braking performance of ABS under different road surfaces were evaluated. Based on the simulation results, final conclusions were drawn with regards to the analysis and detailed recommendations for future work directed towards the improvement of the tool were provided.

This work was funded by the industry members of the Center for Tire Research (CenTiRe)

Dedication

To my parents and teachers who made me what I am today

Acknowledgements

I would like to express my profound gratitude to my academic advisor and mentor Dr.Saied Taheri for providing me the opportunity to work under his guidance at the Center for Tire Research. His motivation kindled my passion for engineering research and his constant support and timely advice played a huge role in completing my thesis. Dr.Taheri, it has been an honor and great pleasure to work with you.

I would like to thank Dr.Mehdi Ahmadian and Dr.Robert West for their participation in my thesis committee, and other faculty at Virginia Tech especially Dr.Pablo Tarazaga and Dr.Steve Southward for their excellent courses which enhanced my technical skills in vibrations and control.

I would also like to thank all the industry mentors of this project including Hankook Tires, Michelin, Honda, Bridgestone etc. for their valuable comments and feedback throughout the course of this study which kept the project moving in the right direction. A special mention goes to all my lab-mates at CenTiRe especially to Ali for all the technical discussions, insights and suggestions.

Finally, I want to acknowledge my roommates and all my friends who have been of immense emotional support to me during my research and writing my thesis.

Contents

List of Figures

List of Tables

Chapter 1

Introduction

Rapid advancements in technology and computational ability to quickly solve differential equations at affordable costs has led to widespread adoption of simulations for design in the engineering industry, particularly in the automotive and tire sectors. Today, computer simulations have become indispensable and are an integral part of any product design and development process. The availability of an advanced and accurate simulation model is considered a competitive advantage as this enables engineers to analyze multiple test cases without experimentation and rapidly optimize their final product design. This also reduces the cost of prototyping and improves product development time. Over the last few decades, there have been numerous theories and models proposed, both from academia and industry to simulate the behavior of various vehicle subsystems. This includes multiple modeling approaches ranging from complex and computationally intensive Finite Element (FE) based models to simplified lumped parameters discrete models. With each iteration, there has been progress towards improving the accuracy of the simulations by validating the model with experimental results. Realizing their importance, companies tend to invest considerable effort towards developing in-house models for tires, vehicles and related safety systems for their product development work-flow. Some of these models are considered trade secrets as they served a critical purpose for their design. In addition to this, there are also companies

which exclusively develop simulation tools and commercially license such products to the industry.

Although fairly advanced multi-body dynamics models exist for calculating the response of the entire vehicle, modeling a pneumatic tire is considered a challenge because it is one of the most complex components of a vehicle consisting of multiple structural elements. Early tire models were merely simple mass-spring-dampers and were used for comfort and durability studies. Over the years, advanced tire models have been developed which could predict the dynamic response of the tire under various operating conditions and road inputs. Some of these models require fairly high amount of computational capability.

1.1 Motivation

One of the most important application of tire and vehicle models is in the development of safety systems such as Anti-lock Braking System (ABS) and Vehicle Stability Control (VSC) which are essential features in all modern automobiles. As the control algorithms for these systems become more advanced, there is a requirement to accurately predict and understand the forces generated due to the dynamic response of the rolling tire due to road contact, short wavelength road disturbances, brake torque variations and the interaction of the tire with the vehicle. From the standpoint of the automotive manufacturer, this is important because tires are responsible for transmitting forces from the ground to the vehicle for traction, braking and steering. A deeper understanding of the factors governing the dynamic force response of tires would provide immense scope towards evaluating and optimizing the performance of their controllers. For the tire manufacturer, an ABS braking simulation model would assist engineers in modifying their tire design to maximize braking performance.

In the current scenario, each tire and automotive manufacturer use their own in-house simulation code to evaluate ABS braking performance. Each model has its own disadvantages. This is due to the fact that the tire manufacturers would not have access to commercial ABS

control algorithms and models since they are considered Intellectual Property (IP) and are not revealed. Vehicle manufacturers lack the expertise of the tire industry in dynamic tire models as these are also considered equally critical to protect. Due to the lack of a common evaluation tool, engineers from both industries might not be able to target the same issue and work towards a solution.

The need for such evaluation tools employing dynamic tire models have been validated through previous studies by Pauwelussen [2] and Jansen [3] which conclusively state that the effect of tire belt vibrations on ABS braking is significant and cannot be neglected.

1.2 Objective

The objective of this study is the develop a simulation tool that would serve as a common platform for both tire and automotive manufacturers to analyze the effects of tire belt vibrations, road disturbances and high frequency brake torque variations on the performance of ABS in a vehicle. Once deployed into the industry, this tool could eventually be integrated into the development work flow of engineers.

1.2.1 Model Requirements

Understanding the key requirements from the simulation model is essential to ensure proper implementation of the tool. Developing the tool without complete knowledge of expected features will lead to either spending unnecessary effort in modeling factors that are not required or falling short of satisfying key requirements, which are listed below:

- The simulation tool should be capable of modeling the dynamic response of the tire for excitations up to 100 Hz on any type of uneven road including short wavelength disturbances and simulate all kinds of braking maneuvers.

- The model should be capable of calculating results at a relatively fast speed with low computational effort.
- The simulation results should be accurate within the operating limitations of the models and verifiable through experiments.
- A parameterization procedure needs to be developed to ensure that the simulation tool is capable of performing calculations for any general tire.
- The parameters required for the simulation model should be kept to a minimum with low experimental effort required for parameter estimation.
- Standard formats should be adopted for the exchange of experimental data and tire parameters for model parameterization and validation to avoid ambiguity and improve integration into the existing design work-flow.
- The ABS algorithm should be based on a commercial ABS system installed in a production vehicle with comparable performance and response.
- Implementation of the model should be done on a commonly used simulation platform and should be capable of being adopted to other platforms or run as a standalone application.
- The simulation tool should be capable of being adapted for real-time applications such as Hardware-In-the-Loop (HIL) simulations.
- Tire and ABS models should be able to interface with commercial vehicle dynamic software such as CarSim®.

1.3 Research Approach

In order to fulfill the final objective, the work was divided into multiple tasks which would serve as individual blocks that can be built upon towards the completion of the final model.

The following steps, which are explained in subsequent chapters in this thesis were taken towards achieving the final objective:

- Comprehensive literature review of all the available tools and existing technology which can be leveraged towards the development of the tool.
- Detailed mathematical modeling of all components based on a set of assumptions and modeling requirements.
- Identification of simulation platform, implementation and integration of individual models into larger simulation models.
- Development of estimation procedure to parameterize the tire model from experimental data for model generalization.
- Detailed analysis of simulation results and their comparison with experimental data.

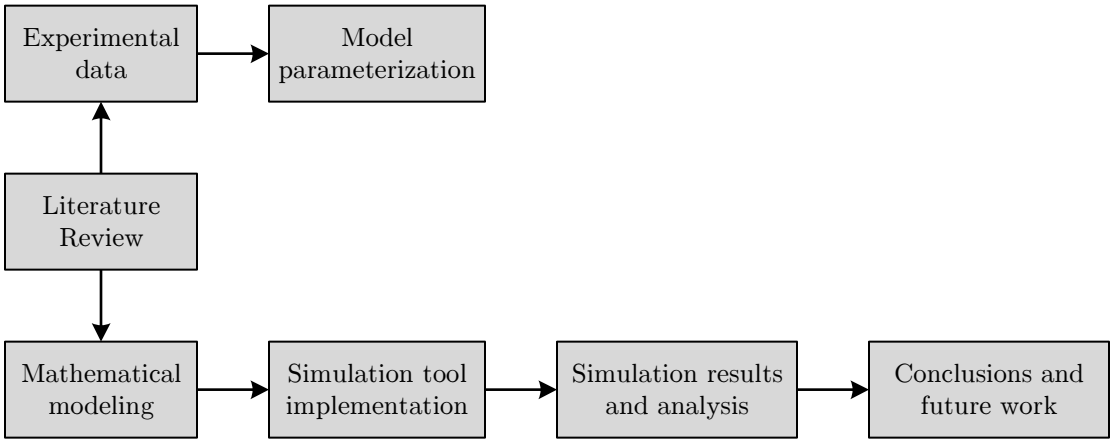

Figure 1.1: Thesis outline.

1.4 Thesis Outline

The chapters are organized in the same order as outlined in the research approach adopted in this thesis. Chapter 2 provides a detailed background relating to all the models which were

implemented. Chapter 3 explains the mathematical modeling of the tire, vehicle and the ABS model followed by the implementation of the tool which is further explained in Chapter 4. The procedure developed to estimate the parameters of the tire model is described in Chapter 5. Detailed analysis of simulation results for various test cases are explained in chapter 6. Final conclusions and recommendations for future work are provided in Chapter 7. Figure 1.1 illustrates the outline of this thesis.

Chapter 2

Background

This chapter provides a detailed overview of the state-of-the-art in the modeling and simulation of automotive tires, braking systems and their integration with vehicle models from published literature. The modeling and implementation of the tool components which are explained in subsequent chapters are largely built upon the work detailed in the literature. The rationale behind the choice of simulation models are explained here.

2.1 The Pneumatic Tire

In order to understand the behavior of a pneumatic tire, it is essential to understand its construction. The tire is a composite element which is essentially a torus made of visco-elastic rubber reinforced with high-tensile strength cords. Figure 2.1 shows the internal composition of radial-ply tire. This tire has parallel cords, known as carcass plies running from one bead to another. There are two stiff belts made of fabric and reinforced by steel that runs around the circumference of the tire. The belt plies, typically aligned at 20deg to the circumference and the pressurized sidewalls provide structural and directional stability to the tires. The soft carcass provides for ride comfort and the stiff belts are essential for

the cornering properties of the tire. Treads block are rubber components which are required for hydroplaning and for adhesion to maintain contact with the road. They have a major influencing factor in the generation of forces at the contact zone. The beads are made of steel cables and they are responsible for anchoring the tire and maintaining a tight seal between the tire and the wheel rim to hold pressurized air.

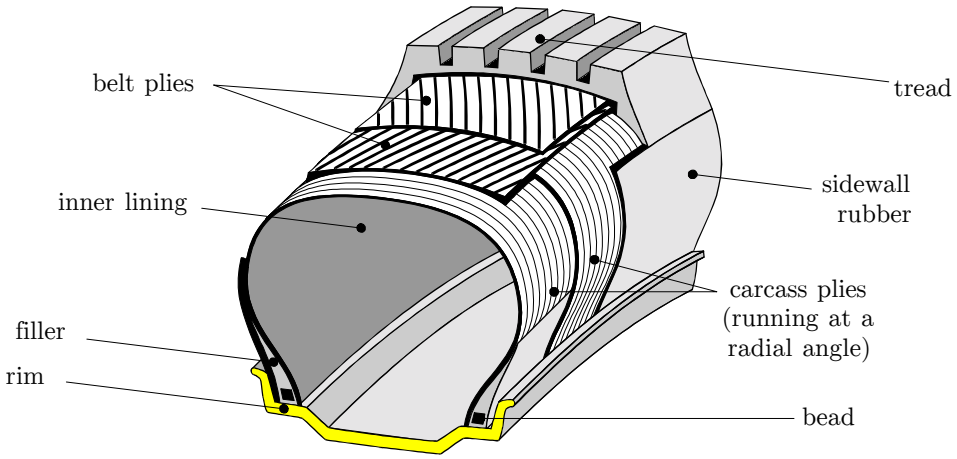

Figure 2.1: Detailed view of a pneumatic tire. Adapted from Zegelaar, P. (1998). *The dynamic response of tyres to brake torque variations and road unevennesses.* Delft University of Technology. Used under fair use, 2013.

2.2 Tire Modeling

For vehicle dynamic analysis, tires are critical components and play a pivotal role in the smooth operation of a vehicle. They also interact with other vehicle subsystems including steering, braking and suspension systems. Hence, understanding their behavior by modeling their force response under various operating conditions is required to ensure proper design of other components in the vehicle. Designing suspension or steering systems without consideration of tire behavior might lead to unfavorable results during the operation of the vehicle in terms of comfort and safety.

2.2.1 Classification

Tire modeling is an active area of research owing to its sheer complexity. Various theories and methods were proposed towards modeling the behavior of tires. The type of tire model used is heavily dependent on their targeted application which can span multiple domains including material characterization, thermal response, strain mechanics and dynamics. The primary focus of this section is towards tire models which can be used for vehicle dynamic analysis. Based on the type of response, tire models can be classified as:

Steady-State Response A steady state condition is a situation in which there are low variations in the input quantities to the tire (vertical load, slip). Some of the scenarios that match this condition involve slow steering maneuvers such as cornering and lane changing. Steady state tire models are the most widely used and can be both physical and empirical.

Transient Response Steady state tire models lose their validity under conditions where are rapid variations in slip with time. This is because the force generation in tire does not instantaneously follow slip variations. The time constant of this response is described using the concept of relaxation length which is defined as the distance traveled before force generation in response to a step variation in slip. Transient tire models account for the effect of relaxation length using various differential equations and predict the force response more accurately at shorter time steps. In some methods, the transient effects are calculated by physically modeling the tire mass in contact with the ground through differential equations. Transient responses are mainly required under fast events such as lane change at high velocities, ABS braking and traveling on a rough road to name a few. Relaxation length is required to model the shimmy phenomenon [4] which occurs on the front wheels of vehicles and also on the landing gear of aircraft.

According to H.B.Pacejka [5], tire models (both transient and steady state) can be broadly classified into four categories, as shown in Figure 2.2. Each of these models have their own

advantages and shortcomings with varying levels of accuracy. The choice of model to be used in this thesis is based on current modeling requirements. Some of the most important tire models which fall into one of these categories are explained below:

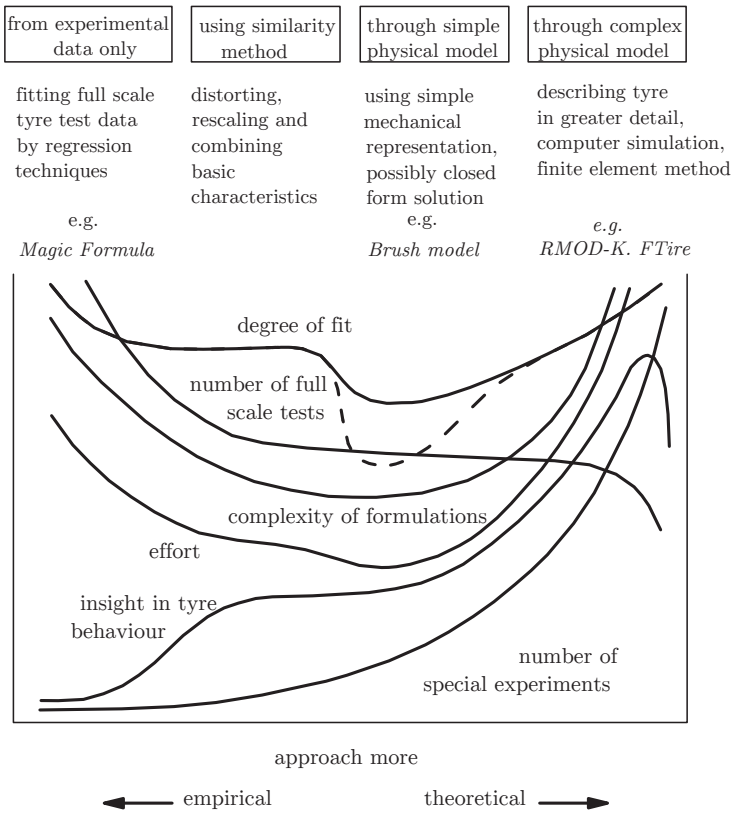

Figure 2.2: Classification of tire models. Adapted from Pacejka, H. B. (2012). *Tire and Vehicle Dynamics (3rd ed.)*. Butterworth-Heinemann. Used under fair use, 2013.

2.2.2 Empirical Tire Models

These are mainly linear or non-linear mathematical relations which are derived based on fitting experimental data. The biggest advantages of such models is their high accuracy in predicting force response as their outputs are based on regressive analysis of previously collected experimental data under similar conditions. Some their shortcomings are that the equations formulated through this method are purely algebraic curves and have very

little physical significance as one cannot correlate the parameters of such models to the actual properties of the tire. Also, parameterization of such models would require extensive experimental data which can prove to be expensive.

Some of the most popular example of an empirical tire models is the Magic Formula by Pacejka [6] which is considered a standard tire model in the industry for vehicle dynamic simulations. The Magic Formula has been improved over the years with the addition of more empirical relations to account for transients and inflation pressure changes [7, 8]. Braghin et al proposed an extension to the Magic Formula by developing MF-Relax [9], which accounts for the dynamic effects of the tire with a focus towards Anti-lock Braking System simulations.

2.2.3 Physical Tire Models

These are based on analytical derivations that are actually based on a set of assumptions that would define the tire in a physical sense. The parameters of such models are based on actual measurable entities of the tire such as belt mass, rotational moment of inertia, vertical stiffness etc. Since these models are analytically derived, their outputs tend to have higher scope in terms of analysis as one can correlate outputs to specific tire parameters. Hence, they are extensively utilized during the design stage of the tire. The earliest application of physical tire models were in ride and durability studies were the tire was a simple lumped mass, spring and a damper. Such models are still being used to model vibration response for both passive and active suspension design.

One of the most widely used physical models with a simplified formulation for vehicle dynamic studies is the HSRI model, also known as the 'brush model' developed by Dugoff, Francher and Segel [10] which was later improved by Bernard, Segel and Wild [11]. Some of the recent advances in developing simple, unified physical models for all kinds of analysis include UniTire [12]

Tire Enveloping Property

The behavior of a tire while rolling over obstacles is a complex phenomenon as the tire is in contact with the ground at multiple points. This effect is clearly evident when the road disturbances have short wavelengths as the tire contact creates a filtering effect by smoothening out sharp obstacles. This is known as the enveloping property of the tire, which is illustrated by Zegelaar [1] in Figure 2.3. As a result of the enveloping effect, the effective road disturbance which acts on the tire is different from the actual road surface.

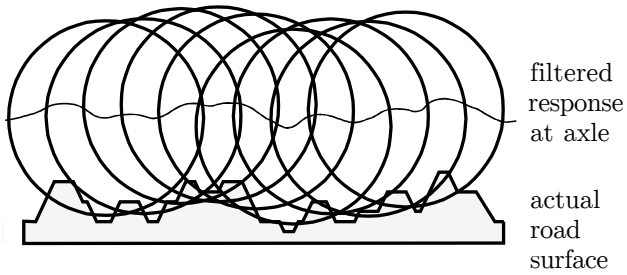

Figure 2.3: Tire enveloping property. Adapted from Zegelaar, P. (1998). *The dynamic response of tyres to brake torque variations and road unevennesses.* TU Delft. Used under fair use, 2013.

When the tire rolls over uneven roads, the assumption of a single point of contact might not hold true. Hence, various enveloping model, both physical and semi-empirical have been proposed to simulate this effect of the tire. A broad list of various methods used for enveloping models found in literature are shown in Figure 2.4 . The overview provided here is based on the work previously done by Schmeitz [13]

Point Contact Model The is the most popular model in which a single point of rolling contact is assumed at the tire-road interface which is connected to the axle by a spring and a damper. Although this generates a filtering effect, the accuracy is highly reduced for sharp obstacles such as cleats because this model is valid only for longer wavelengths (greater than 3m).

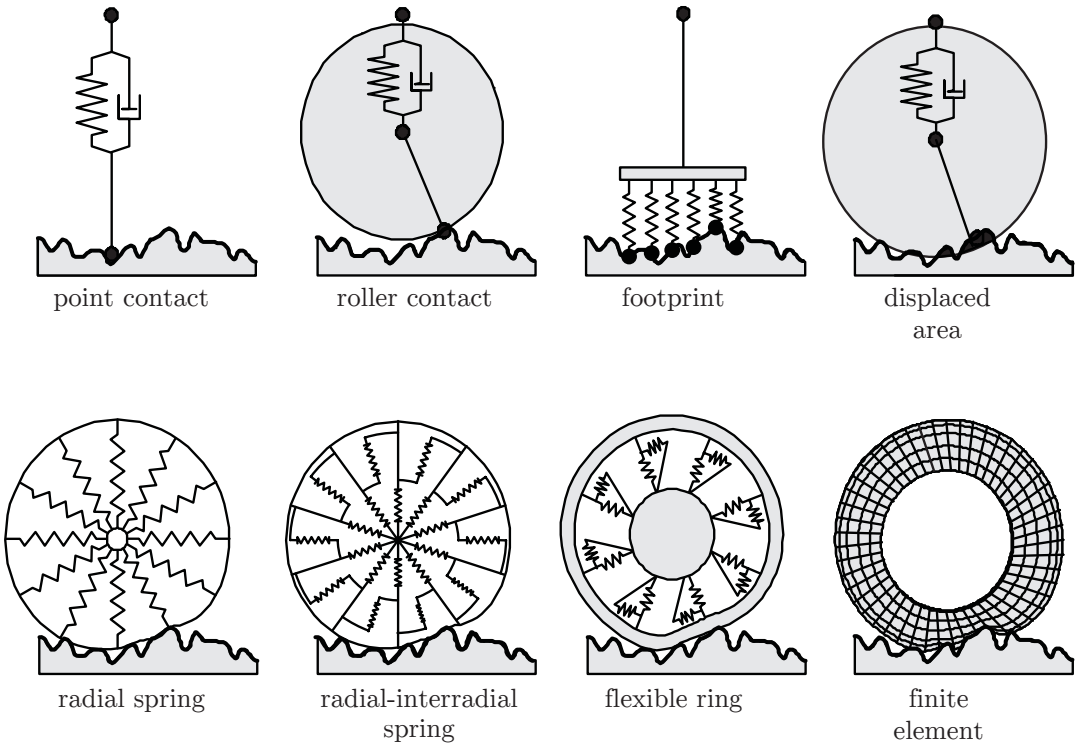

Figure 2.4: Tire enveloping models. Adapted from Schmeitz, A. J. C. (2004). A Semi-Empirical Three-Dimensional Model of the Pneumatic Tyre Rolling over Arbitrarily Uneven Road Surfaces. Delft University of Technology. Used under fair use, 2013.

Roller Contact Model This type of model, initially proposed by Guo [14] offers more accuracy in comparison to a point contact model but fails to account for the deformation of the tire which can cause high accelerations when used with dynamic tire models.

Footprint models In this type of model, the excitations are modeled using a linearly distributed stiffness and damping over the contact area. This gives more accurate results than the point contact model but fails to account for tire geometry at the contact zone. Recent advances in this model includes the work by Frey [15]

Radial Spring Model In this model, a radially deformable body is used instead of a rigid wheel. The model is a network of circumferentially distributed springs which can either be linear or quadratic. An enhanced variant of this model was developed by

Badalamenti [16].

Flexible Ring Models This type of model simulates enveloping behavior though a flexible tread-band and distributed stiffness for sidewalls. These were developed using different methods such as modal analysis by Gong [17] and Zegelaar [18] and finite element methods by Mousseau [19]. Although this model has good accuracy it has a high computational load. Other examples include the REF model [20]

Empirical Models Based on the analysis conducted by Lippmann [21], various attempts have been made to develop empirical models that can be used for computing enveloping characteristics. Based on the findings on Bandel [22], a basic function approach, was developed by Zegelaar [1], which involved summing elementary curves to obtain the effective road profile. This was later improved by Schmeitz [23].

A semi-empirical approach was adopted by Schmeitz [24, 13] using two tandem rigid elliptical cams which roll over the uneven road surface. The average height of the cams is considered to be the effective road surface or excitation to the tire. This model has the advantage of being suitable for arbitrary road profiles and can be extended to all three dimensions. A variation of this model has been proposed by Allen [25] to reduce the experiments required for parameterization.

Displaced Area Models These are based on the assumption that the resultant force acts along the centroid of the total displaced area and the wheel center. Although these models offer better results than the point contact model, they lose their accuracy at sharp obstacles.

Dynamic Tire Models

Dynamic Tire Models are physical models used to simulate the dynamic response of the tire under situations where there are high-frequency variations in the inputs to the tire and the transient response of the tire play a significant role in deciding the force response. Some

of these models are capable of calculating the response at high frequencies up to 250 Hz. One specific aspect which is of importance is their ability to simulate dynamics while rolling over uneven surfaces, Schmeitz [13] provides a general classification of dynamic tire models for uneven road surfaces as shown in Figure 2.5. These models were taken from literature based on the simulation requirements and the most suitable model is implemented in this thesis. A detailed literature survey of all transient dynamic tire models has been done by Chang et al [26].

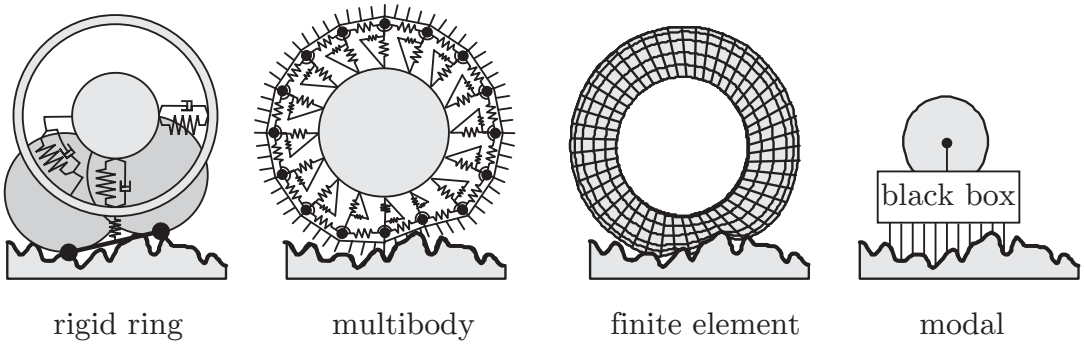

Figure 2.5: General classification of dynamic tire models. Adapted from Schmeitz, A. J. C. (2004). *A Semi-Empirical Three-Dimensional Model of the Pneumatic Tyre Rolling over Arbitrarily Uneven Road Surfaces.* Delft University of Technology. Used under fair use, 2013.

Rigid Ring Model This modeling approach assumes a rigid ring which represents the tire belt to be rolling on the road surface. This ring is connected to the axle through a set of springs and dampers which represent the pressurized sidewall. Since rigid ring models are based on a single point of contact, they are generally used in conjunction with an enveloping model which can be chosen by the availability of parameters and modeling requirements. The rigid ring model is valid under frequencies up to 100 Hz as the belt behaves as a rigid body in this range. Early models on rigid ring model were developed by Takayama et al. [27]. Newer implementations of the rigid ring models were based on detailed studies undertaken by Gong [17] which were then developed for simulation by Zegelaar [18] for in-plane dynamics and extended by Maurice [28, 29] to

account for out-of-plane dynamics. Other implementations of this model include the work done by Allison and Sharp [30] and Bruni et al [31]. The rigid ring model has been used for various commercial simulation tools for tires including MF-SWIFT by TNO Automotive [32] and more recently, the UniTire model [33].

Multi-body Models In a multi-body simulation model, the tire belt is constructed as an elaborate discrete point mass network which are interconnected through tension and rotational springs. Multiple elastic belts with a similar discrete mass arrangement are assumed to simulate lateral behavior which are again connected to each other in a similar fashion. The elastic belts are connected to the axle through radial and tangential springs. The tread elements are assumed to be brushes like that can slide over or stick to the road surface. Eichler [34] introduced a three-dimensional version of this model which was later commercially implemented as FTire [35, 36] and there were studies on in-plane force transmissions which were conducted based on this model by Dorfi [37]. Although these models are accurate, they tend to be computationally heavy and difficult to parameterize.

Finite Element Models These models are constructed using detailed geometry and descriptions of the tire. They are generally the most accurate in terms of simulation output and can be directly used for simulating dynamic tire response. One of the major drawbacks of this method is that they have the largest computational effort among all models and are hence unsuitable for vehicle dynamic simulations. Finite element models are generally used in conjunction with simpler discrete models as a virtual prototyping tool to improve the speed of the simulations. Explicit finite element models have been developed by Wu et al. [38] and Shobanie [39]. Some of the recent work on finite element modeling which are usable in rigid ring tire models have been done by Chae [40, 41]

Modal Models Generally, modal analysis is considered to be a 'black-box' approach where the relation between inputs (axle motion, road deflections) and outputs (spindle forces)

are identified using modal dynamics of the tire. One can either derive them through FEA [22, 31] or through experimental modal analysis. One of the drawbacks with these models is their linearity which fails to account for a lot of factors including the effect of non-linear enveloping behavior, transient slip and the variations in longitudinal force due to rolling velocity variations. Although they can be used up to frequencies of 250 Hz, they have greater applicability for noise and vibration analysis than for vehicle dynamics.

2.3 Anti-lock Braking Systems

The two primary functions of a braking system are to retain control of the vehicle at a steep inclination or a declination and to bring the vehicle to a complete stop in the shortest distance possible. Conventionally, braking is accomplished in automobiles using a hydraulic circuit. When the driver presses the brake pedal, it pushes fluid through the master cylinder into the hydraulic circuit. This eventually translates into a pressure which would push the brake shoes against the wheel and generate braking torque through friction.

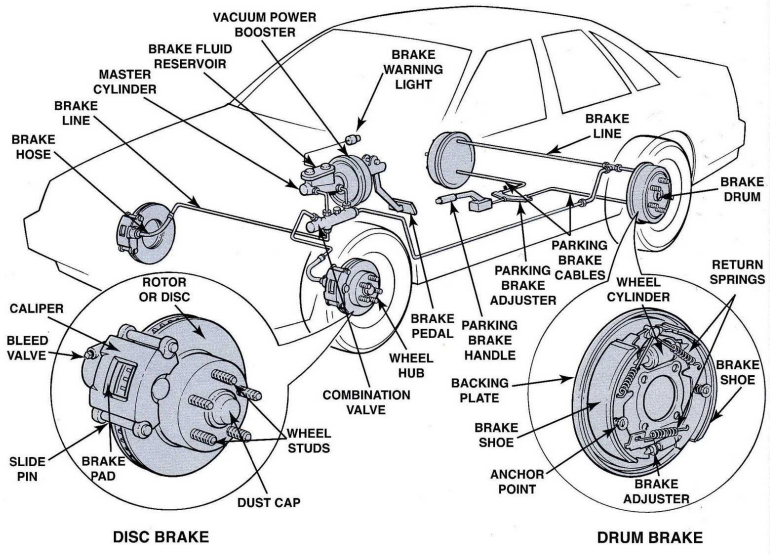

Figure 2.6: Conventional vehicle braking system.

Initial systems were based on drum brakes on all four wheels where the drum is mounted on the wheel with brake shoes positioned inside the drum. The hydraulic actuators press the brake shoes against the drum and this would cause braking due to frictional force. Currently, vehicles are equipped with disc brakes since they were more efficient during braking and had a better heat dissipating mechanism. In this, a caliper is mounted on a wheel solid disc which is attached to the wheel. The calipers are actuated through hydraulics and generate braking force by clamping the disc through brake pads. A detailed diagram of a vehicle braking system with disc brakes on the front and drum brakes on the rear is shown in Figure 2.6

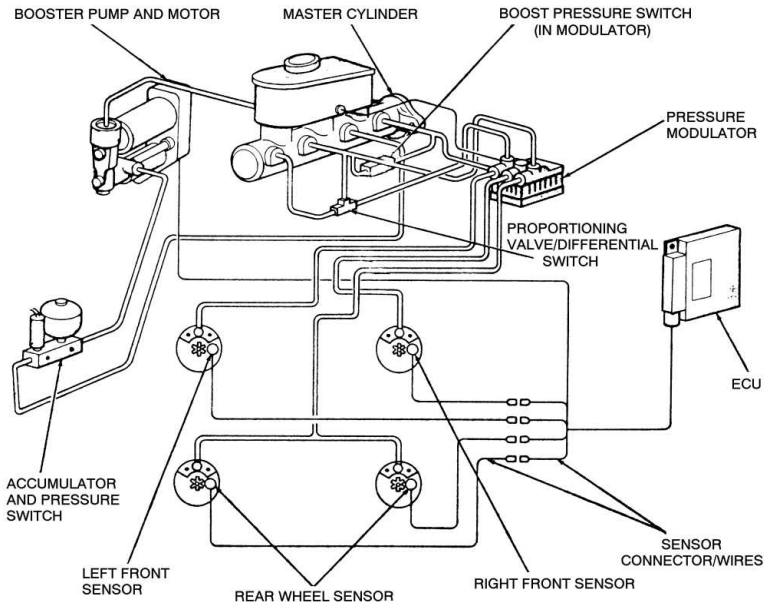

Figure 2.7: Bendix ABS System Schematic.

Improvements in electronics led to the development of reliable control systems which could be used for the improvement of safety systems. This led to the development of the Anti-lock Braking System (ABS). This was a revolutionary concept in which the ABS controller cycles the braking action such that the wheel is always at a desired optimum slip ratio and wheel lock up is also prevented. As a result, this system retains directional control to the driver even during severe braking events and prevents the vehicle from going unstable due to the wheel slipping. Earlier versions of ABS began to appear in aircrafts as early as 1929 and they

remained exclusive due to their high costs. Modern ABS systems for use in automobiles were introduced in 1971. The automotive industry was interested in utilizing this technology for incorporating it as a safety system in their vehicles and began to adapt them for the consumer level. Following their introduction in vehicles, ABS systems came to be widely adopted as they drastically reduced the number of automotive-related accidents. Currently, ABS in a vehicle is considered a critical safety system and is mandatory in many countries. Figure 2.7 shows a detailed overview of an ABS system. A time-line of the development of ABS systems is described as an SAE Standard [42].

2.3.1 Principle of Operation

The operation of an ABS is centered around the longitudinal force versus slip characteristic of a tire. From Section 2.2 we know that the force generated at the contact patch is dependent on the slip ratio. This is the braking force that is generated in the direction opposite to the motion of the vehicle. Figure 2.8 shows the variation of longitudinal force with slip ratio for a generic tire. From this, we can notice that the braking force peaks at a particular slip ratio and then reduces. The braking force available when the tire is fully sliding (unstable region) is also comparatively less. Hence one would expect to see a reduction in braking distance if the wheel slip ratio is maintained around this peak.

The ABS achieves this through a Hydraulic Control Unit (HCU) which is essentially a complex circuit of control valves which are actuated through solenoids. Based on the current wheel slip ratio, the ABS control algorithm, which is generally implemented through a micro-controller, calculates the optimum braking torque based on wheel speed information from sensors and correspondingly chooses whether to increase, hold or reduce the pressure in the brake line by actuating the solenoid valves. This way, the ABS controller achieves its objective of maintaining wheel slip in the desired range and in the stable region for all four tires. Typically, an ABS controller executes control signals at the rate of 10-20 Hz.

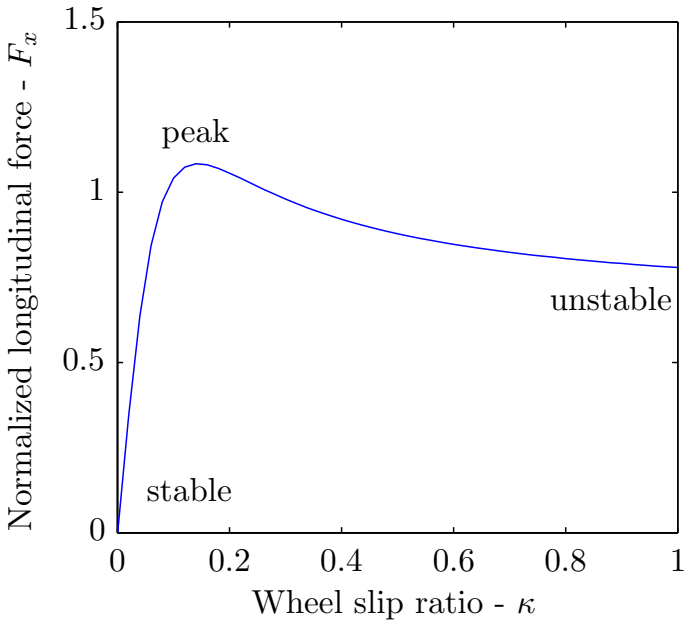

Figure 2.8: General variation of tire longitudinal force with slip.

2.3.2 ABS Control Algorithms

The ABS control algorithm mainly performs two tasks: prediction and re-selection. Prediction involves the judgment of the controller on whether the wheel is going towards lock-up and re-selection is when the controller decides to re-apply brakes based on its assessment of whether has sufficiently accelerated.

The performance of an ABS is decided to a large extent by the controller algorithm being used in the micro-controller that sends signals to the solenoids in the modulator circuit. Unlike regular controllers, ABS control algorithms have multiple layers of redundancies written into them to ensure failsafe operation. The type of control algorithm used depends on the state variable being controlled. Most of the algorithms on production ABS today are based on a combination of the control of two states which are described below.

Wheel Slip Control In this method, the wheel slip is continuously calculated through wheel speed and vehicle speed sensors and is sent as a state to the ABS controller

which, based on various control methodologies drives the wheel slip to the desired value. For wheel slip control, a model based law is adapted and currently this is the most widely used method for advanced ABS systems used in modern automobiles. As new control methodologies are formulated, various ABS algorithms have been proposed and evaluated over the years towards creating a more robust system that would operate under varying surface conditions. Slip control systems are known to work well for non-decreasing force conditions.

Some of the earliest work done in this area includes the work done by Guntur [43, 44] who proposed an adaptive brake control system. Taheri [45] investigated the use of non-linear control laws for ABS and proposed a sliding mode based control algorithm [46], a variation of which was also proposed by Drakunov et al [47]. Some authors including Mauer [48] have proposed intelligent controllers based on fuzzy logic. Robust adaptive control based on the Lyapunov method was suggested by Yu [49]. Due to the complex nature of the hydraulic actuators which cause the pressure change in the brake line, PID controllers are considered to be very robust and are popularly implemented at the lower level, such as the ones proposed by Taheri and Law [50]. Recent advances in sensor-based estimation techniques have led to the development of ABS control methods based on intelligent tires as explained by Singh et al [51]. A comprehensive review of various ABS wheel slip control algorithms has been explained by Aly [52].

Wheel Acceleration Control The concept of an ABS based on the measurement of peripheral angular acceleration of the wheel is implemented using a rule-based approach. In this system, the braking cycle is designed to operate in three states: 1. Apply 2. Hold 3. Release. The ABS controller is supplied with an exhaustive look-up table that would account for different braking scenario. This table is essentially a set of threshold values for wheel deceleration and slip ratios that would decide the brake state during the prediction and re-selection stage. In a typical system, the ABS would activate when the wheel deceleration drops below a specific value. The brake states are continuously regulated such that the wheel deceleration and slip are within the

provided thresholds. This method is considered to be an indirect way of controlling wheel slip because it requires careful adjustment of wheel acceleration thresholds to achieve optimum performance.

Although more advanced controllers have been developed since their introduction, wheel acceleration based ABS controllers are still popularly implemented in multiple vehicle simulation models which require the inclusion of an ABS. One of the most widely used algorithms in this regard is the Bosch® HVE version 1 algorithm which has been explained in detail by Roberts et al [53] and in their automotive handbook [54].

Ding et al [55, 56] implemented an improved version of this algorithm which was originally designed for the 2002 Volkswagen® Jetta with additional braking states and self-adjusting thresholds and reference speeds. The Hardware-In-the-Loop (HIL) validation [57] of this algorithm has also been explained in detail to demonstrate its performance in comparison to a commercial ABS.

2.4 Previous Work on Dynamic Tire Models with ABS

Due to sustained interest from the industry to understand the influence of the dynamics of tires and uneven roads on the performance of braking systems, various studies have been undertaken using mutiple dynamic tire models. Earlier research by Zegelaar [58] involved understanding the response of the rigid ring tire model to brake torque variations and their experimental validation. Following this, Jansen et al [3] have focused on demonstrating the potential of dynamic tire models such as the rigid ring model and their comparison with steady-state and transient tire models for the analysis of the performance of ABS systems. Following this, Paulwelussen et all [2] implemented the MF-SWIFT model in a full vehicle with an ABS model and analyzed the braking response of their model at different velocities under varying road conditions. Rangelov [59] constructed a simulink model of a quarter car with MF-SWIFT and Bosch® ABS algorithm and analyzed the performance of different

control methodologies. In addition to this, Adcox et al [60] developed a ring model with a torsional spring and specifically analyzed the sensitivity of tire torsional dynamics on the control effort of ABS and braking performance.

2.5 Conclusions

A review of literature of all the modeling aspects involved in this study has been conducted in detail. Based on this, the following conclusions have been drawn:

- The reaction forces generated by a tire are influenced by vibrations induced in the belt due to road unevenness, variations in brake torque and the oscillations in axle height. The direct resultant of this is their effect on braking performance during the operation of ABS.
- Simple transient models are not sufficient for modeling all the above influencing factors. Various tire models are available to account for such factors.
- Dynamic tire models show considerable difference in response to braking in comparison to steady-state and transient tire models which justify their necessity.
- The enveloping property of the tire should be included in conjunction with the tire model to account for the filtering effect of the tire and the influence of road unevenness on force response.
- Various detailed algorithms for ABS controllers are available in published literature which can be adopted for analysis based on their closeness to commercial implementation.
- Requirements for vehicle models change according to their intended application (design iterations, real-time testing, driving simulator etc.)

After carefully evaluating the advantages and drawbacks of various models described in the literature, the following models have been chosen for implementation in the simulation tool to be developed:

Tire Model For simulating the dynamics of the tire, the rigid ring model developed by Zegelaar [1] is chosen because it is valid up to 100 Hz, accounts for the belt vibrations and has potential for real-time implementation due to its speed.

Enveloping Model The semi-empirical tandem elliptical cam model, which was developed by Schmeitz [13] has been selected due to its proven experimental validity and its applicability to arbitrary uneven road profiles.

ABS Model For modeling the Anti-lock Braking System, an improved variation of the Bosch® ABS algorithm implemented by Ding [55] is chosen due to the availability of source code and the algorithm has been validated to have accurately represented the operation of a comparable commercial ABS system.

Vehicle Model The vehicle model would serve to integrate all the above developed simulation models as a single unit. It is proposed to implement a standalone version of the simulation tool based on a quarter car vehicle model. Individual models also be adapted to be implemented in advanced vehicle dynamic modeling software such as CarSim®.

Chapter 3

Mathematical Modeling

Following the detailed literature review and the consequent selection of available models from available literature, the mathematical modeling of all components needs to be undertaken. This chapter explains in detail the assumptions for each model, the equations and constitutive relations that govern their behavior and their associated parameters. Detailed knowledge of the mathematical aspects of the tire model, enveloping model and the ABS model will form the basis for their implementation on a simulation platform. For the dynamic tire model, most of the equations were based on the work by Zegelaar [1] and Schmeitz [13], which were later improved by TNO Automotive during its commercial implementation as MF-SWIFT and described in their equation manual [61].

3.1 Dynamic Tire Model

Developing the complete tire model involves two components: 1. Tire model and 2. Enveloping model.

3.1.1 Assumptions

Before beginning to derive the mathematical relations for the dynamics of the tire, important assumptions need to be made to simplify the modeling process and remove unnecessary factors that have low influence on the analysis task at hand. The major assumptions made in this model are mentioned below:

- Only in-plane dynamics of the tire-wheel system is considered for modeling. Out-of-plane motions and their related influence on force generation are neglected.
- The model is expected to be valid only up to 100 Hz where the rigid body modes are dominant.
- The reaction forces generated at the wheel axle are calculated only along the longitudinal and vertical direction (F_x and F_z respectively). Moments generated about the lateral axis are calculated for rolling resistance and brake torque.
- The tire-wheel system is assumed to be rolling at an angular velocity of Ω at the start of the simulation.
- Effect of tread element damping is neglected in the calculation of transient slip.
- Tire belt is assumed to be rigid and inextensible in its expected frequency range of operation (<100 Hz).
- The elliptical cams used in the enveloping model are considered to be rigid and constrained to move only in the vertical direction.
- The tire is assumed to be symmetric about its axis of rotation. Loads and forces acting on the tire are assumed to act along the Z-axis at the center of rotation.
- The influence of camber and toe are neglected
- Inflation pressure is assumed to be constant throughout the simulation.

- The maximum height of the road disturbance is assumed to be less than 0.03 m.

3.1.2 Coordinate System

For all calculations, the right-handed cartesian coordinate system according to ISO 8855 is used. For the X-axis, the forward direction is considered positive and is aligned along the intersection of the wheel plane and the road plane. The Z-axis is chosen such that it is aligned perpendicular to the road plane and the upwards direction is considered positive. The Y-axis is chosen such that the axis system is right-handed. When the tire rolls in the positive X direction, the angular velocity about the Y-axis is positive. Traction forces are hence positive and the braking and rolling resistance forces are negative. The vertical reaction force generated by the loaded tire is positive. Figure 3.1 shows the global coordinate system as illustrated by Zegelaar [1].

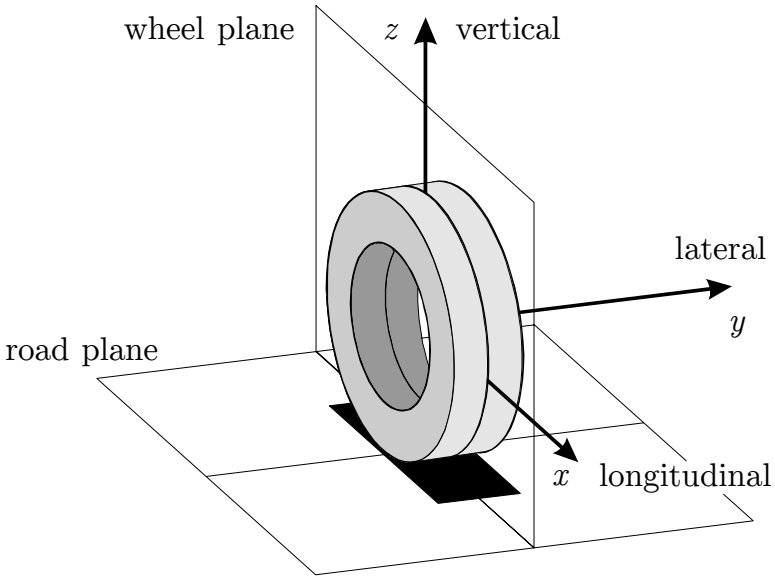

Figure 3.1: Global coordinate system. Adapted from Zegelaar, P. (1998). *The dynamic response of tyres to brake torque variations and road unevennesses.* Delft University of Technology. Used under fair use, 2013.

3.1.3 Tandem Elliptical Cam Model

The enveloping property of the tire is modeled using the tandem elliptical cam model developed by Schmeitz [13]. This is an improvement of the two-point follower method developed by Zegelaar [1]. As explained in the literature, this semi-empirical model assumes two elliptical cams in tandem (connected by rods) rolling over the uneven road surface, constrained to move only in the vertical direction. Figure 3.2 shows a tandem model rolling over an obstacle, as illustrated by Schmeitz [13].

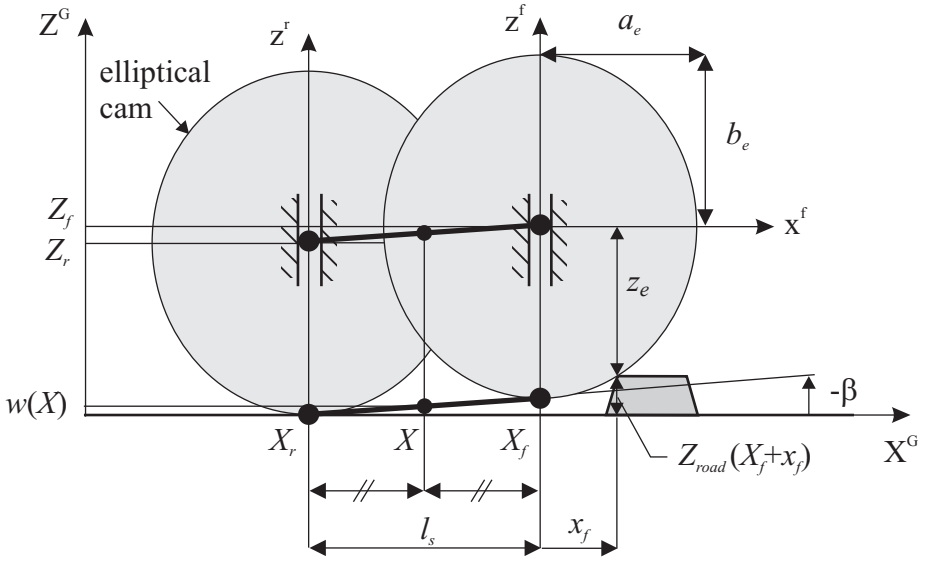

Figure 3.2: Tandem elliptical cam model. Adapted from Schmeitz, A. J. C. (2004). *A Semi-Empirical Three-Dimensional Model of the Pneumatic Tyre Rolling over Arbitrarily Uneven Road Surfaces.* Delft University of Technology. Used under fair use, 2013.

Each elliptical cam has a width a_e and height b_e. The subscripts 'G','f' and 'r' are used to denote the coordinate systems for the global road, front and rear elliptical cam respectively. The cams are separated by a distance l_s. This parameter is a function of the vertical load on the tire and is calculated based on the contact length $2a$:

$$l_s = p_{ls} \cdot 2a \tag{3.1}$$

where p_{ls} is a model parameter estimated through experiments. The distance (shift) between

the cams increases as the load increases. The inputs to this model are the X and Z coordinates of the actual road profile in the global frame of reference. This is transformed into an effective plane height and slope which would serve as an input to the rigid ring tire model. The effective plane height w is calculated for each road position X as the mid-point of the lower tandem rod:

$$w(X) = \frac{Z_f + Z_r}{2} - b_e \tag{3.2}$$

where Z_f and Z_r are the global heights of the front and rear cams respectively. The effective plane slope β is calculated as:

$$\beta(X) = \arctan\left(\frac{Z_r - Z_f}{l_s}\right) \tag{3.3}$$

For the front ellipse, we know its equation in the local coordinate system as:

$$\left(\frac{x_f}{a_e}\right)^{c_e} + \left(\frac{z_f}{b_e}\right)^{c_e} = 1 \tag{3.4}$$

where x_f and z_f are the local position coordinates for the front ellipse. The vertical distance (z_e) between the local X-axis and the ellipse for any local position x_f is calculated based on Equation (3.4) as:

$$z_e(x_f) = \left| b_e \cdot \left(1 - \left(\frac{|x_f|}{a_e}\right)^{c_e}\right)^{\frac{1}{c_e}} \right| \tag{3.5}$$

From Figure 3.2, we can observe the front ellipse rolling over an obstacle of height Z_{road}. Thus the global height of the front ellipse(Z_f) is calculated using a maximal relation as the sum of the road height and the vertical distance between the ellipse contact point and the center:

$$Z_f = \max\left[Z_{road}(X_f + x_f) + z_e(x_f)\right] \quad \forall\, x_f \in [-a_e, a_e] \tag{3.6}$$

Equation (3.6) is a maximal relation because to calculate Z_f it is necessary to find out where the ellipse actually makes contact with the road profile. This is done using an iterative procedure where the road profile is sampled at specific intervals around the global position of the front ellipse X_f with a maximum limit of the ellipse width a_e where the global height of the front ellipse is calculated at each interval using Equation (3.6) and the maximum

obtained value at the end of the iteration is taken as the final global height. The same procedure is also repeated for the rear ellipse.

Special care must be given to the selection of the sample interval and the total scan width because the number of points to scan at each road position would play a major role in determining the speed and accuracy of the algorithm. Scan intervals which are too big might lead to inaccurate results. Also, scanning the entire width of $[-a_e, a_e]$ might severely slow down the calculation speed as this step is repeated at each simulation time step. Generally, the resolution of the road profile is taken as the sample interval and the scan width is adjusted accordingly to achieve the right balance between accuracy and speed. The maximum allowable sampling interval is 2 cm to achieve acceptable results.

3.1.4 Rigid Ring Tire Model

This section details the modeling of the rigid ring dynamic tire model as explained by Zegelaar [1] and adapted based on the current assumptions. This includes the calculations for various properties of the tire including effective loading radius, forces in the contact patch and related equations of motion.

In this model, the tire belt is modeled as a rigid ring connected to the axle or the rim through springs and dampers which represent the pressurized sidewall. The ring is connected to the road through a contact model which is represented as a transient slip model, as illustrated in Figure 3.3. In this model, the translational sidewall stiffness and damping are represented by c_{bx} and k_{bx}. $c_{b\theta}$ and $k_{b\theta}$ denote the rotational stiffness and damping. Vertical sidewall stiffness and damping are represented by c_{bz} and k_{bz} respectively. Since the tire is assumed to be symmetric, the stiffness and damping along the X and Z direction are assumed to be the same.

Figure 3.4 shows deformations occurring in the tire ring of radius r. The tire-wheel system is rotating at an undisturbed angular velocity Ω. The motion of the axle is represented by

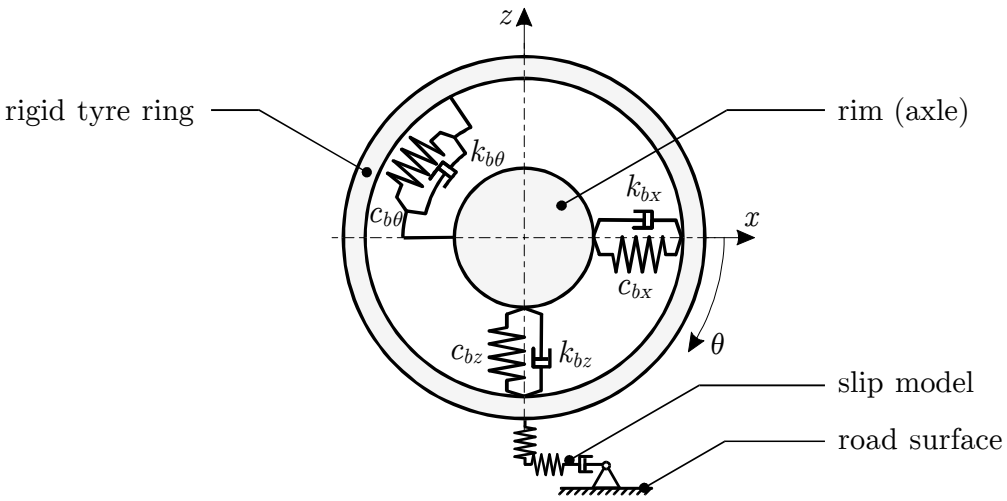

Figure 3.3: Rigid ring tire model. Adapted from Zegelaar, P. (1998). *The dynamic response of tyres to brake torque variations and road unevennesses.* Delft University of Technology. Used under fair use, 2013.

x_a and z_a. Consider a point O in the ring after a rotation of ϕ ($\dot{\phi} = \Omega$). This point then moves to A following the motion of the rim which is rotated by θ_a and translated by x_a and z_a. This then results in a deflection in the sidewall which results in the point moving to B due to a rotation of θ_b and a translation of x_b and z_b in the ring.

Inputs and Outputs

The rigid ring model requires inputs from other models to simulate results, namely:

Axle Motion Axle motion is represented by x_a, z_a, $\dot{x}_a$ and $\dot{z}_a$ which are calculated from the vehicle model. When the tire is loaded, the axle is given an initial vertical displacement (which is negative) to represent the deflection in the tire. In the case of experiments with a fixed axle, z_a is kept constant and $\dot{z}_a = 0$.

Effective Road Profile This consists of the effective plane height w and plane angle β. These values are calculated for each point in the road profile by the enveloping model.

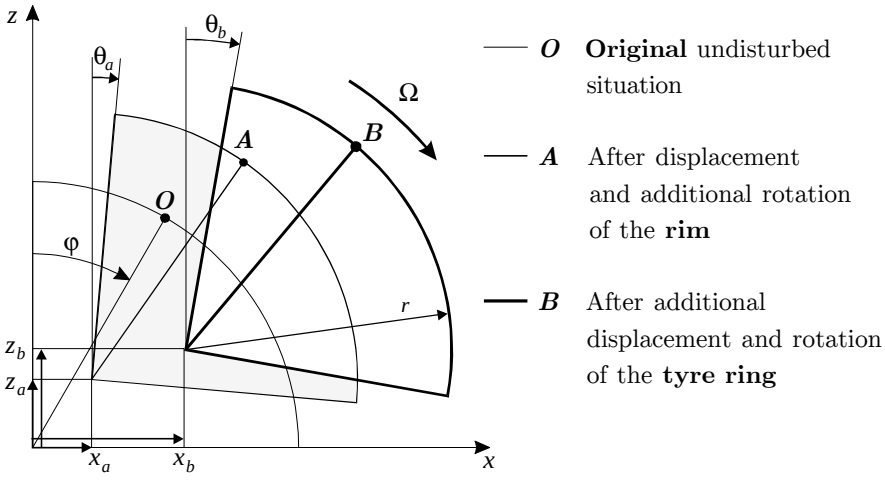

Figure 3.4: Deformations in the tire. Adapted from Zegelaar, P. (1998). *The dynamic response of tyres to brake torque variations and road unevennesses.* Delft University of Technology. Used under fair use, 2013.

Braking Moment This is denoted by M_{ay} and this input is provided by the braking module which calculates the applied torque at the axle during a braking event. This can either be due to ABS or manual braking.

Based on the above inputs, the rigid ring model calculates the following outputs which serve as inputs to the vehicle and the braking model:

Reaction Forces These are the forces acting on the vehicle from the tire, denoted by F_{bx} and F_{bz} and are from the equations of motion for the ring model.

Wheel Slip The dynamics of the tire rolling over uneven surfaces causes fluctuations in the angular velocity of the wheel due to the deformation of the belt in the rotational direction. The practical slip ratio κ, which acts an input to the braking module is calculated from the theoretical slip in the contact patch ζ_{cx} along the longitudinal direction.

Contact Patch Length This is calculated either based on the load acting on the contact patch or the vertical deflection of the tire. The length of the contact patch is denoted

by a and it serves as an input to the enveloping model to decide the shift between the tandem elliptical cams.

Equations of Motion

The four degrees of freedom of the rigid ring model are: (i) Horizontal defection of the belt x_b; (ii) Vertical deflection of the belt z_b; (iii) Angular deflection of the ring θ_b and (iv) Angular deflection of the rim or axle θ_a. The dynamics of the rolling tire are represented through a set of non-linear second order differential equations as shown below:

$$m_b\ddot{x}_b + k_{bx}\left(\dot{x}_b - \dot{x}_a\right) + c_{bx}\left(x_b - x_a\right) - k_{bz}\left(\Omega + \dot{\theta}_a\right)\left(z_b - z_a\right) = F_{cT}\cos\beta + F_{cN}\sin\beta \quad (3.7a)$$

$$m_b\ddot{z}_b + k_{bz}\left(\dot{z}_b - \dot{z}_a\right) + c_{bz}\left(z_b - z_a\right) + k_{bz}\left(\Omega + \dot{\theta}_a\right)\left(x_b - x_a\right) = F_{cN}\cos\beta - F_{cT}\sin\beta \quad (3.7b)$$

$$I_{by}\ddot{\theta}_b + k_{b\theta}\left(\dot{\theta}_b - \dot{\theta}_a\right) + c_{b\theta}\left(\theta_b - \theta_a\right) = -r_e F_{cT} + M_{cy} \quad (3.7c)$$

$$I_{ay}\ddot{\theta}_a + k_{b\theta}\left(\dot{\theta}_a - \dot{\theta}_b\right) + c_{b\theta}\left(\theta_a - \theta_b\right) = M_{ay} \quad (3.7d)$$

Equation (3.7) involves the use of multiple parameters, force and moment inputs where some of them stay constant throughout the simulation. Calculation of these parameters are based on non-linear relations which are explained in subsequent sections.

Inertial Parameters

The inertial parameters of the ring model are measured through experiments or already assumed to be known through design. The belt-mass is denoted by m_b and its moment of inertia about the Y axis is denoted by I_{by}. Axle moment of inertia I_{ay} is a combination of the rotational inertia of the wheel, axle and the brake calipers. Hence, this is a vehicle dependent parameter.

Sidewall Stiffness and Damping

The vertical and rotational stiffness and damping of the sidewall are calculated from the natural frequencies of the in-plane rigid body modes of the unloaded, inflated tire which is mounted on a fixed spindle without touching the ground. Sidewall stiffness and damping values are calculated as:

$$c_{bx0} = c_{bz0} = 4\pi^2 \cdot m_b \cdot f_{long}^2 \tag{3.8a}$$

$$c_{b\theta 0} = 4\pi^2 \cdot I_{by} \cdot f_{windup}^2 \tag{3.8b}$$

$$k_{bx0} = k_{bz0} = 4\pi \cdot \zeta_{long} \cdot m_b \cdot f_{long} \tag{3.8c}$$

$$k_{b\theta 0} = 4\pi \cdot \zeta_{windup} \cdot I_{by} \cdot f_{windup} \tag{3.8d}$$

where f_{long} is the primary eigen-frequency (in Hz) and ζ_{long} is the dimensionless damping factor of the vertical/longitudinal motion of the belt, also known as the in-plane vertical mode. f_{windup} and ζ_{windup} are correspondingly the eigen-frequency and damping factor of the rotational motion of the belt, also known as the in-plane torsional mode. The subscript '0' denotes stiffness and damping values of the tire at non-rolling conditions. Equation (3.8) is valid only for rigid body modes because under such situations, the belt moves as a rigid body and can be approximated to have the same behavior as a single degree of freedom mass, spring and damper. During the modal analysis, the spindle is clamped to ensure the belt mass is the primary inertial component.

Based on previous studies by Vinesse [62] and Zegelaar [58], it is understood that the natural frequencies of the rolling tire change with velocity. Hence, the actual sidewall stiffness is much lower than the values obtained from the natural frequencies at stationary condition using Equation (3.8). In order to account for this effect, the sidewall stiffness is made dependent

on the rolling velocity, pressure and load through correction factors:

$$c_{bx} = c_{bx0}\left(1 + 0.65 \cdot dp_i\right)\left(1 - q_{bVx}\sqrt{Q_V}\right) \tag{3.9a}$$

$$c_{bz} = c_{bz0}\left(1 + 0.65 \cdot dp_i\right)\left(1 - q_{bVz}\sqrt{Q_V}\right) \tag{3.9b}$$

$$c_{b\theta} = c_{b\theta 0}\left(1 + 0.49 \cdot dp_i\right)\left(1 - q_{bV\theta}\sqrt{Q_V}\right) \tag{3.9c}$$

where the variable Q_V is a non-dimensional quantity which represents the rate of deformation of the tire due to rolling, calculated using the relation:

$$Q_V = \frac{\left|\Omega + \dot{\theta}_a\right|}{V_0}\sqrt{(x_b - x_a)^2 + (z_b - z_a)^2} \tag{3.10}$$

where V_0 is the nominal rolling velocity in m/s. The pressure dependency of sidewall stiffness is included using empirical factors. The variable dp_i measures the change in inflation pressure:

$$dp_i = \frac{P - P_0}{P_0} \tag{3.11}$$

where P_0 is the nominal inflation pressure and P is the current inflation pressure, measured either in bar or kPa.

Normal Force in the Contact Patch

The normal force in the contact patch is represented by F_{cN} which is a product of the residual stiffness and the residual deflection in the contact patch. This occurs due to the fact that the total deformation of the tire is larger than the displacement of the rigid ring. The total vertical stiffness is hence a combination of the sidewall stiffness c_{bz} and the residual stiffness. The normal force in the contact patch has a non-linear relation with the residual deflection and is represented as a third order polynomial:

$$F_{cN} = \begin{cases} q_{Fzr3}\rho_{zr}^3 + q_{Fzr2}\rho_{zr}^2 + q_{Fzr1}\rho_{zr} & \text{if } \rho_{zr} > 0 \\ 0 & \text{if } \rho_{zr} \leq 0 \end{cases} \tag{3.12}$$

The polynomial coefficients in Equation (3.12) are calculated from the sidewall stiffness c_{bz} and the parameters q_{Fz1} and q_{Fz2} which are the linear and quadratic factors in the total vertical load-deflection characteristic:

$$q_{Fzr1} = \frac{c_{bz} A_1}{c_{bz} - A_1} \tag{3.13a}$$

$$q_{Fzr2} = \frac{c_{bz}^3 A_2}{(c_{bz} - A_1)^3} \tag{3.13b}$$

$$q_{Fzr3} = \frac{c_{bz}^4 A_2^2}{(c_{bz} - A_1)^5} \tag{3.13c}$$

where:

$$A_1 = \frac{q_{Fz1} F_{z0}}{r_0} \left(1 + \frac{q_{V2} |\Omega_a| r_0}{V_0}\right) \tag{3.13d}$$

$$A_2 = \frac{q_{Fz2} A_1}{q_{Fz1} r_0} \tag{3.13e}$$

The constant parameters F_{z0} denotes the nominal vertical load (in N) and r_0 the free-tire radius at non-rolling condition. The factor q_{V2} accounts for the increase vertical stiffness with speed. Ω_a replaces Ω and is the angular velocity of the rim, which is the sum of the undisturbed rolling velocity and the rate of deflection of the rim:

$$\Omega_a = \Omega + \dot{\theta}_a \tag{3.14}$$

The normal force in the contact patch is influenced by the effective road profile, radial and tangential deflection of the belt and these factors are accounted through the residual deflection:

$$\rho_{zr} = w - z_b + \Delta r - q_{Fcx} \rho_x^2 \tag{3.15}$$

In this, q_{Fcx} is a model parameter. The variable Δr represents the centrifugal growth of the free-tire radius due to rolling:

$$\Delta r = r_0 \left(q_{re0} + q_{V1} \left(\frac{\Omega_a r_0}{V_0}\right)^2\right) \tag{3.16}$$

where q_{re0} and q_{V1} are the model parameters which can be estimated. The influence of the horizontal deflection ρ_x is observed at high levels of braking torque and constant axle heights,

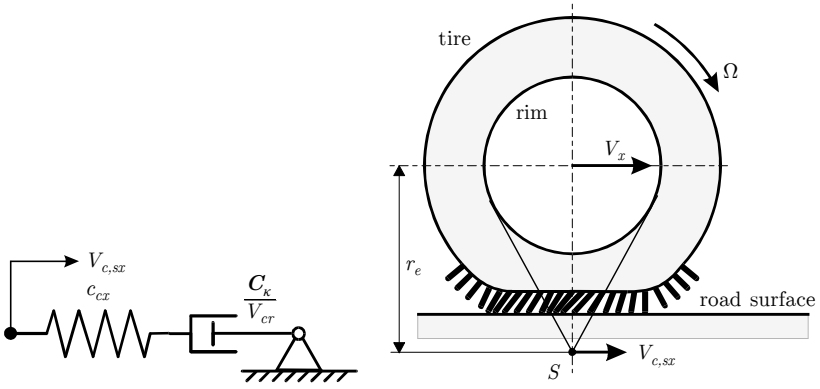

(a) Tread element model. (b) Brush-type tread elements.

Figure 3.5: Tire-road contact model. Adapted from Zegelaar, P. (1998). *The dynamic response of tyres to brake torque variations and road unevennesses.* Delft University of Technology. Used under fair use, 2013.

which is calculated as:

$$\rho_x = (x_b - x_a) + r_0(\theta_b - \theta_a) \tag{3.17}$$

Tire-Road Contact Model

The tangential force acting in the contact patch is represented by F_{cT}. This force is generated due to slip ζ_{cx} occurring in the contact patch. The dynamic interactions between the tread elements of the rolling tire and the ground leads to variations in the slip. The slip is also influenced by the deformation of the belt and variations in the effective rolling radius. This plays a crucial role in the analysis of ABS systems.

Hence, a contact model is required for the tread elements to simulate the transient slip. This is accomplished using an analytical model, as shown in Figure 3.5(a) where the non-steady state slip variations are modeled using a first-order approximation which is based on the relaxation length σ_{cx} and slip velocities calculated from belt deflections:

$$\sigma_c \cdot \dot{\zeta}_{cx} + |V_{cr}| = -V_{c,sx} \tag{3.18}$$

where σ_c is the relaxation length of the contact patch. The slip ζ_{cx} is limited to avoid numerical stability issues. The linear rolling velocity of the belt V_{cr} is calculated as:

$$V_{cr} = r_e \left(\Omega + \dot{\theta}_b\right) \tag{3.19}$$

Slip Velocity

The slip velocity of the belt in the contact zone $V_{c,sx}$, as illustrated in Figure 3.5(b) is calculated as a difference between the linear velocity of the center of the ring along the road surface and its rolling velocity as shown in Equation (3.20). An additional term is included to account for the effect of road disturbance on the effective rolling radius.

$$V_{c,sx} = V_{cT} - V_{cr} = (\dot{x}_b \cos\beta - \dot{z}_b \sin\beta) - r_e \left(\Omega + \dot{\theta}_b\right) + \rho_z \frac{d\beta}{dt} \tag{3.20}$$

where ρ_z is the total vertical deflection of the tire:

$$\rho_z = w - z_a + \Delta r - q_{Fcx}\rho_x^2 \tag{3.21}$$

Effective Rolling Radius

In order to calculate the rolling velocity from Equation (3.20), the effective rolling radius r_e needs to be obtained, which is calculated through an empirical relation:

$$r_e = \Delta r - \frac{F_{z0}}{C_z}\left(D_{reff} \arctan\left(B_{reff}\frac{F_{cN}}{F_{z0}}\right) + F_{reff}\frac{F_{cN}}{F_{z0}}\right) \tag{3.22}$$

where B_{reff}, D_{reff} and F_{reff} are model parameters. The total vertical stiffness C_z, which is dependent on the inflation pressure is calculated using the relation:

$$C_z = C_{z0}\left(1 + p_{Fz1} \cdot dp_i\right) \tag{3.23}$$

where p_{Fz1} denotes the linear dependence of the vertical stiffness on inflation pressure. C_{z0} is the nominal vertical stiffness of the tire:

$$C_{z0} = \frac{F_{z0}}{r_0}\sqrt{q_{Fz1}^2 + 4q_{Fz2}} \tag{3.24}$$

Tangential force from brush model

The value of the transient slip ζ_{cx} obtained from the slip model described in Equation (3.18) and the vertical load in the contact patch F_{cN} obtained from Equation (3.12) are used as inputs to a brush model to calculate the tangential force F_{cT} in the contact patch.

The brush model, as illustrated in Figure 3.5(b) is a steady-state physical tire model where the tread elements are assumed to have the behavior of bristles with a stiffness c_{px} per unit length of the tread. The tangential force F_{cT} is given by:

$$F_{cT} = \begin{cases} \mu F_{cN} \left\{ 3 \left| \theta \zeta_{cx} \right| - 3 \left| \theta \zeta_{cx} \right|^2 + \left| \theta \zeta_{cx} \right|^3 \right\} \operatorname{sgn} \left(\zeta_{cx} \right) & \text{for } \left| \zeta_{cx} \right| \leq 1/\theta \\ \mu F_{cN} \cdot \operatorname{sgn} \left(\zeta_{cx} \right) & \text{for } \left| \zeta_{cx} \right| > 1/\theta \end{cases} \tag{3.25}$$

where the composite parameter θ is defined as:

$$\theta = \frac{2}{3} \frac{c_{px} a^2}{\mu F_{cN}} \tag{3.26}$$

An alternative approach is to use the steady-state Magic Formula for calculating the tangential forces, which requires a practical slip κ as an input instead of the theoretical slip ζ_{cx}. This is explained in detail by Zegelaar [1] in the appendix of his thesis.

Relaxation Length

The relaxation length σ_c used in Equation (3.18), is calculated from the local slip stiffness C_κ and the slip stiffness at free rolling $C_{\kappa 0}$:

$$\sigma_c = \sigma_{c0} \frac{C_\kappa}{C_{\kappa 0}} \tag{3.27}$$

where σ_{c0} is the relaxation length at free rolling equals half the contact length ($\sigma_{c0} = a$). The slip stiffness at free rolling $C_{\kappa 0}$ is calculated from the unit tread element stiffness c_{px} and half the contact length a:

$$C_{\kappa 0} = 2 c_{px} a^2 \tag{3.28}$$

The local slip stiffness C_κ is calculated as:

$$C_\kappa = \left(\frac{\partial F_x}{\partial \zeta} \right)_{\zeta = \zeta_{cx}} \tag{3.29}$$

Calculation of the relaxation length based on Equation (3.27) although accurate can be computationally expensive due to partial derivatives used in (3.29). Hence, an approximation is used based on an adhesion factor m:

$$\sigma_c = \frac{ma}{1 + \zeta_{cx}} \tag{3.30a}$$

with m calculated based on the composite parameter θ using Equation (3.25):

$$m = \begin{cases} 1 - \theta \dfrac{|\zeta_{cx}|}{1 + \zeta_{cx}} & \text{if } \dfrac{|\zeta_{cx}|}{1 + \zeta_{cx}} < \dfrac{1}{\theta} \\ 0 & \text{otherwise} \end{cases} \tag{3.30b}$$

The minimum value of the relaxation length is constrained to ensure the numerical stability of the simulation.

Contact Length

When the tire is loaded, the deformation leads to a flattened contact surface between the tire and the ground. This patch is assumed to have the shape of an ellipse. As the contact patch grows larger with increasing loads, the length of the contact patch is assumed to have a non-linear relationship with the vertical load (or deflection) which can be expressed as:

$$a = r_0 \left(q_{ra2} \frac{F_{cN}}{C_z \cdot r_0} + q_{ra1} \sqrt{\frac{F_{cN}}{C_z \cdot r_0}} \right) \approx r_0 \left(q_{ra2} \frac{\rho_z}{r_0} + q_{ra1} \sqrt{\frac{\rho_z}{r_0}} \right) \tag{3.31}$$

where a is half of the contact length and q_{ra1} and q_{ra1} are polynomial fit parameters which are calculated through experiments.

Rolling Resistance

Rolling resistance is the opposition experienced by the tire as it rolls over a surface. This effect is accounted in Equation (3.7) by assuming an external torque M_{cy} that acts on the

ring:

$$M_{cy} = -r_e f_r F_{cN} \cdot \text{sgn}\left(\Omega + \dot{\theta}_b\right) \tag{3.32}$$

where f_r is the rolling resistance coefficient. This coefficient is assumed to vary as a non-linear polynomial function of speed and is expressed as:

$$f_r = \left(q_{sy1} + q_{sy3}\left|\frac{V_x}{V_0}\right| + q_{sy4}\left(\frac{V_x}{V_0}\right)^4\right)\left(\frac{P}{P_0}\right)^{q_{sy8}} \tag{3.33}$$

Forces at the Axle

The forces generated by the tire at the axle serve as the outputs from the tire model to the vehicle model. They are calculated from the belt forces based on Equation (3.7) as:

$$F_{xt} = c_{bx}\left(x_b - x_a\right) + k_{bx}\left(\dot{x}_b - \dot{x}_a\right) - k_{bx}\left(\Omega + \dot{\theta}_a\right)\left(z_b - z_a\right) \tag{3.34a}$$

$$F_{zt} = c_{bz}\left(z_b - z_a\right) + k_{bz}\left(\dot{z}_b - \dot{z}_a\right) + k_{bz}\left(\Omega + \dot{\theta}_a\right)\left(x_b - x_a\right) \tag{3.34b}$$

3.2 Anti-lock Braking System Model

An ABS model consists of two main components: 1. Control algorithm and 2. Pressure model. Both these components are very essential to produce accurate results because having an advanced control algorithm with a simplistic pressure model can lead to un-realistic results. Also, having a detailed pressure model without a robust algorithm can also lead to unfavorable results. Hence, a balance needs to be maintained to ensure confidence in simulation results.

3.2.1 Inputs and Outputs

Since the ABS unit is only responsible for braking control, the system has a limited set of inputs and outputs:

Inputs : The ABS unit requires longitudinal slip κ and the wheel acceleration ϵ from the tire model.

Outputs : Based on the inputs, the ABS with the included pressure model calculates the braking torque M_{ay} which is again sent to the tire model.

3.2.2 Assumptions

The hydraulic circuit of a braking system is an extremely complex system. A number of assumptions were made which were aimed towards simplifying the modeling process and on removing factors that had low influence on ABS performance:

- The ABS controller is assumed to know wheel slip and vehicle speed information through sensors.
- Pressure in the master cylinder is assumed to be a constant value.
- Braking torque at the axle is considered to be linearly proportional to the pressure in the brake line.
- Wheel slip and acceleration thresholds do not change during the simulation.
- The delay in the valves is represented as a first order delay.
- Mechanical delay in converting the pressure in the brake line to torque is taken to be a constant value in time.
- The rate of increase and decrease of pressure during different brake states remain constant and cannot be changed during the simulation.
- A minimum speed is required for the operation of the ABS system below which the braking module switches to manual braking.

3.2.3 Brake States

The operating algorithm of an ABS is characterized by the number and the type of brake states utilized by the ABS to achieve optimal control of slip and wheel acceleration. The ABS control logic, as designed by Ding et al [55] has the following primary states for the braking system:

Initialize The ABS begins in this state where the output pressure in the wheel cylinder is set to the master cylinder pressure. This is done to ensure proper build up of pressure before regulation.

Hold Brake Pressure In this state, the ABS directs the wheel cylinder pressure to be maintained in the previous control cycle. This is generally used when the slip and wheel acceleration fall in the desired range.

Increase Brake Pressure In this, the brake pressure in the wheel cylinder is set to increase from its current level up to the master cylinder pressure at a normal rate. The behavior of the wheel cylinder is modeled according to Equation (3.35).

Fast Increase Brake Pressure The wheel cylinder pressure is regulated to increase at a faster rate than the normal rate. This is generally done in cases where a sudden increase in braking force is required (changing surface conditions etc.).

Decrease Brake Pressure This is also known as the pressure release state where the brake pressure in the wheel cylinder is set to decrease from its current to atmospheric pressure. The behavior of the wheel cylinder is modeled according to Equation (3.36).

Step Increase Brake Pressure This is a hybrid-state in which two operations are done in a cycle: 1. Increase 2. Hold. This was introduced to increase the brake pressure and also maintain the wheel acceleration without waiting for the controller to re-calculate until the next cycle. Apart from the regular thresholds in the controller, this stage has

a separate wheel acceleration threshold where the pressure is set to hold for a specific amount of time when exceeded.

Step Decrease Brake Pressure The operation of this state is based on the same principle as the step increase in brake pressure with the only difference being in this case the brake pressure is decreased in cycles of decrease and hold (for a specified time).

Exit Braking This state is used when the vehicle is below a minimum speed where the ABS shuts off and switches to manual braking.

3.2.4 ABS Control Cycling

An ABS system deployed in a vehicle is designed to control four wheels with a single controller. In a general scenario, it might be too difficult to calculate control signals all four wheels in a single cycle. This is accomplished by the use of controller flags where one wheel is controlled during a cycle and this is rotated after each cycle. This way, all four wheels are controlled at a reasonable rate. This method is illustrated in Figure 3.6.

3.2.5 State Selection Rules

The selection of brake states are made using a state-flow based approach where the decisions are made based on a set of rules and thresholds. Figure 3.7 shows the chart used in this system for the selection of states. Here, κ denotes the wheel slip and ϵ denotes the peripheral acceleration of the wheel. This was previously designed at the Intelligent Transportation Laboratory with a fixed set of thresholds which are being used.

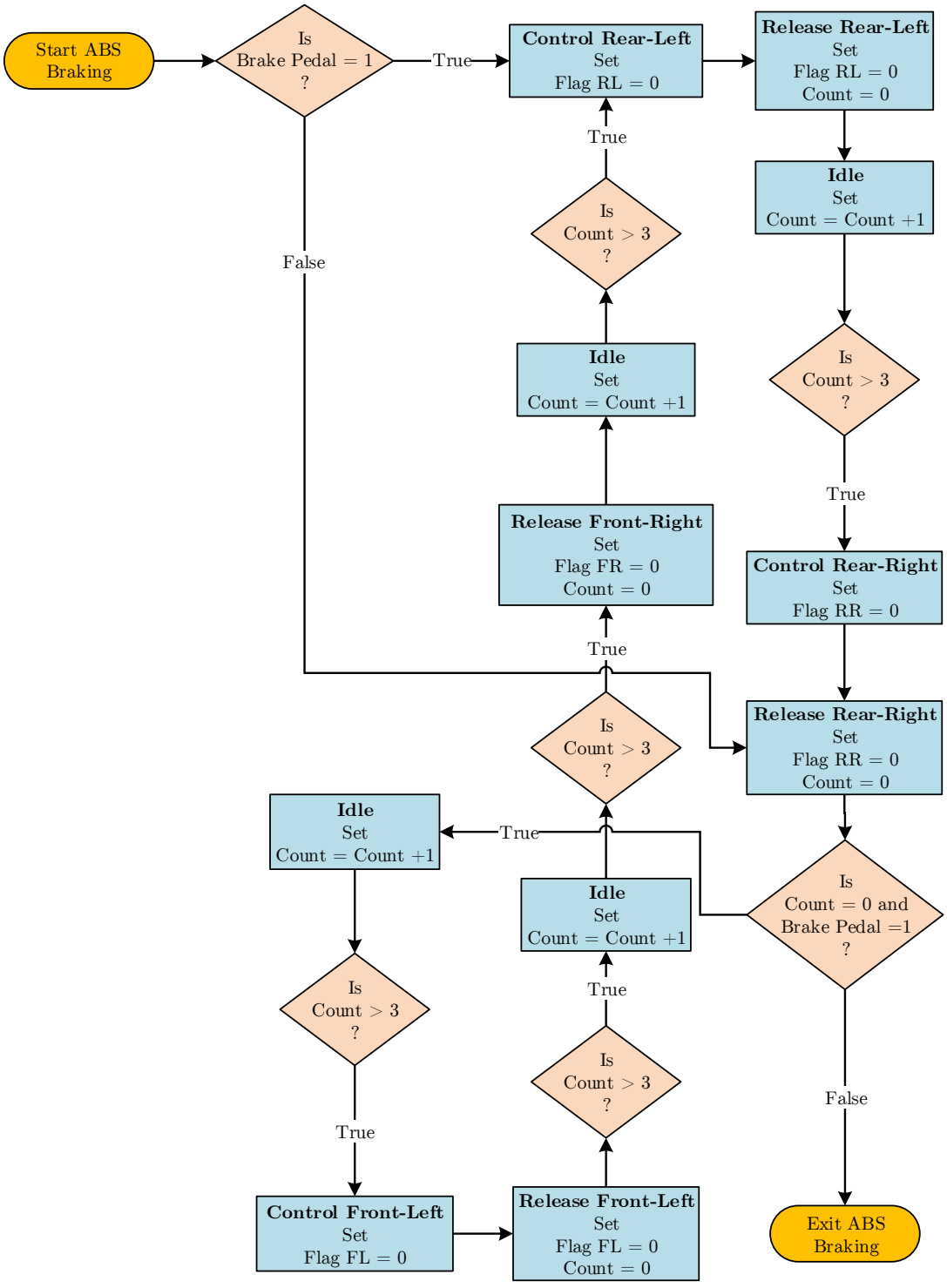

Figure 3.6: ABS control cycling between different tires.

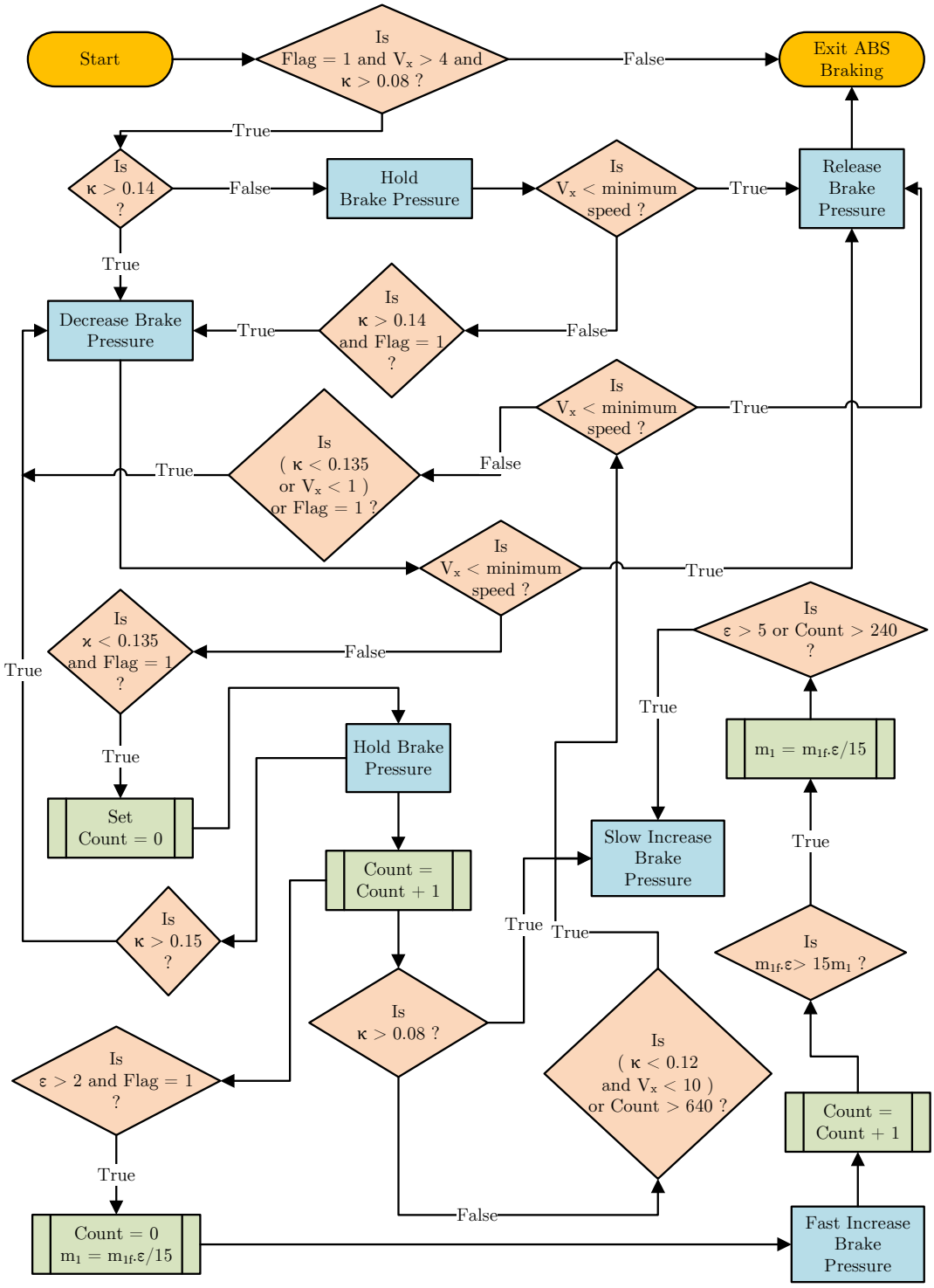

Figure 3.7: Flowchart for the selection of brake states.

3.2.6 Pressure Model

In an ABS system, the brake pressure is regulated by means of electromagnetic valves that are installed in the Hydraulic Control Unit (HCU). The pressure can be regulated through three states: 1. Pressure increase; 2. Pressure hold; and 3. Pressure release.

In the pressure increase mode, the wheel cylinder pressure P_w is assumed to have an exponential increase and is calculated as:

$$P_w(t) = P_m - \left[(P_m - P_{w0})^{\phi_{inc}} - K_{inc}\phi_{inc}(t - t_0)\right]^{1/\phi_{inc}} \tag{3.35}$$

where P_{w0} is the wheel cylinder pressure at the previous simulation time-step t_0. P_m is the pressure at the master cylinder. K_{inc} and ϕ_{inc} are model parameters for the response characteristics of the brake system.

In the pressure release mode, the pressure in the brake cylinder pressure is governed by the following expression:

$$P_w(t) = \left[(P_{w0} - P_a)^{\phi_{dec}} - K_{dec}\phi_{dec}(t - t_0)\right]^{1/\phi_{inc}} + P_a \tag{3.36}$$

where P_a is the atmospheric pressure. The parameters K_{dec} and ϕ_{dec} are selected based on the desired behavior for pressure decrease. The pressure in the wheel cylinder is retained in its previous value during the hold phase.

The pressure in the wheel cylinder P_w is then converted into brake torque M_{ay} using the relation:

$$M_{ay} = P_w \cdot C_p \tag{3.37}$$

where C_p is the brake torque gain (N.m/Pa) and this value is different for the front wheels and rear wheels . The brake torque is applied to the tire model after a first-order transport delay to account for the dynamics of the valve.

3.3 Quarter Car Model

The quarter car model is the most commonly used for ride analysis and braking studies. The model considered here is assumed to have suspensions in both X and Z directions. Inputs to this model constitute reaction forces from the dynamic tire model to the axle. Desired outputs are the axle motions that serve as inputs to the tire model. The quarter car model is illustrated as shown in Figure 3.8.

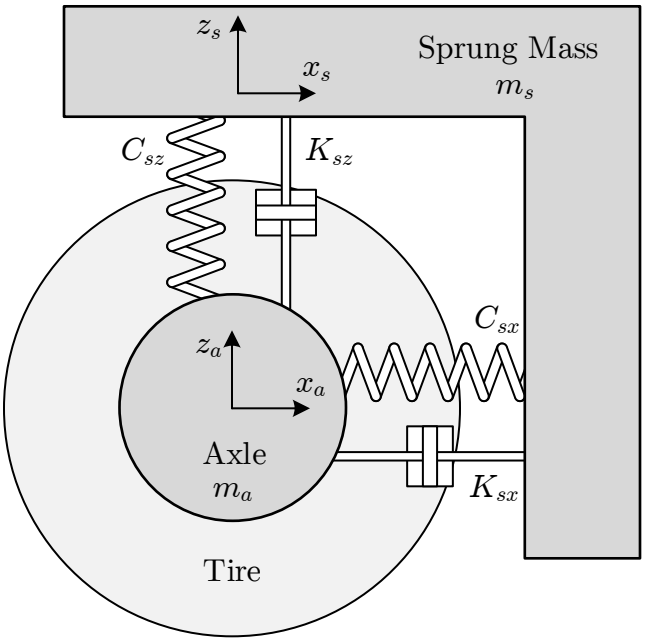

Figure 3.8: Quarter car model.

The equations of motion of the quarter car model are calculated as:

$$m_a \cdot \ddot{x}_a + K_{sx}(\dot{x}_a - \dot{x}_s) + C_{sx}(x_a - x_s) = F_{xt} \tag{3.38a}$$

$$m_s \cdot \ddot{x}_s + K_{sx}(\dot{x}_s - \dot{x}_a) + C_{sx}(x_s - x_a) = 0 \tag{3.38b}$$

$$m_a \cdot \ddot{z}_a + K_{sz}(\dot{z}_a - \dot{z}_s) + C_{sz}(z_a - z_s) = F_{zt} + m_a g \tag{3.38c}$$

$$m_s \cdot \ddot{z}_s + K_{sz}(\dot{z}_s - \dot{z}_a) + C_{sz}(z_s - z_a) = m_s g \tag{3.38d}$$

where C_{sx}, C_{sz}, K_{sx} and K_{sz} are the suspension stiffness and damping values along the X and Z directions respectively. m_s is the vehicle sprung mass and m_a is the unsprung mass

which consists of the mass of the axle including the suspension and braking elements. Since the tire is modeled as a separate rigid ring element, their inertial properties are not added to the axle mass. Here, the assumptions are that the stiffness and damping elements are linear and the deflection along the X axis and Z axis are independent of each other.

3.4 Conclusions

Detailed mathematical models of all the subsystems of the simulation tool, including the dynamic tire model, ABS model and the vehicle model were developed. This was done by deciding on a set of assumptions for simplifying the model and the equations were derived based on the literature. These models were then used to develop a simulation platform and integrated to optimize performance as discussed in subsequent chapters.

Chapter 4

Implementation

Following the derivation of equations for the models, it was necessary to develop their models in a platform that can conduct the simulations and can be used to analyze the results. This chapter describes the methodology adopted towards the selection of simulation platform, development of models and the requirements for the exchange of experimental and parameter data.

4.1 Design Requirements

Based on the objectives of the model defined in Section 1.2.1, the following design requirements are outlined that are relevant towards model development:

- The simulation platform must be capable of running multiple test cases.
- There should be capability to support real-time simulations.
- ODE solvers in the platform should be computationally efficient to deliver results in minimum time. Miscellaneous calculations should be efficient to ensure they do not slow down the ODE solvers.

- The subsystems should be modular in nature and must be easy to modify. They should be able to adapt to other simulation models or commercial software.
- The source for the simulation should be easy to interpret and modify.
- The output data from simulations should be in an open format which can be easily extracted for plotting and analysis.

4.2 Simulation Platform

Based on the design requirements, an appropriate simulation was selected platform was for model development. In this study, Matlab-Simulink® was used because of its popularity and widespread adoption as a simulation platform and it block diagram based approach which is easier to understand and interpret. Their solvers for differential equations are considered to be very efficient and they have the capability to export to C for standalone applications and real-time simulations. Also, this platform can be used with commercial software such as CarSim® for future extensions in the model.

4.2.1 Simulink Modeling

The simulink model was developed based on the same differentiation as the modeling procedure explained in Chapter 2. The developed model consists of three major subsystems: 1. Tire model; 2. ABS model and 3. Vehicle model. These major subsystems were further divided into multiple divisions based on the respective variable or also on the degrees of freedom to reduce confusion while constructing the model. Special focus was placed towards making all subsystems modular to improve interoperability with other subsystems that the manufacturer would like to include, such as proprietary ABS models and vehicle models. Figure 4.1 shows an overview of the complete simulation model with all three major

subsystems. These subsystems have their own organization and they are further explained below.

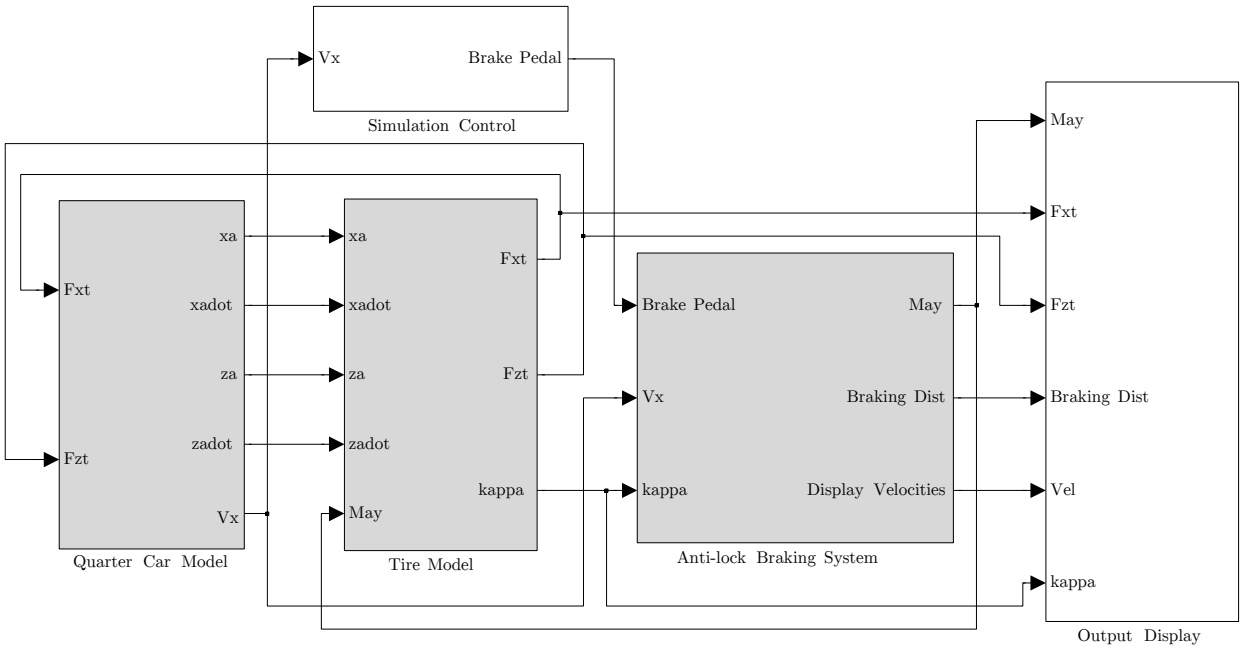

Figure 4.1: Vehicle simulation model.

Tire Model

The tire model is the most complex module of the simulation tool with multiple subsystems. An overview of the tire model with the enveloping model is shown in Figure 4.2. The enveloping model shown here is written as a Matlab® embedded function, which is converted to C during runtime. This is because the model is based on an iterative procedure and developing Simulink models for this case would make the model highly complex and reduce readability of code. This subsystem calculates the effective road height at each time-step for any road profile in real-time. Various subsystems of the tire model, developed as a Simulink subsystem are shown in Figure 4.3.

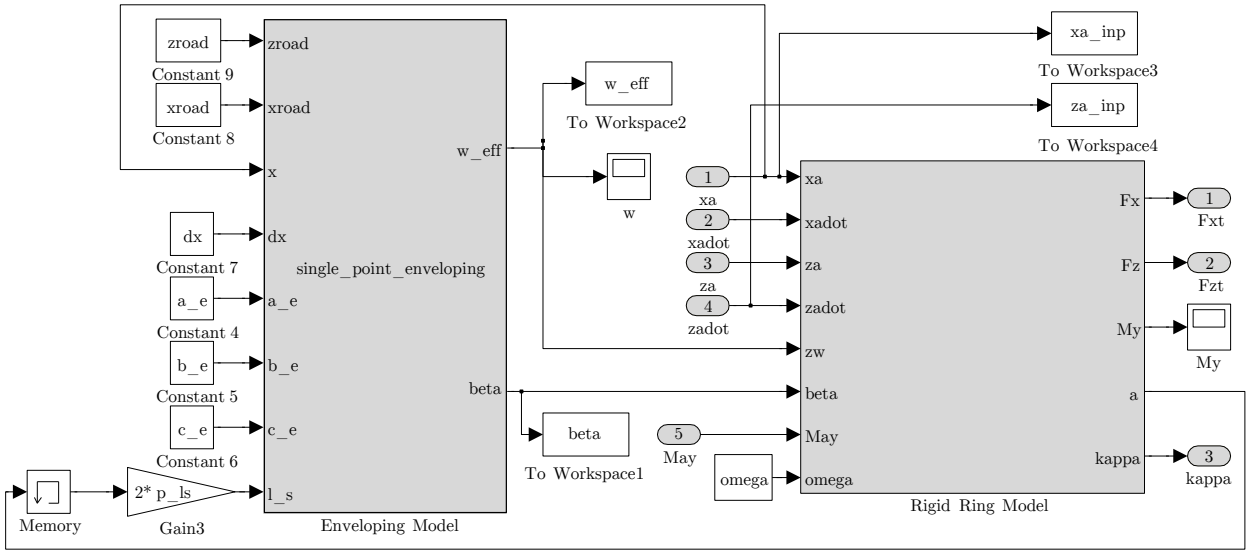

Figure 4.2: Tire model and enveloping model in Simulink.

ABS Model

The ABS model consists of the controller algorithm and the pressure model. The simulink model has been illustrated in Figure 4.4.

Vehicle Model

The quarter vehicle model has two subsystems for the motion of the sprung mass in the X and Z directions. The quarter car subsystem is shown in Figure 4.5.

4.3 Solvers and Time-steps

The selection of solver is extremely important for maintaining the right balance between accuracy of results and speed. In addition to this, the time step should also be selected appropriately. The solver used for all simulations were set to ODE4 (Runge-Kutta) discrete time step in view of its low computational load and satisfactory accuracy.

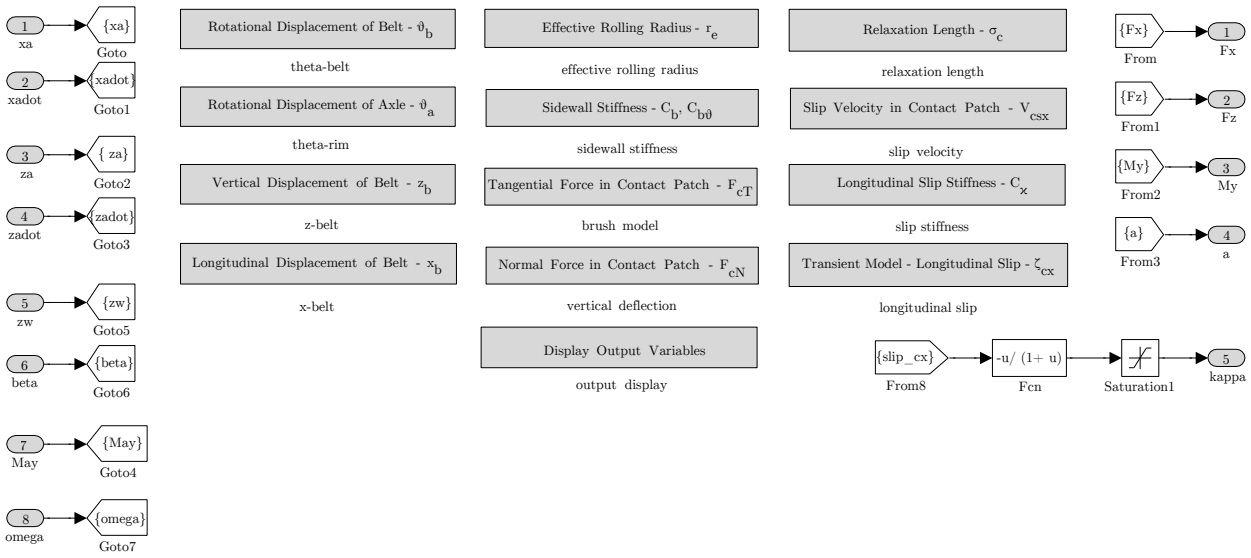

Figure 4.3: Rigid ring tire model in Simulink.

During simulations with a fixed axle with the dynamic tire model, the discrete time step was chosen to be 1 ms. For ABS simulations with a quarter car model, a 0.25 ms discrete time step was chosen because the thresholds and the various timers that are used in the controller algorithm were originally designed based on this time step.

4.4 Data Exchange Standards

The main expectation out of this tool is their implementation among both tire and vehicle manufacturers. In order to achieve this, exchange of experimental data and tire parameter files might be required among cooperating industries. Hence, some form of standardization in the format of the data being transferred is required to avoid any confusions of experimental data. To solve this issue, it was decided to utilize the Tyre Data Exchange (TYDEX) standard. This was standard conceived by the international tire working group to facilitate easy exchange of experimental data between different industries. A detailed explanation of the TYDEX standard has been given by its authors Unrau et al in their manual [63].

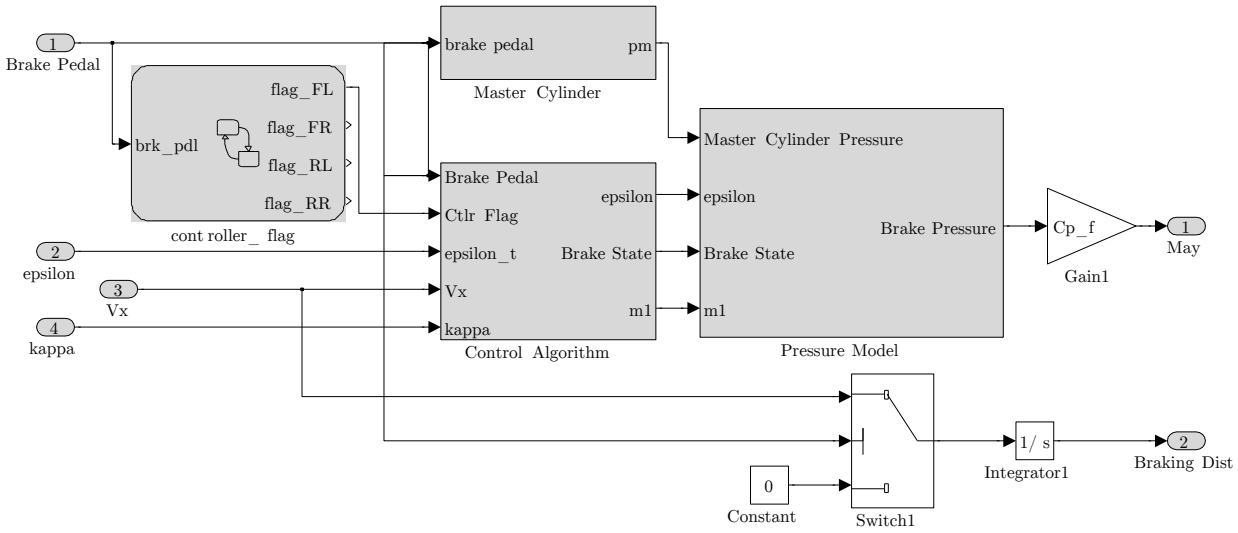

Figure 4.4: ABS subsystem.

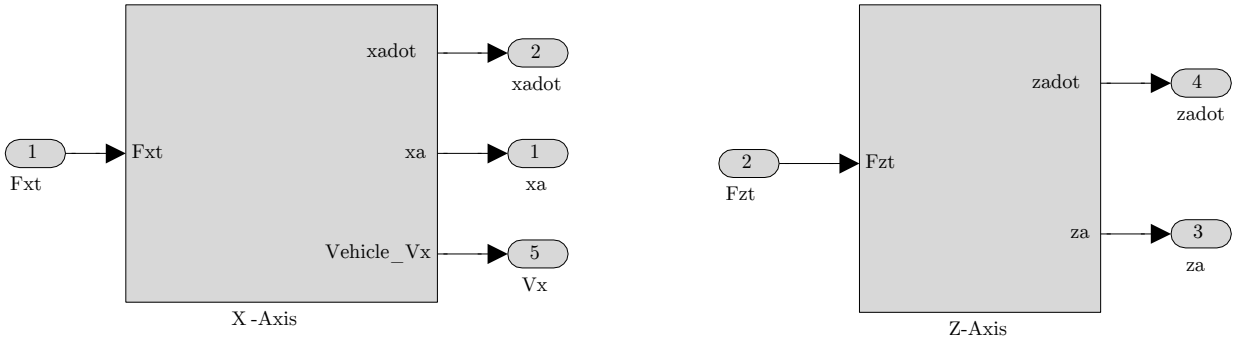

Figure 4.5: Quarter car model in Simulink.

In this study, the capability to read experimental data and parameter values of tires from standard TYDEX files was incorporated to reduce the additional effort involved in the implementation of the tool and its work-flow integration. This would also ensure backward compatibility and with parameter files from other simulation software such as MF-SWIFT which utilize the same standard.

4.5 Model Optimization

When the simulation model was developed and implemented in their current state, it was realized that the performance might not be optimal and feature set might be limited. An important point of concern was that the speed of computation in each subsystem needed to be maintained to ensure it does not slow down the entire simulation. The following optimizations were done to improve the speed of simulation results:

- During initial test runs it was observed that the iterative calculations in the enveloping model was slowing down the entire simulation. This was due to the fact that a process of extrapolation was taking place at every time step. This was then replaced with an indexed array with the road height and horizontal position at fixed intervals. Based on this, the road profile at each time step was approximated to the nearest available point instead of extrapolation. This modification has shown good improvements in the speed of results.

- The scan width of the enveloping model has been set to $[-a_e/6,\ a_e/6]$ to balance between accuracy and achieving faster results without spending computational effort on a bigger scan interval.

- The relaxation length has been approximated using Equation (3.30) to reduce the numerical load in calculating slip stiffness at each time step.

- The calculation of wheel slip κ and wheel acceleration ϵ for the ABS model has been done based the theoretical slip ζ_{cx} to match the rotating coordinate system being used in the tire model and the global coordinate system used in the ABS model.

- All functions used in the simulink model were chosen based on their ability to be converted into equivalent C-functions. This was done keeping future extensions in mind for developing standalone applications.

- After completing the construction of the Simulink model and finalizing model parameters, the simulation file was converted into a Matlab® MEX function, which is a C-compiled executable of the Simulink file. This was found to significantly improve the efficiency of calculations and reduce simulation time.

- All definitions of model parameter constants such as automated extraction from tire parameter (TIR) files, simulation runs and plotting of results were performed using scripts instead of a Graphical User Interface (GUI) based approach to reduce the amount of user intervention required inside the model and to provide a code framework for automated iterations of simulation runs under various test cases for ABS development.

4.6 Conclusions

The simulation model of a quarter car with an ABS system using a dynamic tire model was successfully developed in Matlab-Simulink®. These models were further modified for optimum performance and a code framework has been developed for the automated processing of tire parameter files and conducting simulation runs. Following this, a model parameterization process was developed and simulation runs were conducted for multiple test cases, which are explained in subsequent chapters.

Chapter 5

Model Parameterization

The mathematical model of the dynamic tire involves multiple parameters that are either physical quantities such as sidewall stiffness, damping etc. and also curve fitting parameters to model the non-linear relationships between certain quantities. This chapter describes in detail the procedure developed to parameterize the rigid ring tire model and the enveloping model. Major parts of the procedure and the initial analysis was based on the methods described by Besselink [5] and Schmeitz et al [64]. Also, the Curve Fitting Toolbox™ available in Matlab® has been utilized for the development of the fitting algorithm.

5.1 Reference Tire

In this study, a specific tire was selected as a reference for parameterization and analysis based on the availability of experimental data and available tire parameters. The dimensions of the tire used in this study is denoted as a Goodyear 205/60R15 91V where the numbers are described, and illustrated by Zegelaar [1] in Figure 5.1 and explained in Table 5.1.

Notation	Meaning
205	Section width in mm
60	Ratio between section height and width in % (aspect ratio)
R	Radial tire
15	Rim diameter in inches
91	Maximum allowable load on the tire - 6030 N (load index)
V	Speed rating - 240 km/h

Table 5.1: Reference tire notation

5.2 Experimental Procedure

The physical and empirical parameters of the tire model used in this study are either through direct measurements or based on fitting experimental data. This data is obtained using standard test procedures and measurement conventions. The following experiments are required to be performed in order to completely parameterize the dynamic tire model:

- Geometric and inertial measurements.
- Steady-state longitudinal force vs. slip characteristics.
- Vertical load vs. deflection at multiple inflation pressures.
- Loaded radius, effective rolling radius vs. vertical load and forward velocity at multiple inflation pressures.
- Rolling resistance force vs. forward velocity at various values of inflation pressure.
- Contact patch length vs. vertical load.
- Low-speed enveloping tests on different types of cleats on a fixed axle at multiple loads.
- High-speed cleat tests at different velocities using a fixed axle.

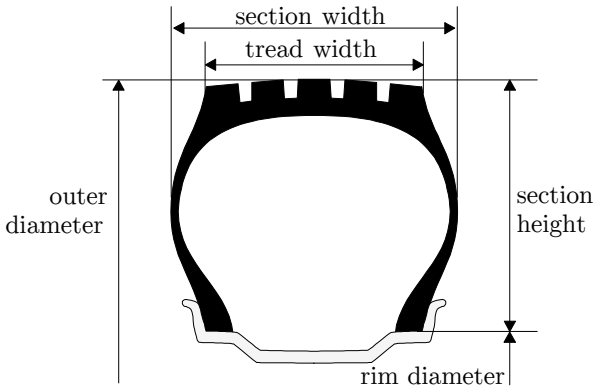

Figure 5.1: Tire dimensions. Adapted from Zegelaar, P. (1998). *The dynamic response of tyres to brake torque variations and road unevennesses.* Delft University of Technology. Used under fair use, 2013.

Generally, experiments that require multiple loads and inflation pressures are based on three distinct values for each, totaling nine experiments. In cases where only one inflation pressure is required, the nominal pressure P_0 is used. Table 5.2 shows the various measurement points used for obtaining data in this study. Here, LI refers to the load index.

Parameter	Values
Vertical load	$L_1 = 0.4 \cdot LI$ $L_2 = 0.8 \cdot LI$ $L_3 = 1.2 \cdot LI$
Inflation pressure	$P_1 = P_0 - 0.5$ bar $P_2 = P_0$ $P_3 = P_0 + 0.5$ bar

Table 5.2: Measurements points for multiple loads and inflation pressures

Since the in-plane dynamics are of major focus in this study, the camber angle and side-slip angle were always set to zero as a pre-condition before performing the experiments. All the

experimental data used in this study were obtained from a trial version of TNO MF-Tool 6.1 [65]. Detailed descriptions of collected experimental data has been provided in their documentation [66].

5.2.1 Nominal Parameters

Before beginning the parameterization process, a set of nominal values need to be fixed for the operating conditions for the tire to ensure that the tire is not used at values that extremely deviate from the nominal set. These would also be used to convert tire parameters into non-dimensional quantities. Their selection is very important because the measurement points are based on them and they need to be fixed throughout the parameterization process. The parameters for the reference tire used in this study are shown in Table 5.3.

Parameter	Symbol	Value
Inflation pressure	P_0	2.2 bar
Vertical load	F_{z0}	4000 N
Rolling velocity	V_{x0}	16.7 m/s

Table 5.3: Nominal parameters for the tire

5.2.2 Inertial and Dimensional Parameters

The major inertial parameters of the tire used in the model involve the mass m_b and rotational moment of inertia I_{by} of the belt along the Y-axis. These are directly measured through experiments. The main dimensional parameter includes the unloaded radius r_0 is also measured directly. The standard procedure adopted for these measurements are explained in SAE J2717 [67]. In the case of absence of experimental data, the following empirical values are assigned for the tire belt inertial parameters:
75% of the tire mass is considered to be belt mass m_b

80% of the rotational inertia of the tire is considered to be the mas of the tire.
They can also be calculated using the unloaded radius and the tread depth h_{tread}:

$$I_{by} = m_b \left(r_0 - h_{tread}\right)^2 \tag{5.1}$$

The measured values of relevant tire dimensional and inertial properties are shown in Table 5.4

Parameter	Value
Unloaded radius r_0	0.3135 m
Belt mass m_b	7.247 kg
Belt rotational moment of inertia I_{by}	0.5698 kg.m^2

Table 5.4: Geometric and inertial parameters of the tire

5.2.3 Sidewall Stiffness and Damping

The initial sidewall stiffness and damping are calculated from the natural frequencies of the in-plane rigid body modes obtained from stationary modal analysis of the tire and converted to stiffness and damping values based on Equation (3.8). The boundary conditions in this case is that the tire is mounted on a fixed spindle and not in contact with the ground. Detailed experimental procedures can be adopted based on the Tire Model Performance Test (TMPT) benchmark [68]. Obtained values of eigen-frequencies and their corresponding stiffness values are shown in Table 5.5

Mode	Frequency, damping	Sidewall stiffness, damping
Translation	77.17 Hz, 0.0558	$c_{bz0} = 1.703 \cdot 10^6$ N/m, $k_{bz0} = 391.938$ N.s/m
Torsion	58.95 Hz, 0.0504	$c_{b\theta 0} = 7.817 \cdot 10^4$ N.m/rad, $k_{b\theta 0} = 21.2654$ Nm.s/rad

Table 5.5: Estimated sidewall stiffness and damping

Zegelaar [1] observed that the stiffness values estimated through stationary modal analysis might be too high due to the fact that the stiffness during rolling is less and Dorfi [69] observed there is a shift in the modal frequencies due to the cycling of rubber and material transport. Hence, a correction factor is recommended to account for such rolling effects, as shown in Equation (3.9). These factors can be determined through an optimization procedure through experimental results obtained from cleat testing. In this study, these correction factors were set to empirical values: $q_{bVx} = 0.3640$ and $q_{bV\theta} = 0.0648$.

5.2.4 Vertical Stiffness

The total vertical stiffness of the tire is determined through the variation of vertical deflection vs. load on the tire. In this study, the deflection test has been performed on a rolling tire at different velocities and inflation pressure. Hence, the deflection is calculated using the loaded radius of the tire. As a first step, the fitting parameters q_{V2}, q_{Fz1} and q_{Fz2} were evaluated using data obtained at nominal pressure P_0 using non-linear curve fitting as shown in Figure 5.2:

$$F_z = \left(1 + q_{V2}\frac{\Omega \cdot r_0}{V_0}\right) \cdot F_{z0} \cdot \left(q_{Fz1}\frac{\rho}{r_0} + q_{Fz2}\left(\frac{\rho}{r_0}\right)^2\right) \tag{5.2}$$

Based on this, the total vertical stiffness is calculated using Equation (3.24). The effect of inflation pressure is then captured through an additional factor p_{Fz1} with data measured at a given vertical deflection (loaded radius) $\rho = 0.0128$ m at multiple loads and rolling velocities using non-linear curve fitting as shown in Figure 5.3:

$$F_z = \left(1 + q_{V2}\frac{\Omega \cdot r_0}{V_0}\right) \cdot F_{z0} \cdot \left(q_{Fz1}\frac{\rho}{r_0} + q_{Fz2}\left(\frac{\rho}{r_0}\right)^2\right)(1 + p_{Fz1} \cdot dP) \tag{5.3}$$

The calculated parameter values are shown in Table 5.6. SAE J2704 [70] can be used for standardized measurement of normal force vs. deflection characteristics without any speed effects. When no experimental data is available, a vertical stiffness C_{z0} is used with $q_{Fz2} = 0$.

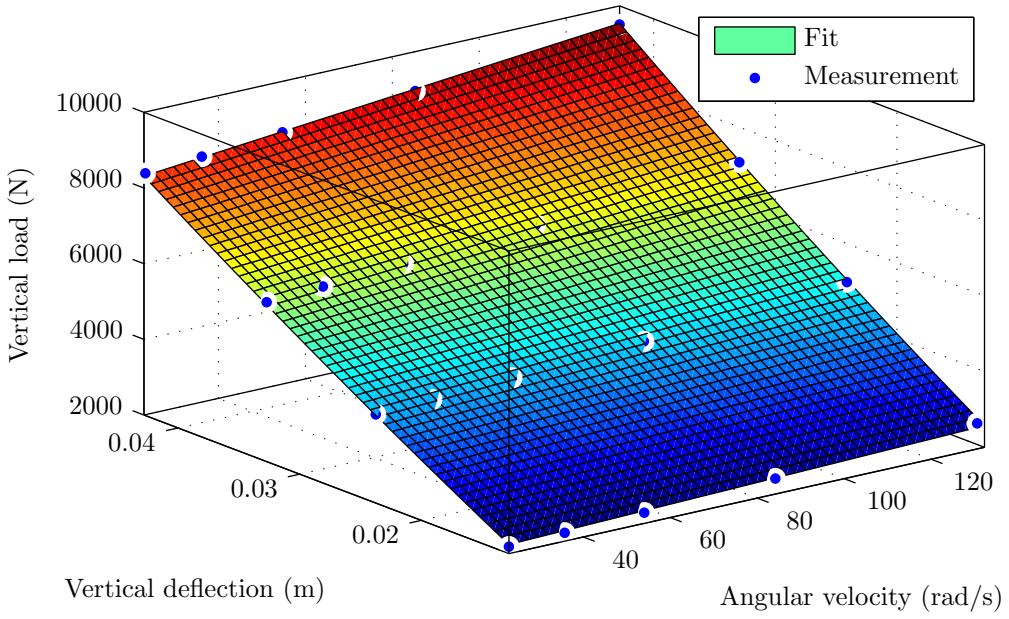

Figure 5.2: Loaded radius measurements at $P = 2.2$ bar.

5.2.5 Effective Rolling Radius

The parameters for effective rolling radius are based on the same experimental data obtained for loaded radius analysis. The calculation of rolling radius is based on an empirical approach through Equation (3.22). The parameters B_{reff}, D_{reff}, F_{reff}, q_{re0} and q_{V1} are calculated based on the variation of the effective rolling radius with load and forward velocity using a non-linear surface fitting procedure. This method assists in capturing the load dependency and the growth in tire radius due to centrifugal forces.

Figure 5.4 shows the final results of the surface fit and the estimated parameters are shown in Table 5.7. In the absence of measurements for effective rolling radius, the following empirical values are suggested for a radial tire: $B_{reff} = 8$, $D_{reff} = 0.24$, $F_{reff} = 0.01$, $q_{re0} = 1$, $q_{V1} = 0$.

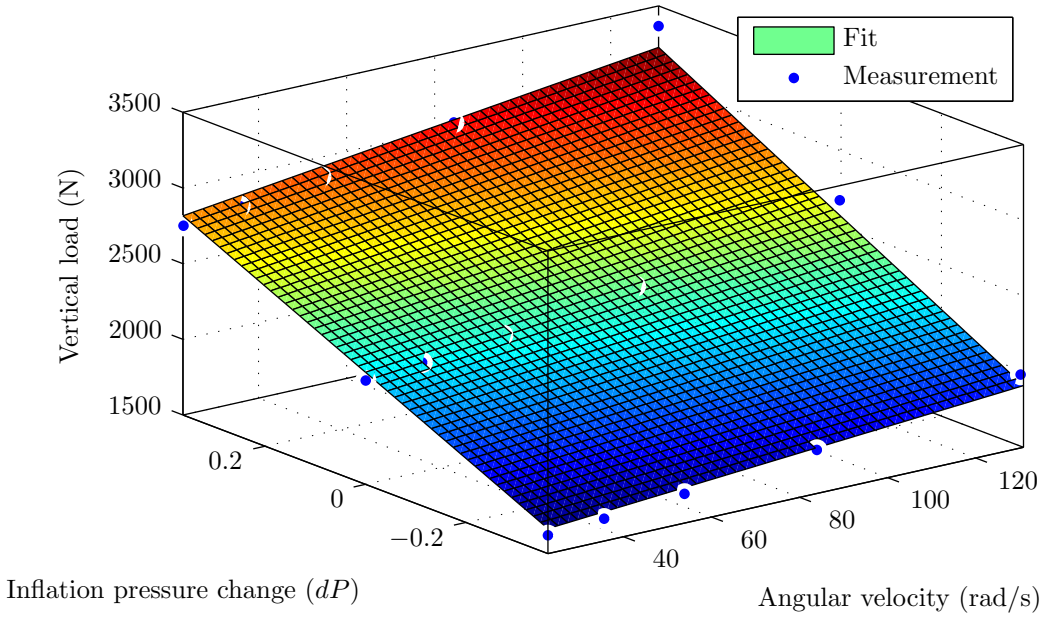

Figure 5.3: Measurements at vertical deflection = 0.0128 m.

5.2.6 Contact Patch

Experimental data obtained from footprint dimension analysis is used to estimate contact patch characteristics. In this, the length of the contact patch is measured at three different loads at nominal inflation pressure. The measurements are then curve-fitted to obtain the fit parameters q_{ra1} and q_{ra2} using Equation (3.31).

The results of the fit procedure are illustrated in Figure 5.5. The obtained parameters are shown in Table 5.8. Detailed documentation for a standardized procedure is given in SAE J2704 [70].

5.2.7 Rolling Resistance

The rolling resistance force is calculated based on the reaction force F_{xr} in the axle during free rolling at a particular velocity and vertical load F_z. This reaction force is then converted

Parameter	Value
C_{z0}	$1.90 \cdot 10^5$ N/m
q_{Fz1}	12.6762
q_{Fz2}	15.2315
q_{V2}	0.0740
p_{Fz1}	0.7064

Table 5.6: Estimated vertical stiffness parameters

Parameter	Value
B_{reff}	2.1733
D_{reff}	0.2140
F_{reff}	0.0567
q_{re0}	0.9822
q_{V1}	$7.4026 \cdot 10^{-4}$

Table 5.7: Estimated parameters for effective rolling radius

to the rolling resistance coefficient f_r using the relation:

$$f_r = \frac{F_{xr}}{F_z} \tag{5.4}$$

Equation (3.33) is then used to obtain a fit for the velocity and pressure dependence of rolling resistance coefficient. Figure 5.6 shows the non-linear surface fit results and the estimated parameters are shown in Table 5.9. ISO standards [71] are required to be followed

Parameter	Value
q_{ra1}	0.6390
q_{ra2}	0.6625

Table 5.8: Estimated parameters for the contact patch

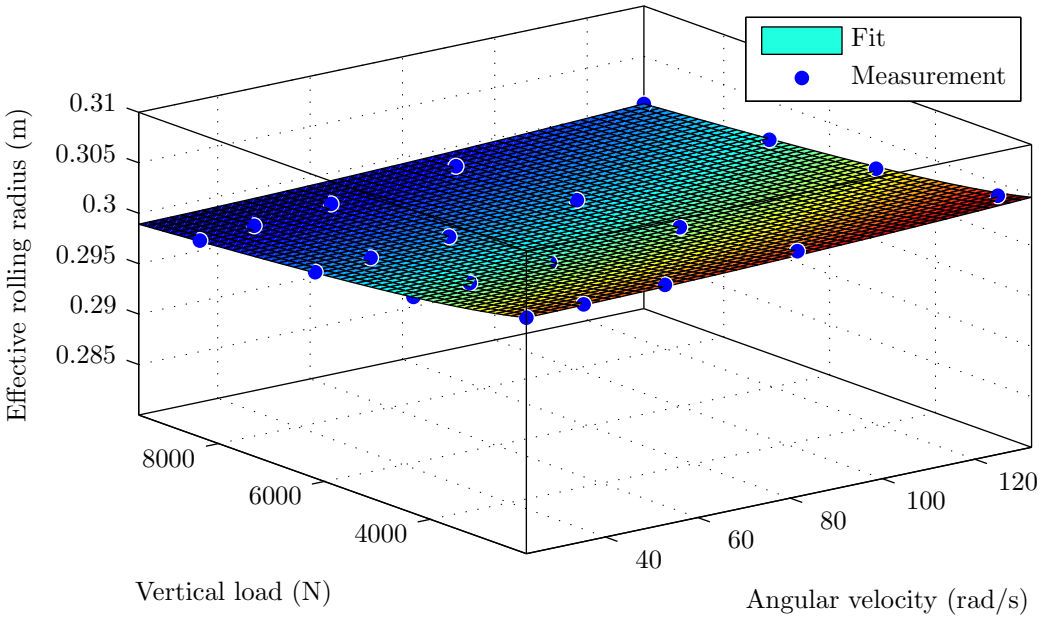

Figure 5.4: Effective rolling radius measurements at 2.2 bar

for measuring rolling resistance.

Parameter	Value
q_{sy1}	0.0070
q_{sy3}	0.0016
q_{sy4}	$9.420 \cdot 10^{-5}$
q_{sy8}	-0.3189

Table 5.9: Estimated parameters for rolling resistance

5.2.8 Tread Element Stiffness

The tread element stiffness c_{px} per unit length is the main parameter involved in the calculation of steady-state tangential forces using the brush model as described in Equation (3.25). This parameter is assumed to be invariable with pressure and is determined from the steady-

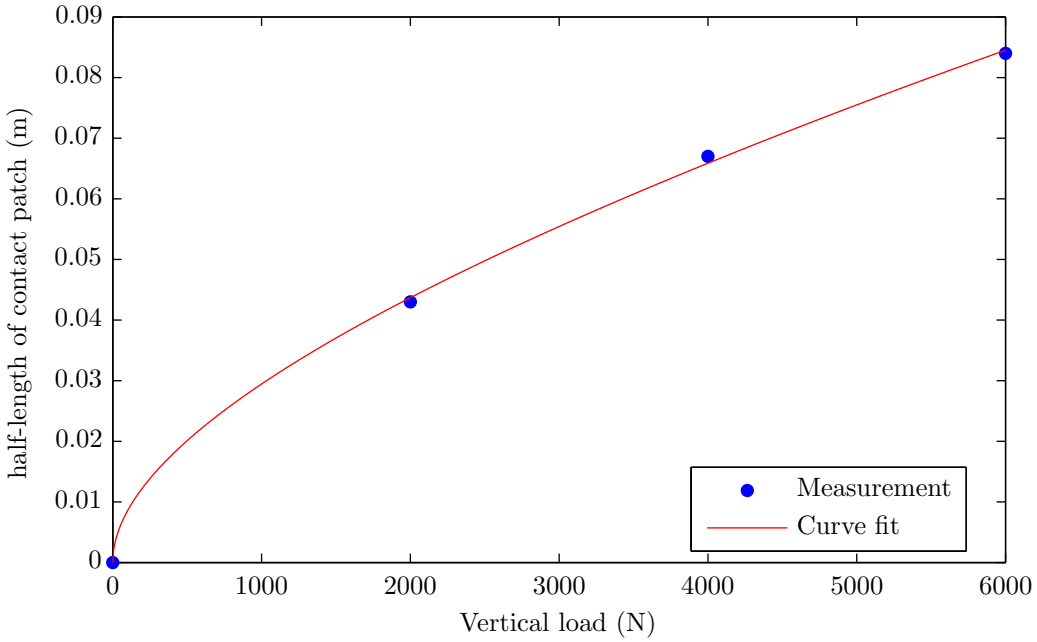

Figure 5.5: Contact patch length vs. vertical load at 2.2 bar.

state longitudinal force vs slip characteristics of the tire using the relation:

$$c_{px} = \frac{C_{\kappa 0}}{2a^2} \tag{5.5}$$

where $C_{\kappa 0}$ is the slip stiffness of the tire at free rolling condition which is the slope of the force-slip curve at $\kappa = 0$. This is calculated from experimentally obtained force-slip characteristics, as shown in Figure 5.7. Alternatively, this data can also be used for fit the Magic Formula [6] if one chooses to use this instead of the brush model.

The half-length of the contact patch a is calculated using Equation (3.31) after accounting for the effect of inflation pressure on the vertical stiffness C_z. The calculated value of tread element stiffness per unit length is shown in Table 5.10.

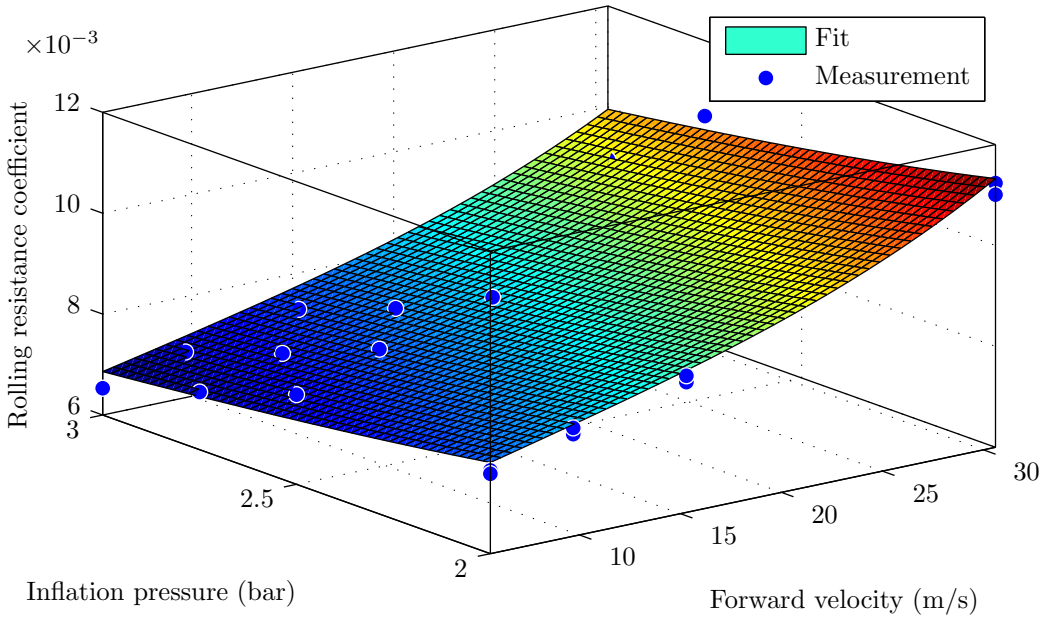

Figure 5.6: Variation of rolling resistance.

Parameter	Value
c_{px}	$10.934 \cdot 10^6$ N/m^2

Table 5.10: Estimated value of tread element stiffness

5.2.9 Enveloping Characteristics

The parameters of the enveloping model primarily involve the dimensions and the order of the tandem elliptical cams. This is the most computationally heavy procedure in comparison to all others because it involves an optimization procedure where the ellipse shape parameters are changed with each iteration and compared with experimental results. The obtained effective height for three types of cleats at different loads is shown in Figure 5.8. To obtain this data, the tire is inflated to nominal pressure and rolled slowly (< 1 km/h) over different sets of cleats at a constant axle height. The reaction forces F_x, F_z at the axle are recorded

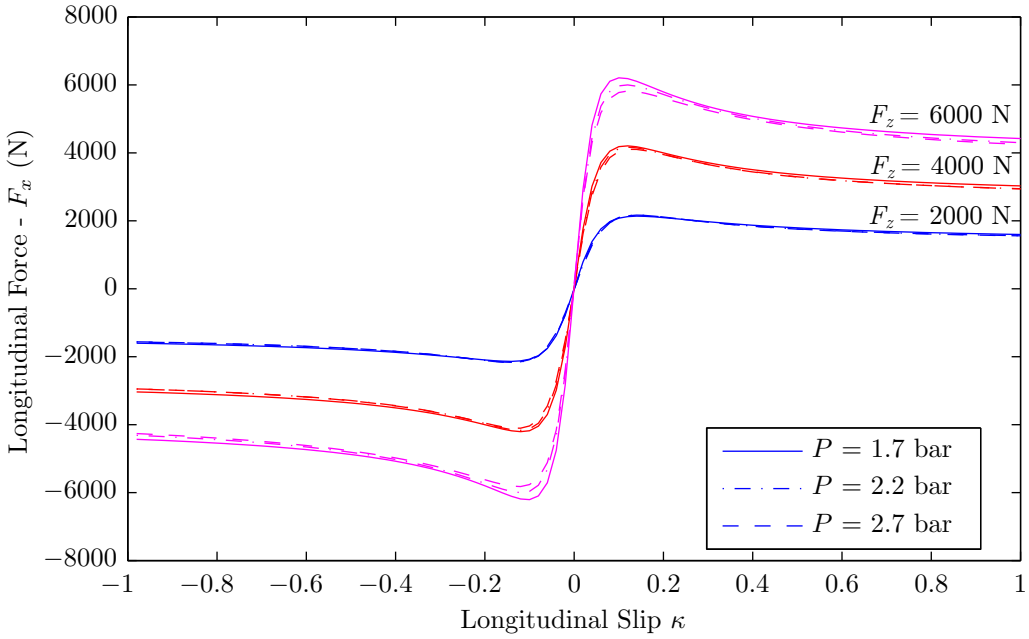

Figure 5.7: Steady-state force vs. slip characteristics.

and are used to obtain the effective road height and plane angle as:

$$w = \frac{F_z - F_{z0}}{C_{z0}} \tag{5.6a}$$

$$\beta = \arctan\left(\frac{F_x}{F_z}\right) \tag{5.6b}$$

The values of w and β are then optimized with the enveloping model to find the shape parameters of the ellipse. This is done using a non-linear least squares fit of the enveloping function to the experimental data. Since the dimensions of the ellipse are generally the same size of the tire, the starting values are assumed to be $a_e = r_0$, $b_e = r_0$, $c_e = 1.8$ and $p_{ls} = 0.8$. The current procedure is designed in such a way that the most minimal set of enveloping data is used for parameterization. Hence, only set of experimental data is used for estimation. This can be improved using multiple sets of experimental data and weighting factors to calculate an optimal set of parameters. From the results of the fitting procedure shown in Figure 5.9, we can see that the enveloping model is able to closely match experimental results. The estimated parameters are shown in Table 5.11.

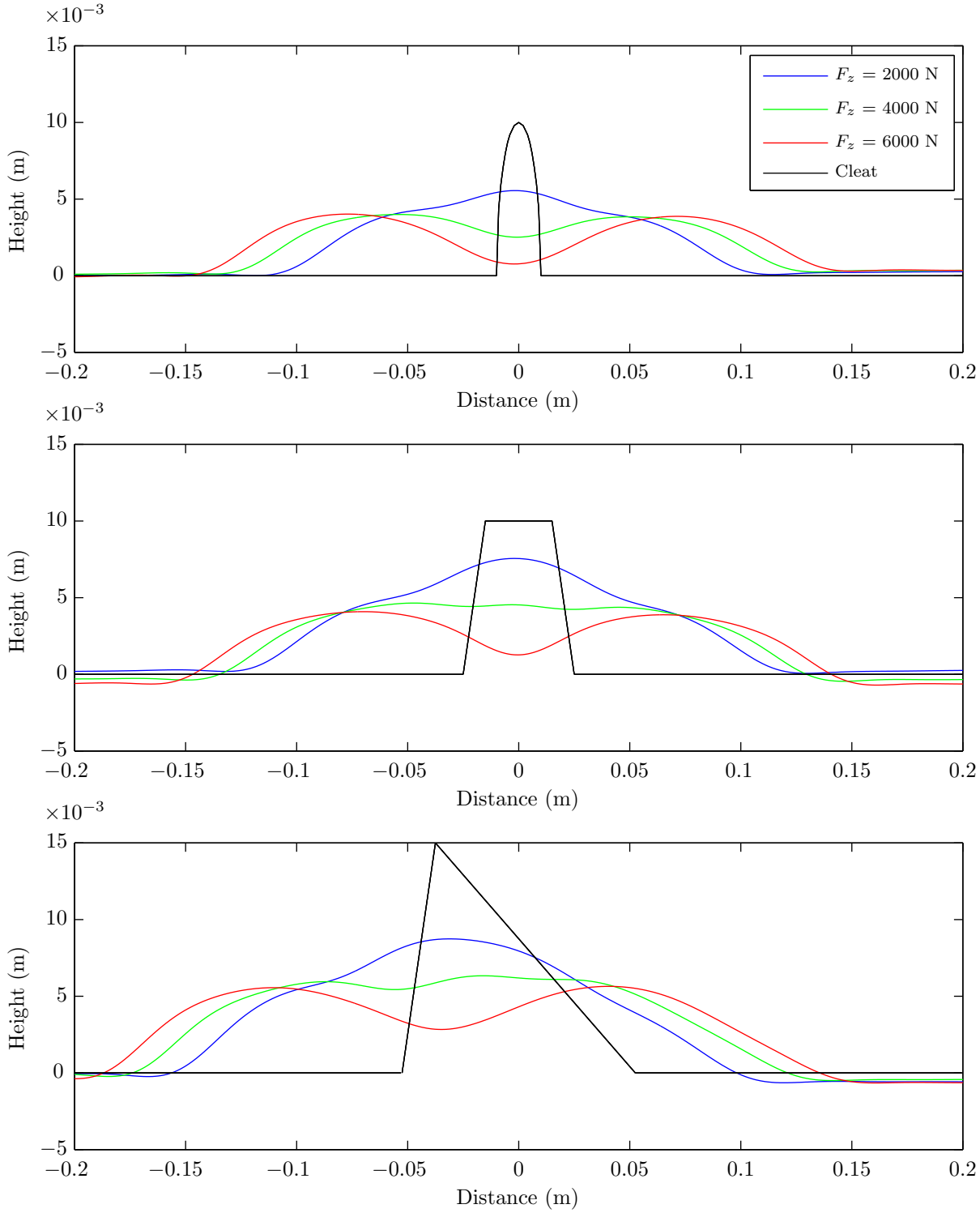

Figure 5.8: Enveloping characteristics for multiple loads.

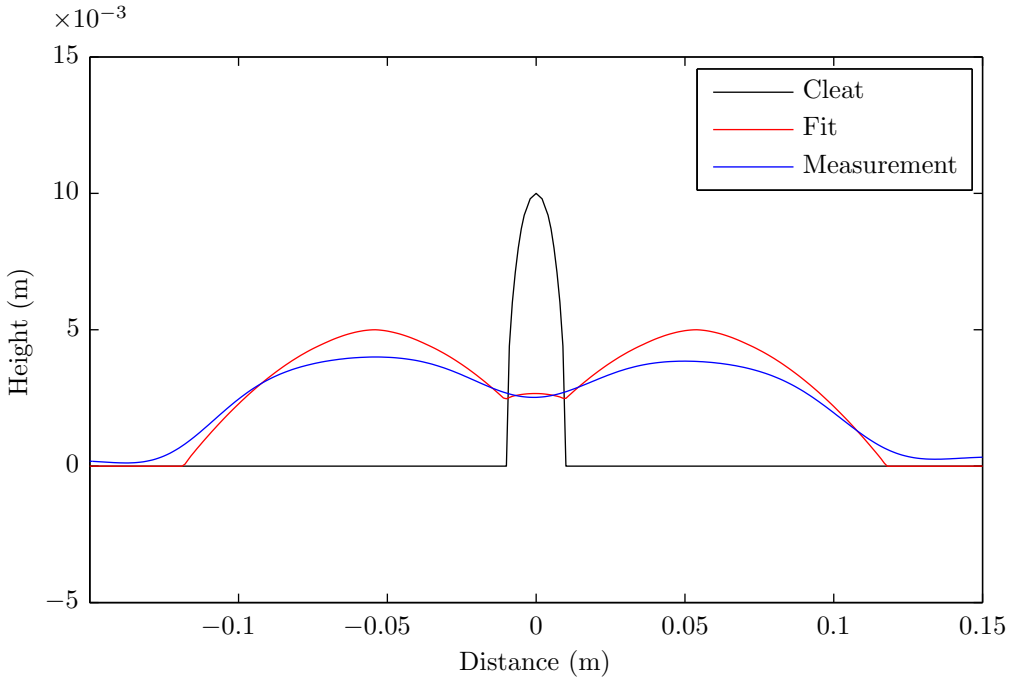

Figure 5.9: Enveloping model fit with experimental data.

An alternative approach towards parameterization of the enveloping model to reduce errors is to fit the enveloping model based on reaction forces rather than through direct calculations. Although this method tends to yield better results, the computational load is much higher due to the fact that this process requires a full simulation at each time-step.

Parameter	Value
a_e	0.3626 m
b_e	0.3580 m
c_e	1.7359
p_{ls}	0.8000

Table 5.11: Estimated parameters for the enveloping model

5.2.10 Alternative Methods of Parameterization

Although experimental results are required to parameterize the dynamic tire model, a prototype tire might not be always available due to various situations. For example, a tire in the design phase might not have a valid prototype. In addition to this, experimental data is expensive to obtain and time consuming. Hence, an alternative method is proposed where the experimental data can be replaced with results from FEA. The FEA model of a tire can be subject to the same operating conditions as a real world testing scenario and these results can be stored in TYDEX files which can be sent as inputs to the parameterization process. Although there is a slight reduction in parameter accuracy in this process, the major advantage here is that this can be used to analyze the performance of tires even during the design stage.

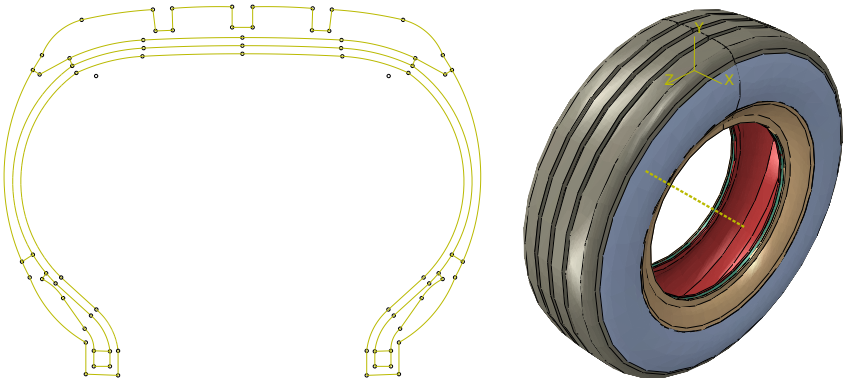

(a) Tire cross-section. (b) Tire assembly.

Figure 5.10: Tire FEA modeling.

Some examples include the work by Balaramakrishna et al [72] who used FEA models to estimate the parameters of the MF-SWIFT tire model. Tounonen et al [73] utilized a combination of instrumented vehicle measurements and FEA based values to parameterize a rigid ring tire model. Currently, modeling work is being undertaken at the Center for Tire Research to replace the experimental data used in this study with simulation results. The tire geometry and assembly diagrams developed in ABAQUS® are shown in Figure 5.10.

5.3 Conclusions

A parameterization procedure for the rigid ring tire model and enveloping model based on non-linear curve fitting has been developed in this chapter and the model parameters were estimated. This is shown in Figure 5.11.

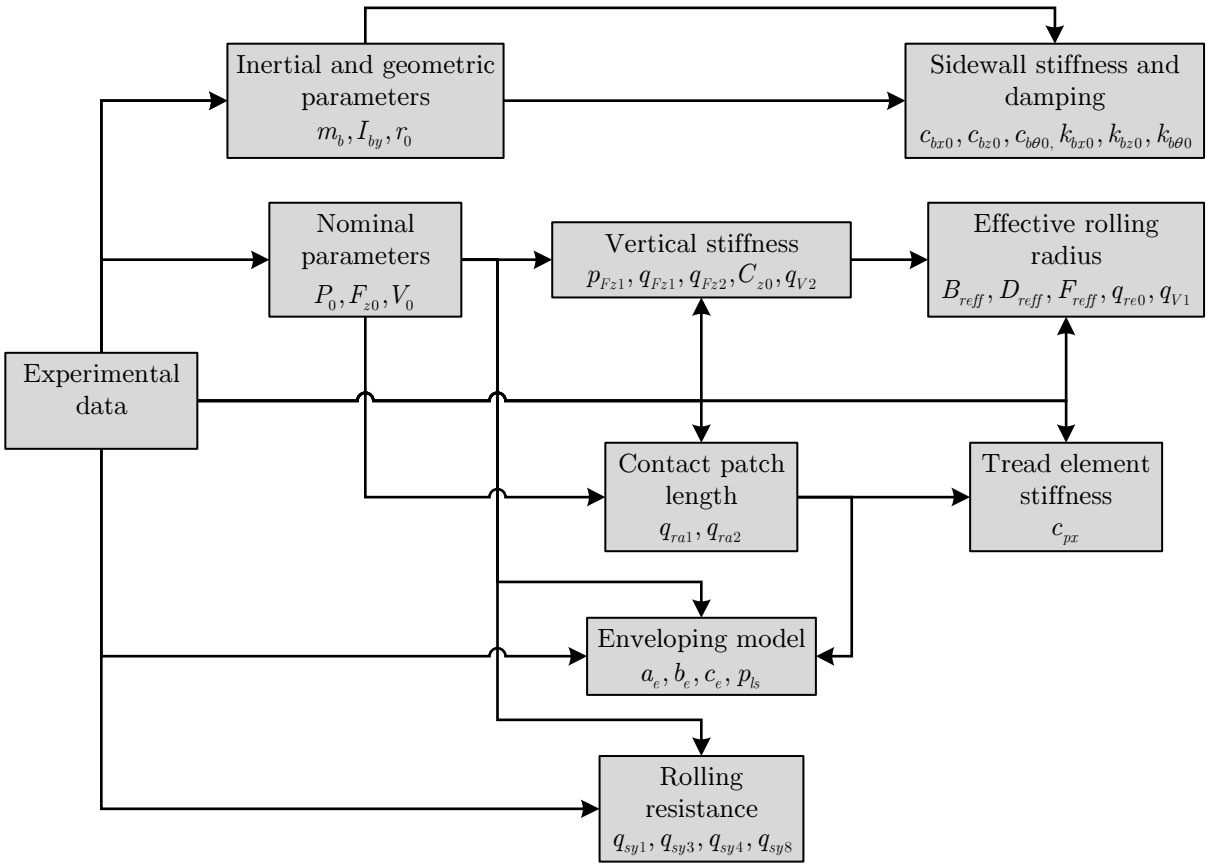

Figure 5.11: Procedure for parameter estimation.

Work on alternative approaches that would supplant experimental data were also explained. The parameters estimated for a 205/60R15 tire based on the current procedure are found to have good correlation with the parameters for the same tire mentioned in literature [5] with an acceptable margin of difference. There is more scope for improvement in the determination of dynamic sidewall stiffness. Subsequent chapters concentrate on the analysis of simulation results and conclusions from them.

Chapter 6

Results and Validation

In order to establish the reliability of the model it is necessary to compare and validate the accuracy of simulation results with experimental data. This chapter explains the validation of the tire model which was done using experimental data available for both high-speed cleat tests and low-speed enveloping tests over different types of cleats. Following this, the complete simulation model with all the components are subjected to various test cases and the results are analyzed.

6.1 Enveloping Model Validation

The validation of the enveloping model involves comparison of the calculations of the effective road profile with actual measurements. For this, the ellipse shape parameters which were obtained in Section 5.2.9 were used to calculate the effective road profile height w and slope β at various vertical loads for three types of cleats: 1. Cylindrical; 2. Trapezoidal and 3. Triangular. It was ensured that the experimental data used for validation studies were not previously used for model parameterization and all tests were conducted at nominal inflation pressure. The test results are shown in Figures 6.1, 6.2 and 6.3.

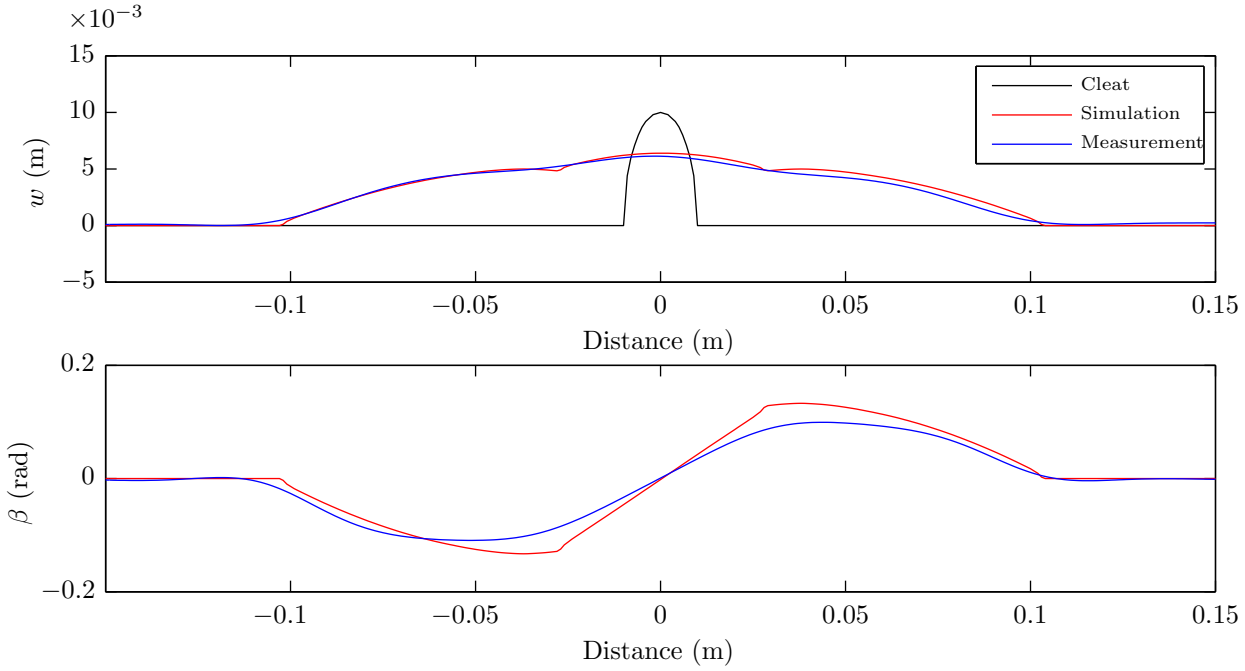

Figure 6.1: Enveloping over a cylindrical cleat at $F_z = 2000$ N.

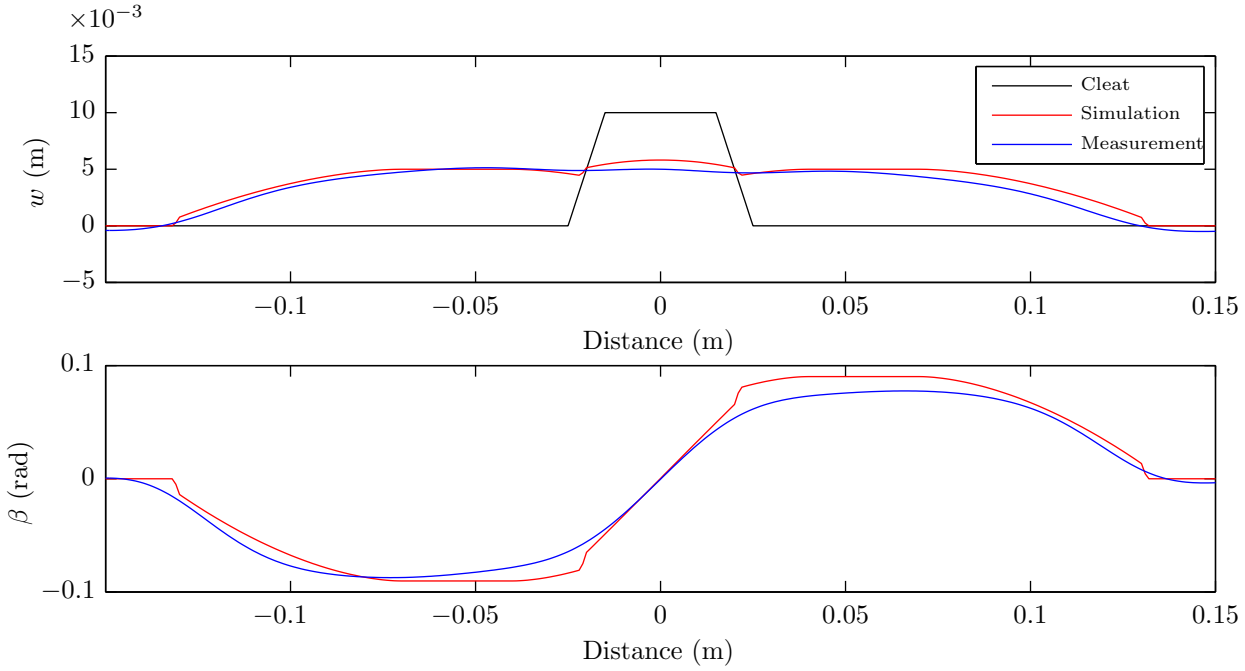

Figure 6.2: Enveloping over a trapezoidal cleat at $F_z = 4000$ N.

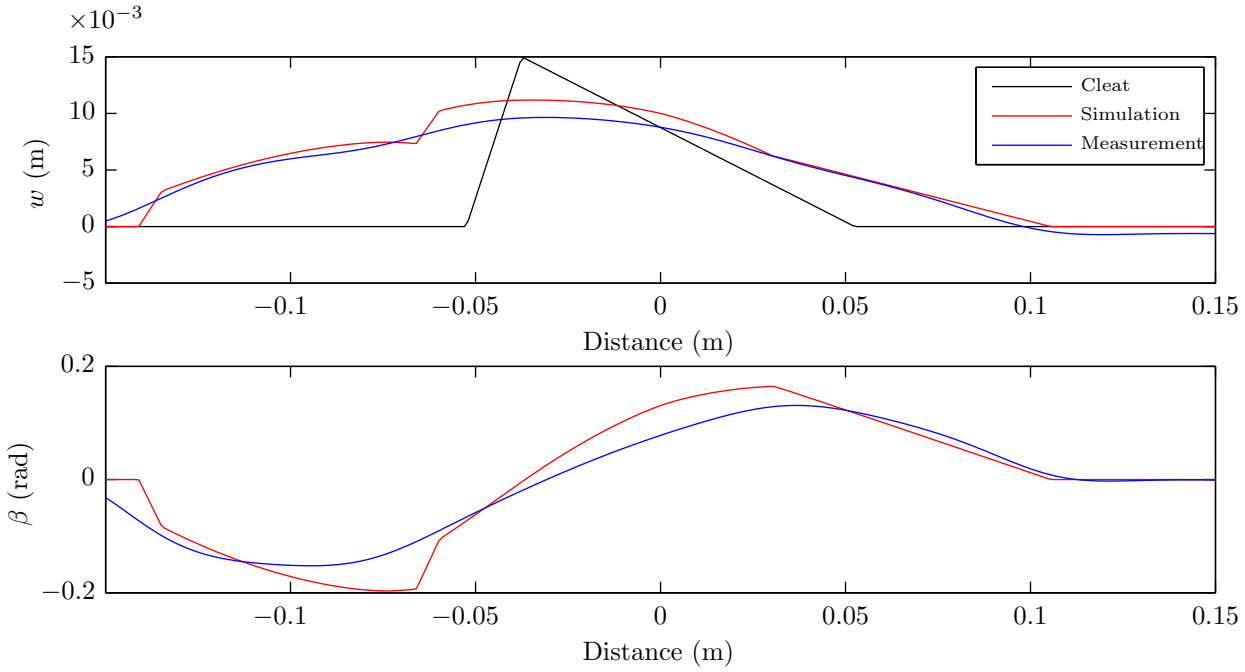

Figure 6.3: Enveloping over a triangular cleat at $F_z = 2000$ N.

From the results, we can see that the enveloping model is able to successfully predict the effective road profile w with minimal error in all three test cases. This demonstrates the capability of the model to be applicable for any general road surface without any significant loss in the level of accuracy.

The various reasons for the observed deviations of the results of the simulation model in some cases with measurements can be interpreted as follows:

- There is a slightly larger deviation in the prediction of plane slope β in comparison to the effective plane height w, but still within acceptable limits. This is due to the fact that the ellipse parameters were optimized based on the effective road profile.

- Figure 6.3 has the most deviation in comparison to other cases due to the sharp triangular obstacle. Also, one can notice that the predicted profile is not completely smooth, which can be seen in the plane slope β. This is due to the limitations of the model as it is based on an algebraic approximation. Also, since the measured values of w and β

are obtained indirectly from the reaction forces at the axle using Equation (5.6), the values tend to be smooth.

- The presence of minor aberrations in Figure 6.3 can be attributed to the scan width and the shift between the ellipse which might not be optimal for all types of obstacles.

In conclusion, the enveloping model based on the current parameterization procedure is able to successfully predict the effective road profile and slope and provide results within acceptable error bounds. Hence, this model is used with the rigid ring tire model for validation in subsequent sections.

6.2 Tire Model Validation

The validation of the dynamic tire model is based on experimental data of the force response that was obtained by rolling a tire over a rectangular cleat at different vertical loads and velocities. In all cases, the axle was kept at a constant height for loading and nominal inflation pressure was maintained. The rectangular cleat has dimensions of 0.05 m (length) and 0.01 m (height). The outputs measured were the reaction forces at the axle and the wheel rotational velocity. This response is then analyzed in both time and frequency domain and compared with experimental data. A detailed description of all procedures adopted to obtained this dataset is given by TNO [66]. SAE J2730 [74] can be utilized as a standard procedure for performing dynamic cleat testing. Four test cases were analyzed for the validation studies.

Four test cases were selected out of the available data and the tire model was simulated under the same operating conditions. Figures 6.4, 6.5, 6.6 and 6.7 show the results of the cleat tests and their comparison with simulation results. Here, the analyzed variables are the change in longitudinal axle force ΔF_x, change in vertical axle force ΔF_z, the change in rotational velocity $\Delta\Omega$ and their respective power spectral densities $S_{F_xF_x}$, $S_{F_zF_z}$ and $S_{\Omega\Omega}$.

The following observations can be made based on the simulation results and their comparison

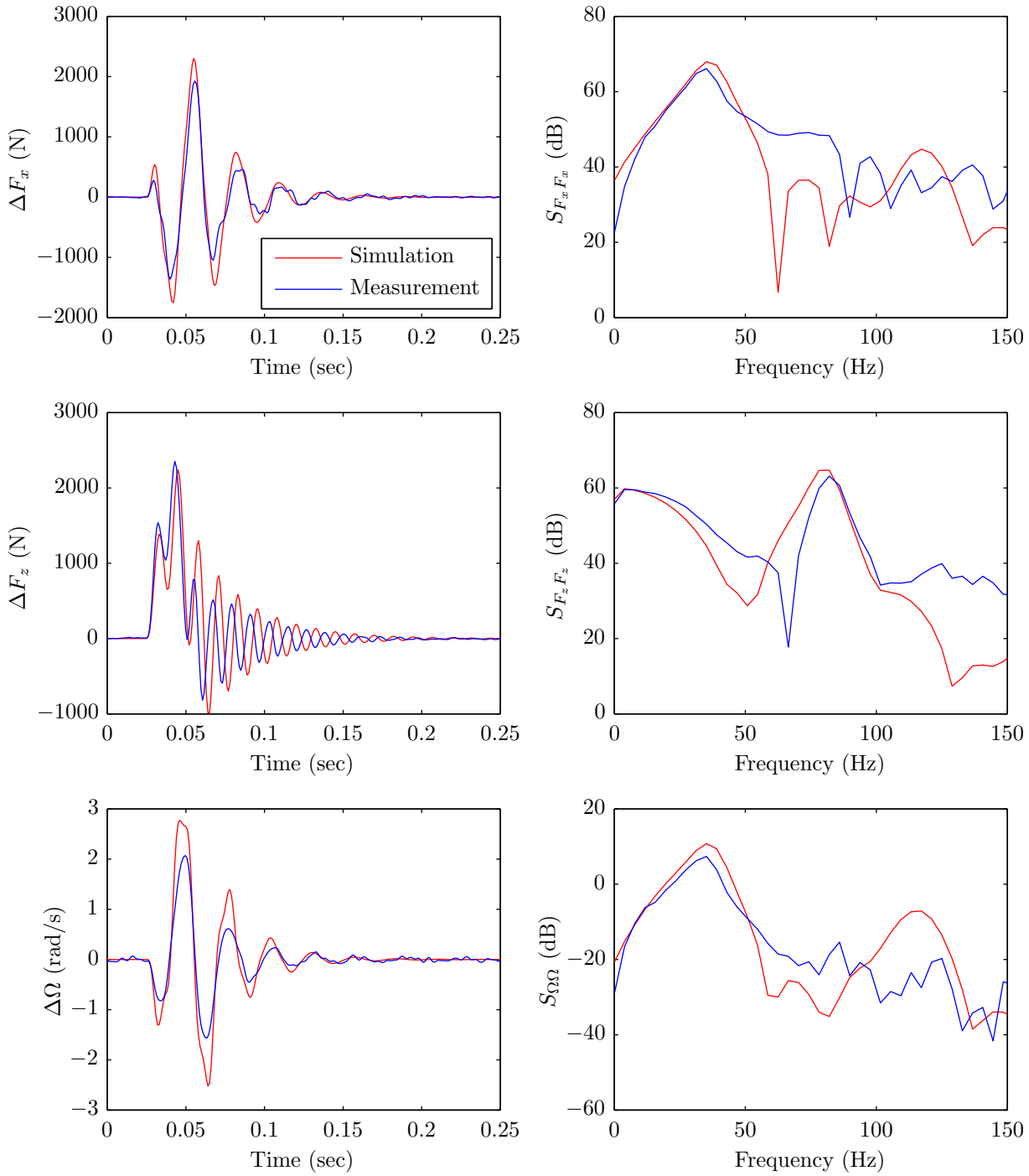

Figure 6.4: Tire rolling over a rectangular cleat at 20 km/h and $F_z = 2000$ N.

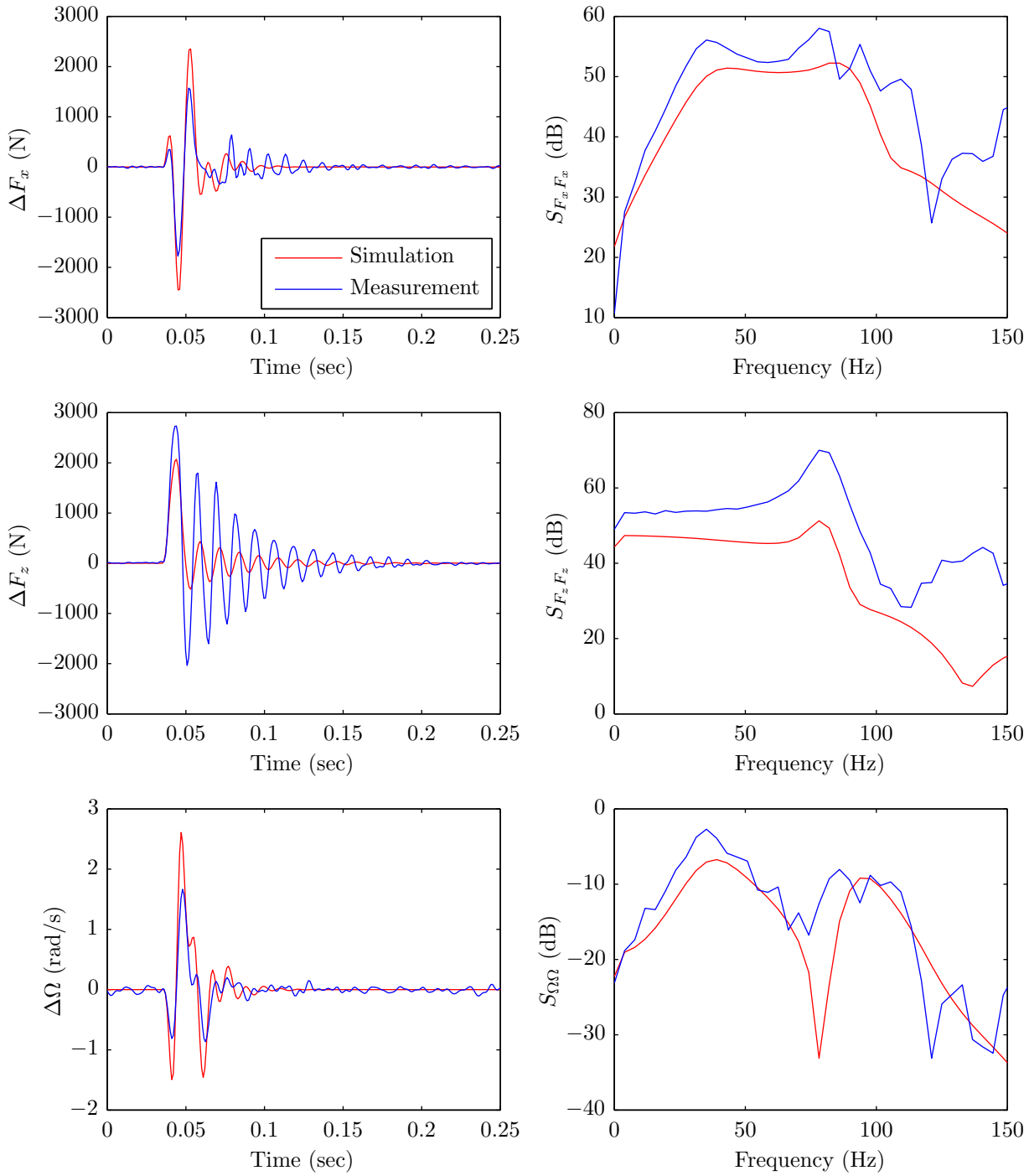

Figure 6.5: Tire rolling over a rectangular cleat at 60 km/h and $F_z = 2000$ N.

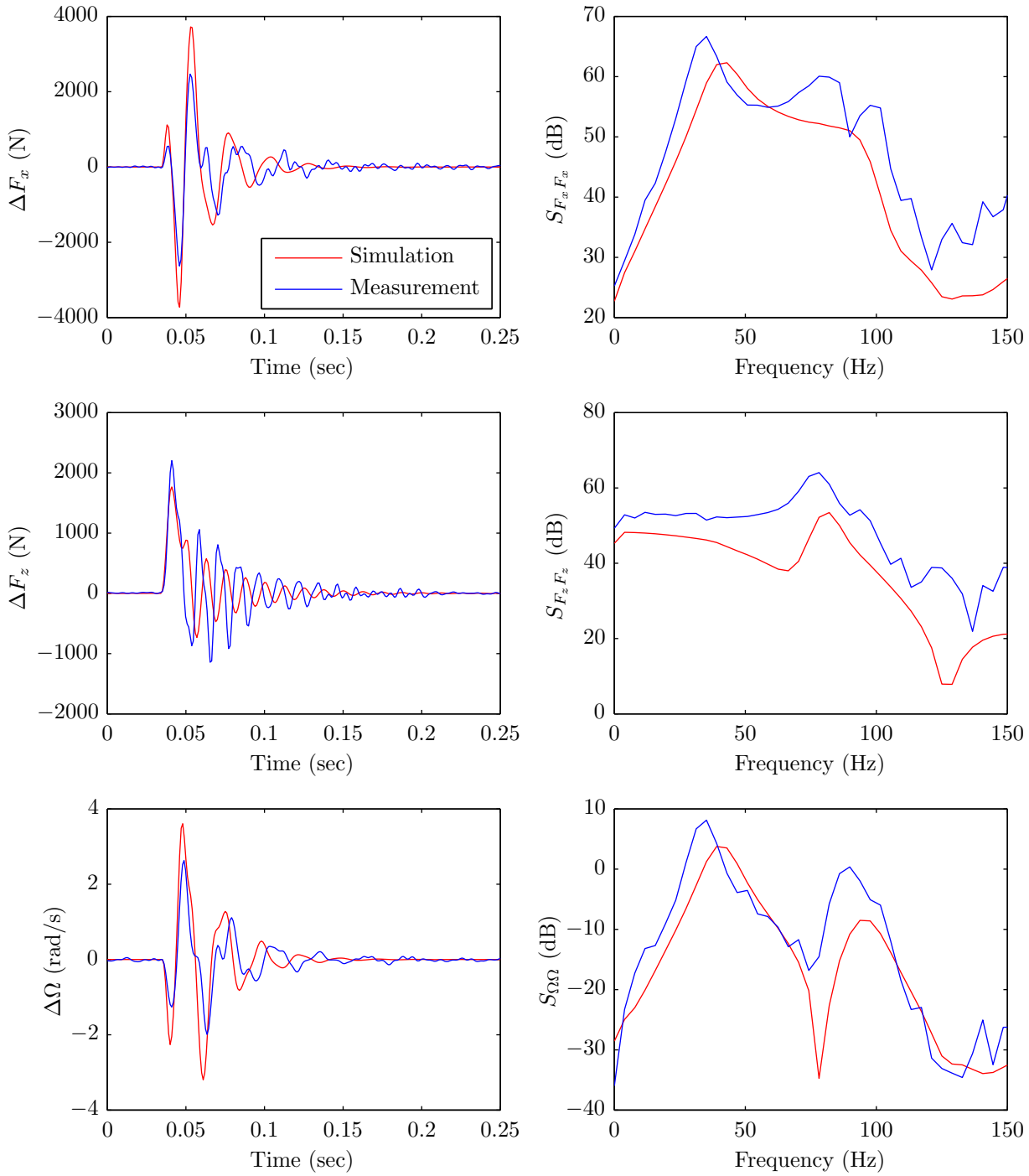

Figure 6.6: Tire rolling over a rectangular cleat at 60 km/h and $F_z = 4000$ N.

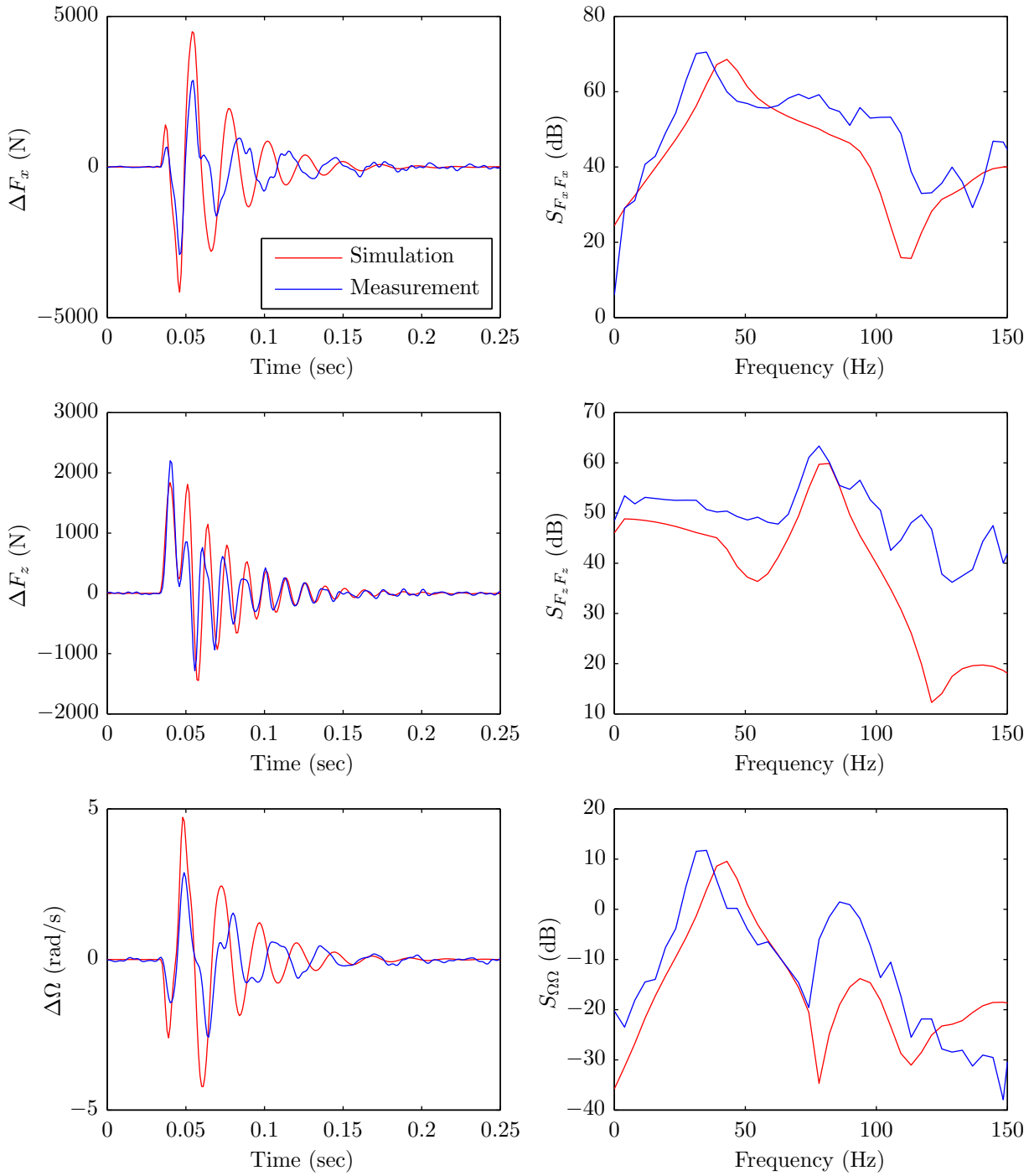

Figure 6.7: Tire rolling over a rectangular cleat at 60 km/h and $F_z = 6000$ N.

with experimental data:

- The time domain response for all four test cases except the vertical force in Figure 6.5 show comparable amplitudes of vibration and have similar settling times.
- The PSD plots show a vertical offset although the peak frequencies show a match. This shift is minor in some plots and larger in a few, especially $S_{F_zF_z}$ in Figure 6.5. This is due to the fact that there is lower damping predicted than measurements at low speeds and a high damping is predicted at speeds of 60 km/h which can be attributed to the relaxation length model with affects the relative damping. The time domain plots reflect this effect through a phase delay between the simulations and measurements as observed in the vertical force response of Figure 6.5.
- The time domain response for the change in horizontal force and angular velocity for Figures 6.4 and 6.5 show good correlation with measurements. This indicates the tire model has higher level of accuracy at lower loads.
- At higher loads of 4000 N and 6000 N, a minor deviation in measurements in the first modal frequency for longitudinal force and angular velocity occurs. This can be attributed to a higher predicted dynamic stiffness which is also reflected with larger oscillations than measurements.
- The extra zeros observed in the simulation results which aren't present in the experimental data are due to the presence of null-points in the enveloping model. In this, the calculated road profile might be zero for certain frequencies due to the geometric setup of the tandem cams. This has been explained in detail by Schmeitz [24].
- From Figures 6.4, 6.5 and 6.7, a minor shift in the natural frequencies of the rigid body modes of the tire at higher velocities can be seen from the experimental data. This effect is also observed in the simulation results. This accounts for the change in sidewall stiffness with rolling velocity.

Overall, a good correlation is observed in the response of the tire model in both time domain and frequency domain. The predicted response and the peaks of the frequency response are found to lie within acceptable levels of error. Hence, it can be concluded that the dynamic tire model is valid over the specified frequency range of operation and the predicted response lies within the expected range and error bounds.

6.3 Frequency Response to Brake Torque

Following the validation studies, it is necessary to understand the influence of in-plane dynamics of the tire during braking events. This is done by performing a comparison of the simulation outputs of a quarter car model based on a Lugre transient model with the rigid ring dynamic tire model. The Lugre model was chosen for comparison due to its widespread usage in ABS simulations. The comparison methods used in this section is based on the work done by Jansen [3] to understand the influence of in-plane dynamics on ABS braking.

For this analysis, an impulse braking torque M_{ay} of high amplitude was chosen as an input to the simulation models as a wide-band excitation to obtain the vertical force F_z and horizontal force F_x at the axle and the angular velocity of the tire Ω. Due to the non-linearities of the simulation model, the Power Spectrum Density (PSD) of the outputs $S_{F_xF_x}$, $S_{F_zF_z}$ and $S_{\Omega\Omega}$ were obtained to plot the amplitude of the response at various frequencies, as shown in Figure 6.8. All responses were normalized before obtaining the PSD and this results in much smaller amplitudes.

From the results, we can see that the Lugre transient tire model matches the response of the rigid ring model up to the wheel-hop mode. At higher frequencies above 10 Hz, the transient model loses its validity as the amplitude of the response begins to fall. This is not seen in the case of rigid ring model as the vertical and rotational rigid-body modes up to 100 Hz can be seen. This demonstrates the validity of the rigid ring model over a higher frequency range in comparison to simple transient tire models which are currently being used.

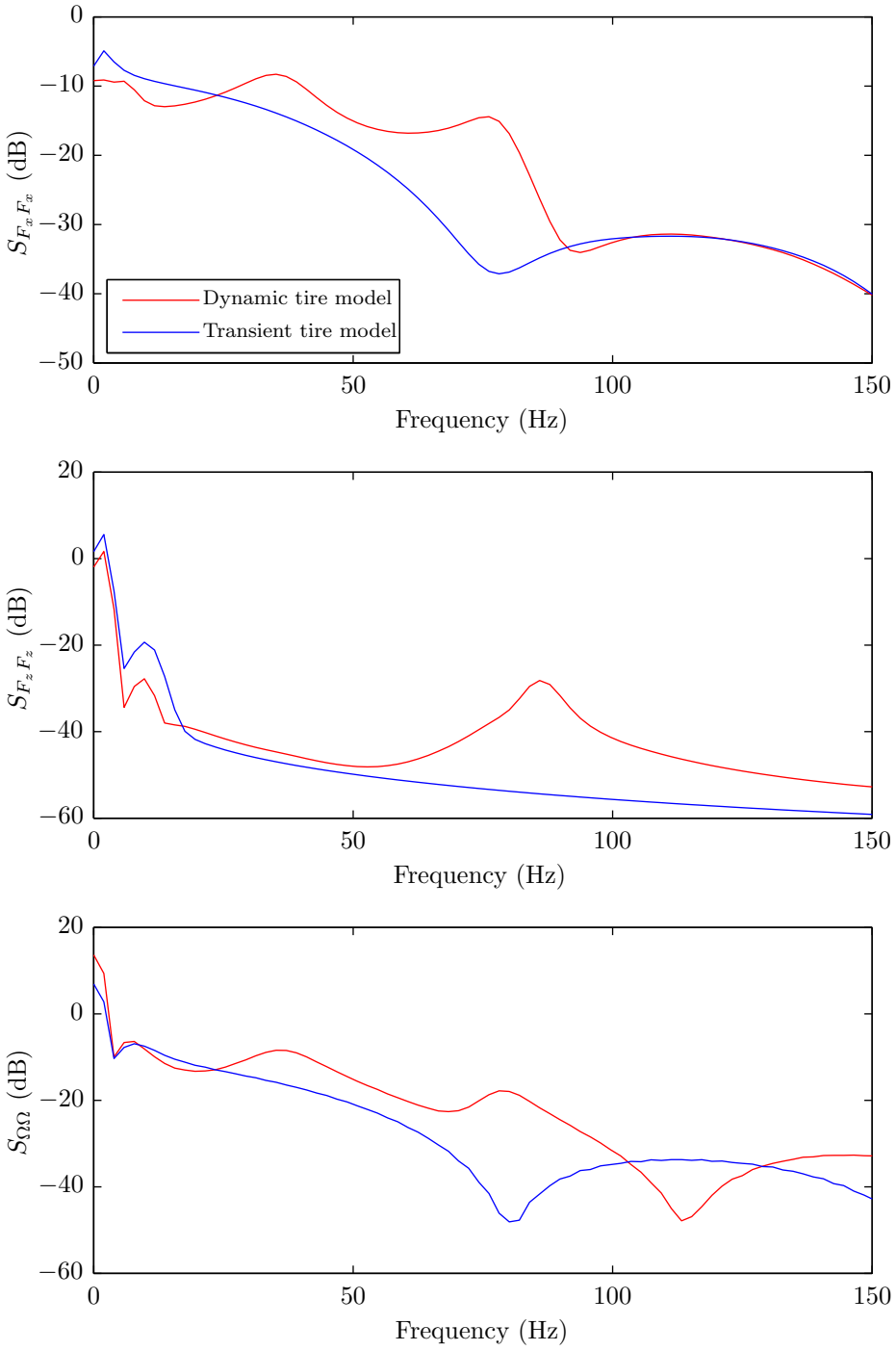

Figure 6.8: Frequency response to brake torque input.

6.4 ABS Simulations

Following the validation of the dynamic tire model, enveloping model and the understanding that the dynamic tire model is valid over a higher frequency range in comparison to transient tire models, simulations are required to be performed on the complete model to assess its capabilities. This includes inducing short wavelength disturbances during ABS operation and assessing braking performance.

6.4.1 Test cases

For this, four test cases with different road profiles were analyzed. In all test cases, the same braking maneuver is adopted where the vehicle is assumed to be moving at 65 km/h before the start of braking on a dry road surface of coefficient of friction $\mu = 0.9$ to serve as a standard for braking assessment. For experimental validation, the best practices described in SAE J2909 [75] is recommended. The four types of road profile used for simulations in this study are described below and shown in Figure 6.9:

Smooth Asphalt Road This is the road profile for asphalt concrete on bound base, as shown in Figure 6.9(a) and was obtained from the Long Term Pavement Performance (LTPP) database [76] for a stretch of highway from the state of Oklahoma. This profile has the lowest level of disturbance and would serve as a baseline measure of braking distance. These are measured at longer intervals of 150 mm.

Jointed Pavement Concrete Road This road profile, as shown in Figure 6.9(b) was also obtained from the LTPP database, measured at intervals of 150 mm for a highway in Oklahoma and this has sharper disturbances when compared to the asphalt road but is still classified as a smooth road.

ISO Grade D Asphalt This standard road profile was available from the Center for Tire Research and would assist in understanding the braking distance variations on a road

with short wavelength disturbances. The road profile has been shown in Figure 6.9(c).

Uneven Road with Sharp Cleats and Potholes This profile, as shown in Figure 6.9(d) was obtained from the smart road at Virginia Tech Transportation Institute (VTTI) for a highly uneven road and consists of sharp bumps and cleats. This would assist in understanding how cleats and potholes impact braking.

6.4.2 Vehicle Parameters

The parameters of the quarter car model were based on a generic vehicle obtained from the work done by Rangelov [59], as shown in Table 6.1.

Parameter	Value
m_s	300 kg
m_a	42.247 kg
K_{sx}	$2 \cdot 10^3$ Ns/m
C_{sx}	$1 \cdot 10^5$ N/m
K_{sz}	$2 \cdot 10^3$ Ns/m
C_{sz}	$2 \cdot 10^4$ N/m

Table 6.1: Quarter car parameters

6.4.3 Simulation Results

The simulation results for all four test cases are shown in Figures 6.11, 6.12, 6.13 and 6.14. The following observations have been made from the simulation results:

- In all four test cases, it can be seen that the ABS is able to successfully cycle around the peak area of the force-slip curve. This demonstrates the effectiveness of the ABS algorithm.

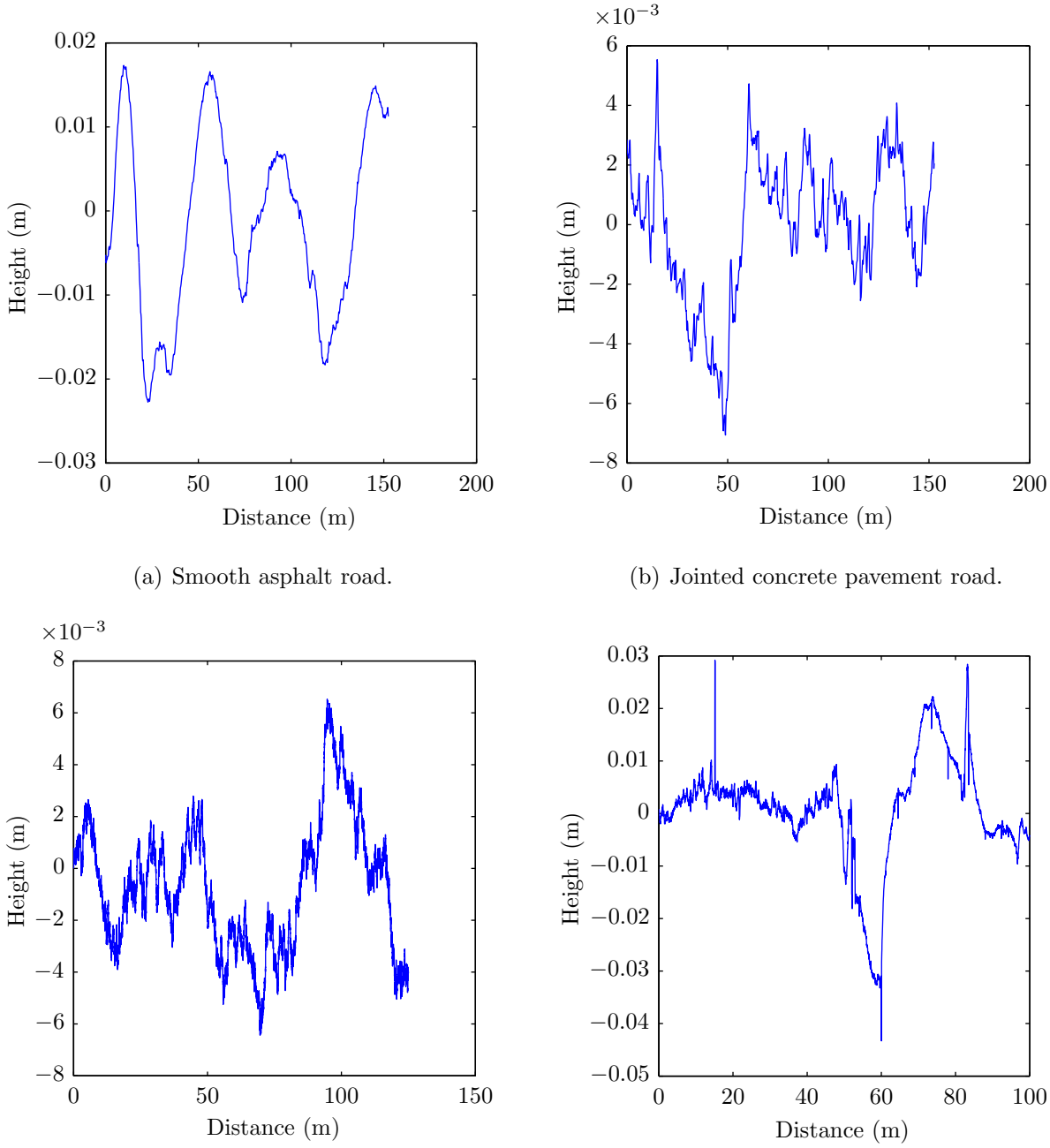

(a) Smooth asphalt road.

(b) Jointed concrete pavement road.

(c) ISO grade D asphalt road.

(d) Uneven road with sharp cleats and potholes.

Figure 6.9: Road profiles for ABS braking analysis.

- The rate of cycling of brake torque is seen to reflect real-world ABS braking scenario as it is done at a much slower rate compared to the simulation time-step.

- Variations in the vertical force F_{zt} are observed to have a direct effect on the braking force F_{xt} generated by the tire at the axle. This effect can be clearly seen in Figure 6.9(d) where there is a sudden drop in braking force due to the tire rolling over a pothole.

- Short wavelength road disturbances are observed to lead to small variations in the angular velocity which can be clearly observed in Figures 6.9(c) and 6.9(d). This is an expected result and demonstrates the capabilities of the tire model to account for such effects.

- From Figure 6.9(c), it is observed that sharp disturbances at longer wavelengths (large intervals) have minimal effect on the rolling velocity of the tire although variations can be seen in the vertical load.

- A combination of sharp cleats and large potholes with short wavelength disturbances can be seen to have an influence towards increasing the average slip during ABS braking.

The braking distance variations for all four test cases can be seen in Figure 6.10. The following observations have been made:

- It is observed that the presence of large cleats and potholes have a direct effect on the braking distance of the vehicle, as seen in the case of braking distance for the uneven road as this test case shows the greatest deviation from the baseline value of smooth asphalt road.

- In this case, the short wavelength disturbances in the ISO grade D asphalt road has been observed to reduce the braking distance due to higher average deflection in the tire.

- Sharp obstacles at larger wavelengths are seen to have minimal effect on the braking distance, as seen in the case of jointed concrete pavement road where the difference

with baseline smooth asphalt road is very less.

Based on the observations it can be concluded that the vibrations of the belt due to short wavelength disturbances have a significant effect on the ABS braking performance of a tire and cannot be neglected. This confirms previous studies done by Zegelaar [58] and Pauwelussen [2]. This effect has been clearly demonstrated by the developed simulation tool with a validated tire model.

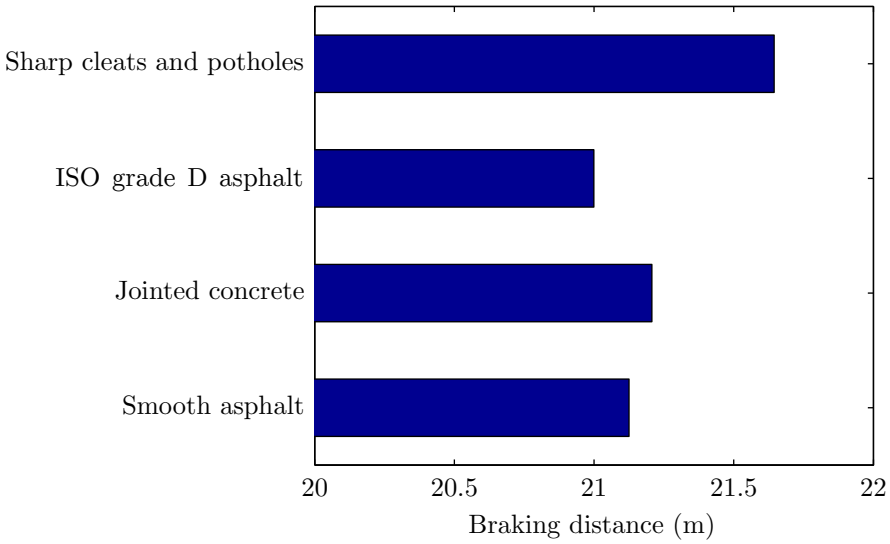

Figure 6.10: Braking distance on various road surfaces.

6.5 Conclusions

The rigid ring tire model and the elliptical cam model were successfully validated against experimental data obtained from fixed axle tests based on the parameters calculated form the estimation procedure and reasons for any discrepancies were analyzed. Results with estimated parameters were found to have equal or better fit with experimental results in comparison with parameters provided by TNO [77]. Simulations with ABS braking maneuvers were conducted on a quarter car model under various road surfaces and the variations in braking distance were also analyzed.

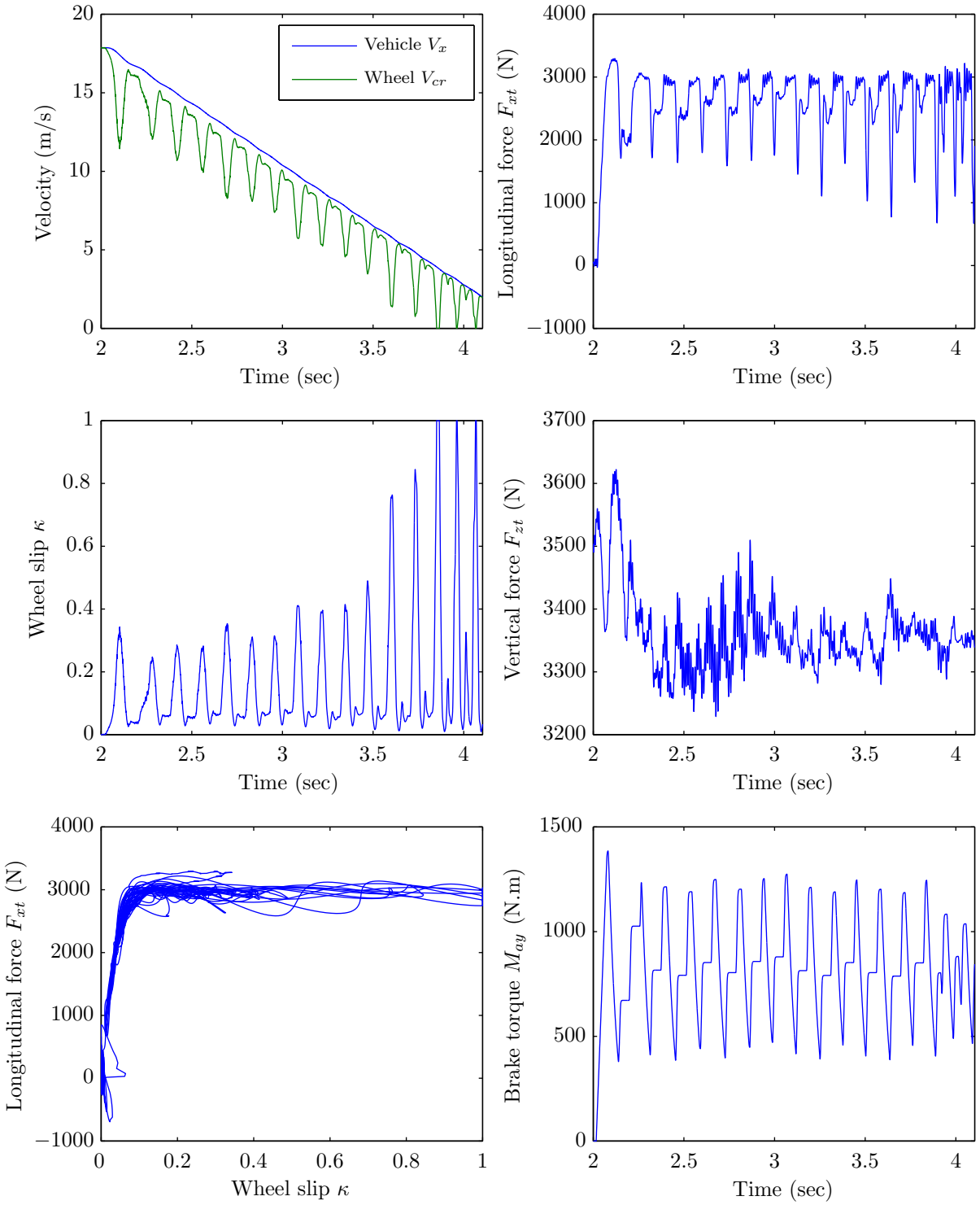

Figure 6.11: ABS braking on smooth asphalt road.

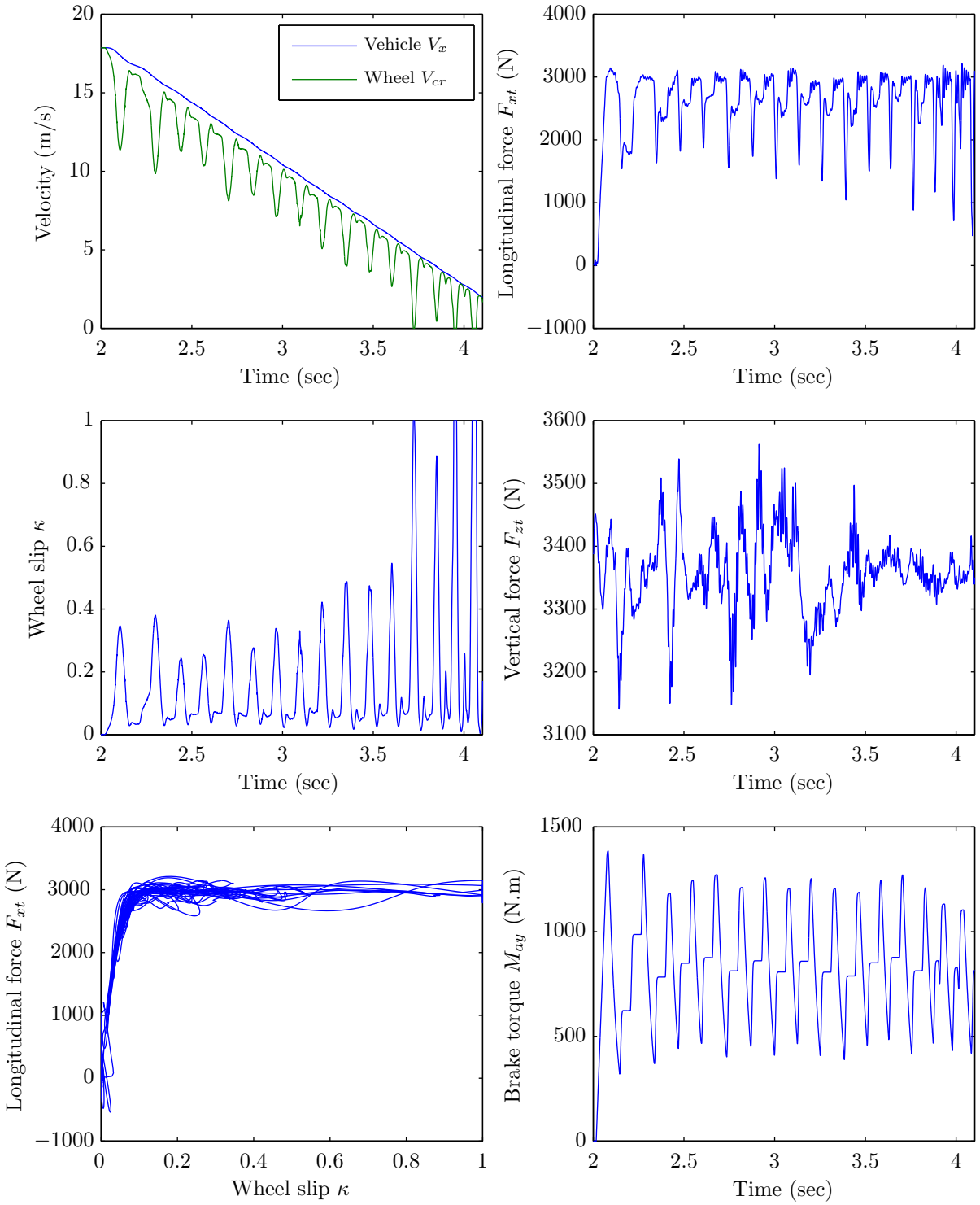

Figure 6.12: ABS braking on jointed pavement concrete road.

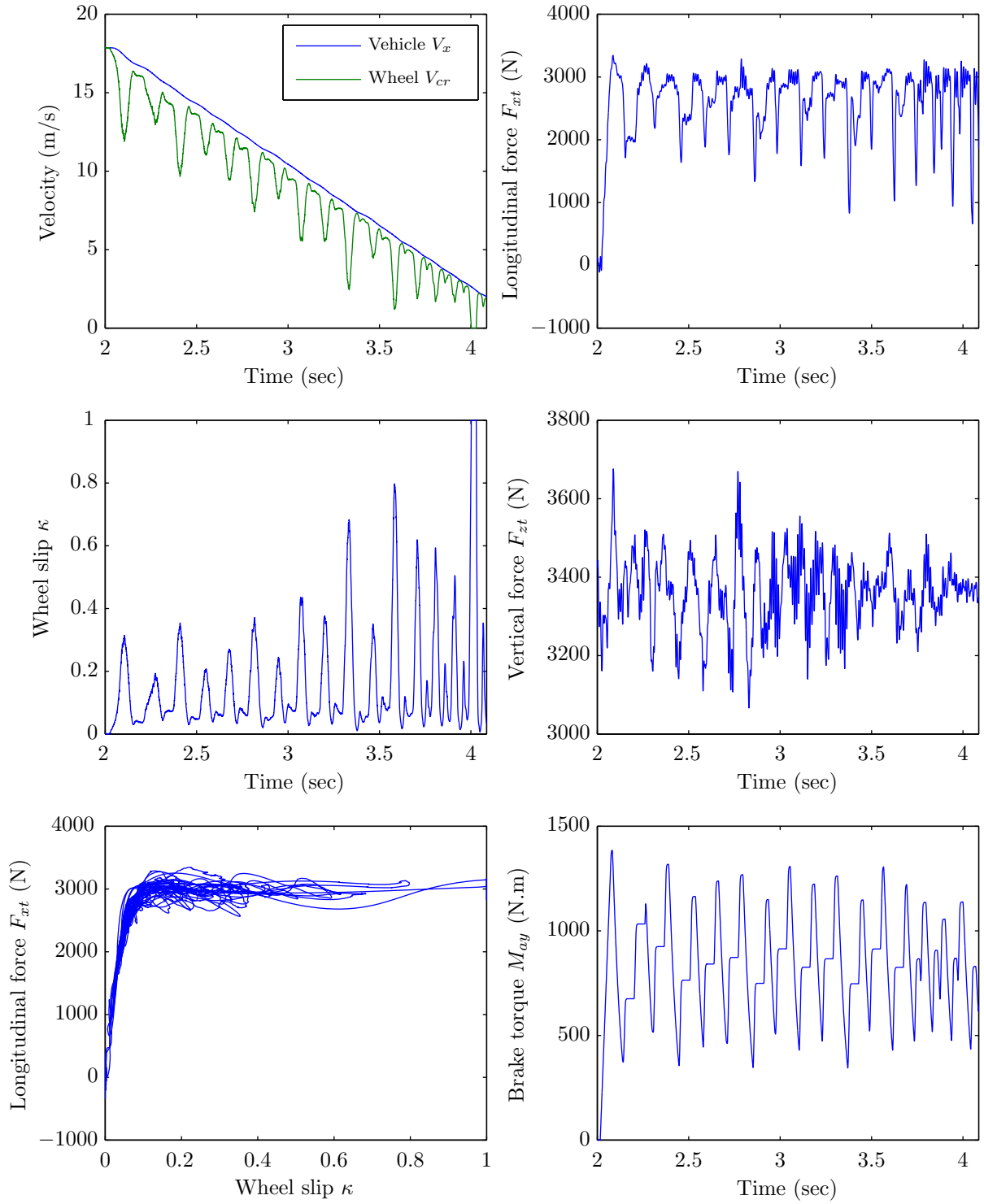

Figure 6.13: ABS braking on ISO grade D poor asphalt road.

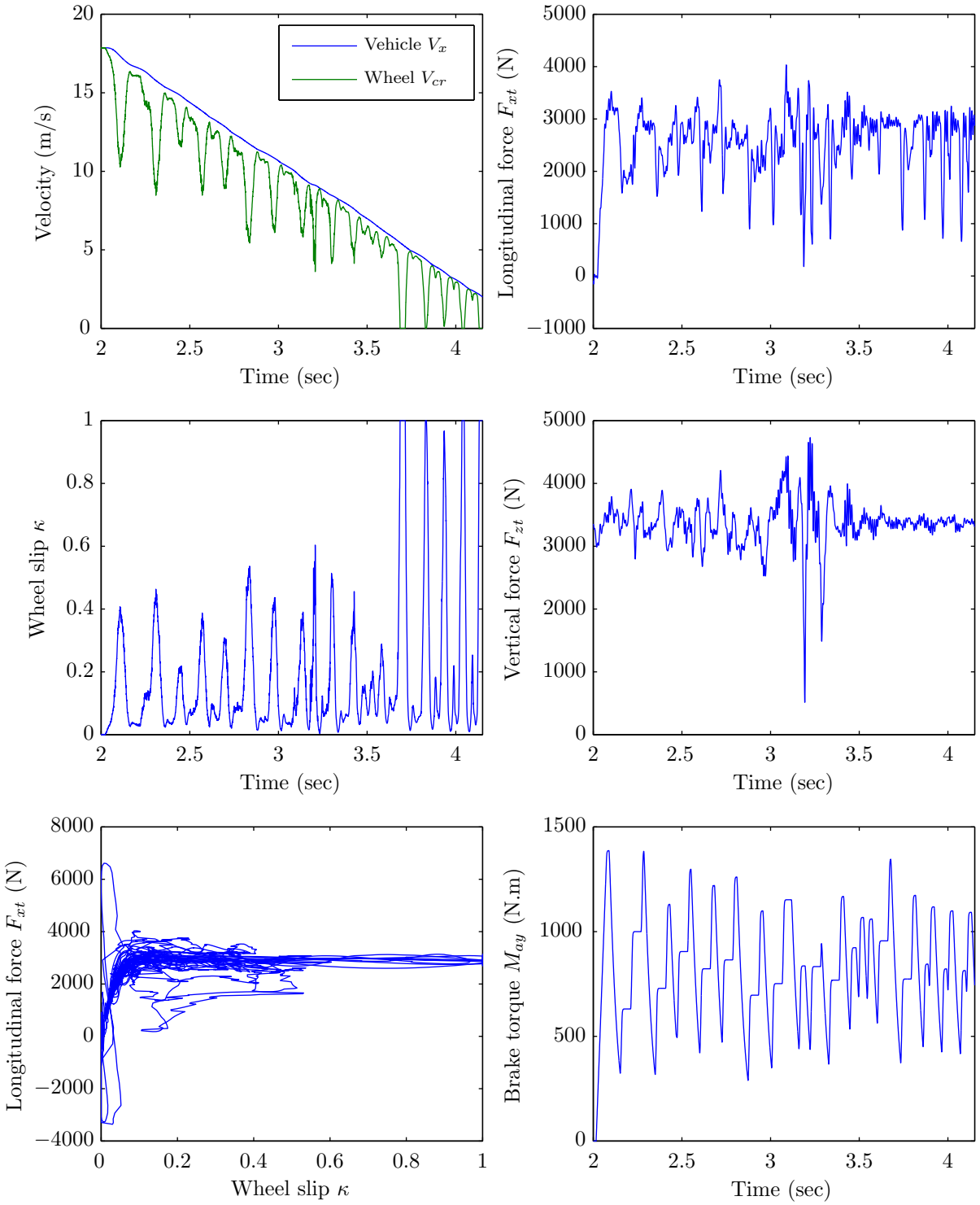

Figure 6.14: ABS braking on uneven road surface with cleats and potholes.

Chapter 7

Conclusions and Future Work

The following activities have been successfully carried out in the course of this study towards the development of a simulation tool that analyze the effect of short wavelength disturbances and brake torque variations on ABS performance:

- A detailed literature review on the development of dynamic tire models and enveloping models and their analysis with respect to braking performance.
- Mathematical modeling of all relevant subsystems of the simulation tool based on the literature, including the rigid ring tire model, tandem elliptical cam enveloping model, ABS model and quarter car model.
- Model development in Matlab-Simulink® with relevant data exchange standards and experimental data further optimization to improve performance.
- Development of a parameterization procedure for estimation of model parameters from experimental data or possibly through FEA in the future.
- Validation of the dynamic tire model including the enveloping model with experimental data from dynamic cleat tests.

- Simulation of ABS braking under various road surfaces and analysis of the effect of short wavelength disturbances on braking performance and other states of the vehicle during ABS braking.

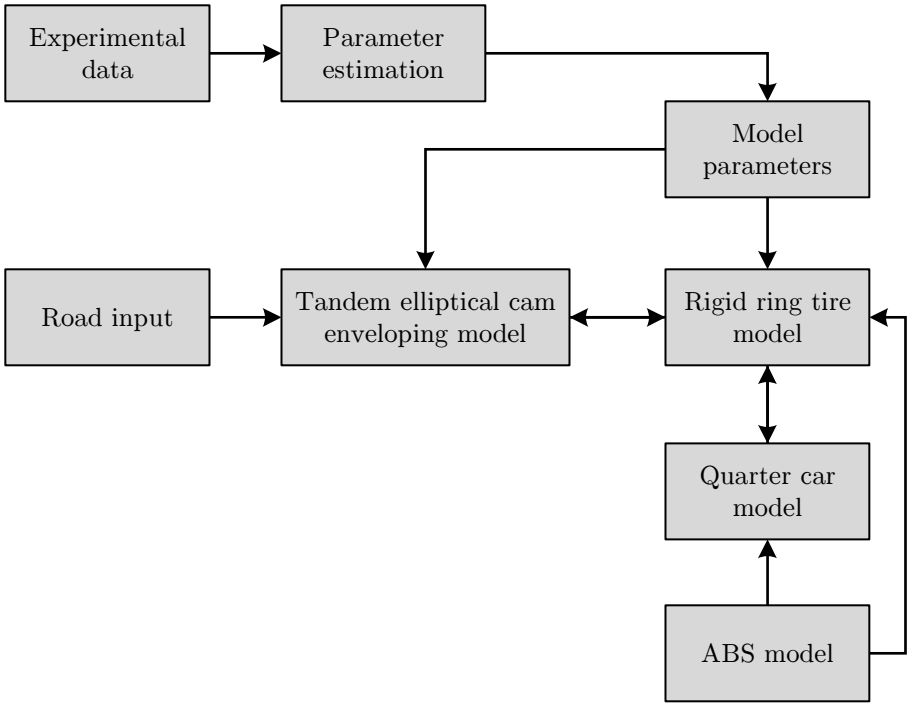

Figure 7.1: Simulation tool overview.

An overview of the developed simulation tool is shown in Figure 7.1. Simulations of ABS braking on the developed tool yield the following analysis results:

- The developed simulation tool provides expected and reliable results for ABS braking simulations and accounts for all intended factors and variations.
- Large wavelength disturbances can lead to variations in vertical load but have minimal effect on braking performance.
- Short wavelength disturbances have a significant effect on the rolling velocity of the vehicle and influence the braking distance.

- Sharp cleats and potholes have a significant effect on the generation of braking force and increase average slip.

7.1 Recommendations for Future Work

The various simulation models and subsystems that were developed in this study towards the final goal of building a simulation tool have numerous scope for improvement. There is also potential towards extending the model for other types of test cases such as ride and comfort analysis for suspensions, evaluating active suspension controllers for robustness, stability controller testing etc. The following recommendations are given for future work pertaining to this study:

- Implementation of a GUI for the simulation tool that would require minimal user intervention for conducting simulations.
- Building the simulation model as a standalone package using C/C++ that can be deployed on any platform.
- Improving the accuracy of the procedure for parameter estimation through weighted curve fitting using multiple sets of experimental data.
- Estimate the dynamic stiffness of the sidewall by fitting the model response to experimental data obtained from high-speed cleat tests.
- Validate the simulations of the quarter car with an ABS system through Hardware-In-the-Loop (HIL) simulations.
- Adapt the simulation tool to handle road profiles over slopes and absolute coordinates.
- Integration of the dynamic tire model and the ABS model in CarSim®.

- Implementation of a magic formula based approach to calculate steady state tangential forces in the contact patch instead of a brush model.
- Facilitate the replacement of experimental data with FEA simulation results and complete the integration process.
- Parameterization of the ABS model to allow for adjustments in wheel acceleration thresholds and compatibility with different simulation time-steps.
- Extension of the rigid ring tire model with additional degrees of freedom for out-of-plane vibrations based on the work by Maurice [29, 28] and Mancosu et al [78] for simulations involving both braking and cornering.

Bibliography

[1] P. Zegelaar, *The dynamic response of tyres to brake torque variations and road unevennesses*. PhD thesis, TU Delft, 1998.

[2] J. Pauwelussen, L. Gootjes, C. Schröder, K.-U. Köhne, S. Jansen, and a. Schmeitz, "Full vehicle ABS braking using the SWIFT rigid ring tyre model," *Control Engineering Practice*, vol. 11, pp. 199–207, Feb. 2003.

[3] S. T. Jansen, P. Zegelaar, and H. B. Pacejka, "The Influence of In-Plane Tyre Dynamics on ABS Braking of a Quarter Vehicle Model," *Vehicle System Dynamics*, vol. 32, pp. 249–261, Aug. 1999.

[4] J. Maas, *A Comparison of Dynamic Tyre Models for Vehicle Shimmy Stability Analysis*. PhD thesis, Eindhoven University of Technology, 2009.

[5] H. B. Pacejka, *Tire and Vehicle Dynamics*. Butterworth-Heinemann, 3 ed., 2012.

[6] H. B. Pacejka and E. Bakker, "The Magic Formula Tire Model," *Vehicle System Dynamics*, vol. 21, pp. 1–18, Jan. 1992.

[7] I. J. Besselink, A. J. Schmeitz, and H. B. Pacejka, "An improved Magic Formula/Swift tyre model that can handle inflation pressure changes," *Vehicle System Dynamics*, vol. 48, pp. 337–352, Dec. 2010.

[8] H. B. PACEJKA and I. J. M. BESSELINK, "Magic Formula Tyre Model with Transient Properties," *Vehicle System Dynamics*, vol. 27, pp. 234–249, Jan. 1997.

[9] F. Braghin and E. Sabbioni, "A Dynamic Tire Model for ABS Maneuver Simulations," *Tire Science and Technology*, vol. 38, pp. 137–154, June 2010.

[10] H. Dugoff, P. Fancher, and L. Segel, "An analysis of tire traction properties and their influence on vehicle dynamic performance," *SAE Technical Paper*, 1970.

[11] J. Bernard, L. Segel, and R. Wild, "Tire shear force generation during combined steering and braking maneuvers," *SAE Technical Paper*, 1977.

[12] K. Guo and D. Lu, "UniTire: unified tire model for vehicle dynamic simulation," *Vehicle System Dynamics*, vol. 45, pp. 79–99, Jan. 2007.

[13] A. Schmeitz, *A Semi-Empirical Three-Dimensional Model of the Pneumatic Tyre Rolling over Arbitrarily Uneven Road Surfaces.* PhD thesis, Delft University of Technology, 2004.

[14] K. Guo, "Tire roller contact model for simulation of vehicle vibration input," *SAE Technical Paper*, 1993.

[15] N. W. Frey, *Development Of A Rigid Ring Tire Model And Comparison Among Various Tire Models For Ride Comfort Simulations.* Masters thesis, Clemson University, 2009.

[16] J. Badalamenti and G. D. Jr, "Radial-interradial spring tire models," *Journal of Vibration Acoustics Stress and Reliability in ...*, no. January, 1988.

[17] S. Gong, *A Study of in-plane Dynamics of Tires.* PhD thesis, Delft University of Technology, 1993.

[18] P. Zegelaar and H. Pacejka, "The in-plane dynamics of tyres on uneven roads," *Vehicle System Dynamics*, no. November 2012, pp. 37–41, 1996.

[19] C. W. Mousseau and S. K. Clark, "An Analytical and Experimental Study of a Tire Rolling Over a Stepped Obstacle at Low Velocity," *Tire Science and Technology*, vol. 22, pp. 162–181, July 1994.

[20] Y. T. Wei, L. Nasdala, and H. Rothert, "Analysis of Tire Rolling Contact Response by REF Model," *Tire Science and Technology*, vol. 32, pp. 214–235, Oct. 2004.

[21] S. A. Lippmann and J. D. Nanny, "A Quantitative Analysis of the Enveloping Forces of Passenger Tires," *SAE Technical Paper*, 1967.

[22] P. Bandel and C. Monguzzi, "Simulation Model of the Dynamic Behavior of a Tire Running Over an Obstacle," *Tire Science and Technology*, vol. 16, pp. 62–77, Apr. 1988.

[23] A. Schmeitz and J. Pauwelussen, "An efficient dynamic ride and handling tyre model for arbitrary road unevennesses," *VDI-Berichte*, no. 1632, pp. 173–199, 2001.

[24] a.J.C. Schmeitz, S. Jansen, H. Pacejka, J. Davis, N. Kota, C. Liang, and G. Lodewijks, "Application of a semi-empirical dynamic tyre model for rolling over arbitrary road profiles," *International Journal of Vehicle Design*, vol. 36, no. 2/3, p. 194, 2004.

[25] J. A. II, M. El-Gindy, and K. Koudela, "Development of a Rigid Ring Quarter-Vehicle Model With an Advanced Road Profile Algorithm for Durability and Ride Comfort Predictions," in *International Design Engineering Technical Conferences & Computers and Information in Engineering Conference*, pp. 1–8, 2008.

[26] Y. Chang, M. E. Gindy, and D. a. Streit, "Literature survey of transient dynamic response tyre models," *International Journal of Vehicle Design*, vol. 34, no. 4, p. 354, 2004.

[27] M. Takayama and K. Yamagishi, "Simulation model of tire vibration," *Tire Science and Technology*, vol. 11, pp. 38–49, 1983.

[28] J. Maurice, "The influence of belt dynamics on cornering and braking properties of tyres," *Vehicle System Dynamics*, no. November 2012, pp. 37–41, 1998.

[29] J. Maurice, M. Berzeri, and H. Pacejka, "Pragmatic tyre model for short wavelength side slip variations," *Vehicle system dynamics*, no. November 2012, pp. 37–41, 1999.

[30] D. Allison and R. Sharp, "On the low frequency in-plane forced vibrations of pneumatic tyre/wheel/suspension assemblies," *Vehicle System Dynamics*, vol. 27, pp. 151–162, Jan. 1997.

[31] D. Belluzzo, F. Mancosu, R. Sangalli, F. Cheli, and S. Bruni, "New Predictive Model for the Study of Vertical Forces (up to 250 Hz) Induced on the Tire Hub by Road Irregularities," *Tire Science and Technology*, vol. 30, pp. 2–18, Jan. 2002.

[32] a. J. C. Schmeitz, I. J. M. Besselink, and S. T. H. Jansen, "Tno Mf-Swift," *Vehicle System Dynamics*, vol. 45, pp. 121–137, Jan. 2007.

[33] K. Guo, "Dynamic tire model used in advanced chassis control," in *2011 International Conference on Electric Information and Control Engineering*, pp. 4957–4961, IEEE, Apr. 2011.

[34] M. Eichler, "A ride comfort tyre model for vibration analysis in full vehicle simulations," *Vehicle System Dynamics*, no. May 2013, pp. 37–41, 1997.

[35] M. Gipser, "FTire: a physically based application-oriented tyre model for use with detailed MBS and finite-element suspension models," *Vehicle System Dynamics*, vol. 43, pp. 76–91, Jan. 2005.

[36] M. Gipser, "FTire, a new fast tire model for ride comfort simulations," *International ADAMS User's Conference Berlin*, 1999.

[37] H. R. Dorfi, "A Study of the In Plane Force Transmission of Tires," *Tire Science and Technology*, vol. 32, pp. 188–213, Oct. 2004.

[38] S. R. Wu, L. Gu, and H. Chen, "Airbag Tire Modeling by the Explicit Finite Element Method," *Tire Science and Technology*, vol. 25, pp. 288–300, Oct. 1997.

[39] M. Sobhanie, "Road Load Analysis," *Tire Science and Technology*, vol. 31, pp. 19–38, Jan. 2003.

[40] S. Chae, *Nonlinear finite element modeling and analysis of a truck tire*. PhD thesis, Pennsylvania State University, 2006.

[41] S. Chae, M. El-Gindy, M. Trivedi, I. Johansson, and F. Öijer, "Dynamic response predictions of a truck tire using detailed finite element and rigid ring models," in *ASME International Mechanical Engineering Congress and Exposition*, pp. 1–11, 2004.

[42] SAE J2246, "Anti-Lock Brake System Review," *SAE Standard*, 1992.

[43] R. R. Guntur and H. Ouwerkerk, "Adaptive brake control system," *Proceedings of the Institution of Mechanical Engineers 1847-1982 (vols 1-196)*, vol. 186, no. 1972, pp. 855–880, 1972.

[44] H. Ouwerkerk and R. R. Guntur, "Skid Prediction," *Vehicle System Dynamics*, vol. 1, no. 2, pp. 67–88, 1972.

[45] S. Taheri, "A Feasibility Study of the Use of a New Nonlinear Control Law for Automobile Anti-Lock Braking Systems," *Transportation Systems*, 1990.

[46] S. Taheri and E. H. Law, "Investigation of a combined slip control braking and closed loop four wheel steering system for an automobile during combined hard braking and severe steering," in *American Control Conference,*, Proceedings of the American Control Conference, pp. 1862–1867, Publ by American Automatic Control Council, 1990.

[47] S. Drakunov, U. Ozguner, P. Dix, and B. Ashrafi, "ABS control using optimum search via sliding modes," *IEEE Transactions on Control Systems Technology*, vol. 3, pp. 79–85, Mar. 1995.

[48] G. Mauer, "A fuzzy logic controller for an ABS braking system," *IEEE Transactions on Fuzzy Systems*, vol. 3, no. 4, pp. 381–388, 1995.

[49] J. Yu, "A robust adaptive wheel-slip controller for antilock brake system," in *Proceedings of the 36th IEEE Conference on Decision and Control*, vol. 3, pp. 2545–2546, IEEE, 1997.

[50] S. Taheri and E. Law, "Slip control braking of an automobile during combined braking and steering manoeuvres," *Advanced Automotive Technologies*, 1991.

[51] K. B. Singh, "An Intelligent Tire Based Tire-Road Friction Estimation Technique and Adaptive Wheel Slip Controller for Antilock Brake System," *Journal of Dynamic Systems, Measurement, and Control*, vol. 135, p. 031002, Feb. 2013.

[52] A. a. Aly, "An Antilock-Braking Systems (ABS) Control: A Technical Review," *Intelligent Control and Automation*, vol. 02, no. 03, pp. 186–195, 2011.

[53] T. Day and S. Roberts, "A Simulation Model for Vehicle Braking Systems Fitted with ABS," in *SAE World Congress and Exhibition*, SAE.

[54] Robert Bosch GmbH, "Automotive handbook," 2004.

[55] N. Ding, W. Wang, G. Yu, W. Zhang, X. Xu, D. Nenggen, W. Weida, Y. Guizhen, and Z. Wei, "Research and Validation of the Adaptive Control Strategy for ABS Based on Experimental Knowledge," *Automotive Engineering*, vol. 31, no. 1, 2009.

[56] W. Weida, D. Nenggen, and X. Xiangyang, "An Improved Self-adaptive Algorithm of Vehicle Reference Speeds for ABS," in *2006 IEEE International Conference on Vehicular Electronics and Safety*, pp. 98–102, IEEE, Dec. 2006.

[57] W. Zhang, N. Ding, M. Chen, G. Yu, and X. Xu, "Development of a Lowcost Hardwareintheloop Simulation System as a Test Bench for Antilocked Braking System," *Chinese Journal of Mechanical Engineering*, 2011.

[58] P. Zegelaar and H. Pacejka, "Dynamic tyre responses to brake torque variations," *Vehicle System Dynamics*, no. November 2012, pp. 37–41, 1997.

[59] Kiril Z. Rangelov, *Simulink Models of a Quarter-Vehicle with an Anti-lock Braking System*. Masters thesis, Eindhoven University of Technology, 2004.

[60] J. Adcox, B. Ayalew, and T. Rhyne, "Interaction of Anti-Lock Braking Systems with Tire Torsional Dynamics," in *Tire Science and Technology*, no. September 2011, pp. 1–18, 2011.

[61] TNO Automotive, "MF-Tyre & MF-Swift 6.1.2 Equation Manual," 2010.

[62] E. Vinesse, "Tyre vibration testing from modal analysis to dispersion relations," *Proceedings of ISATA*, 1988.

[63] H. Unrau and J. Zamow, "TYDEX Manual Release 1.3," *Description and Reference Manual, Release*, pp. 1–55, 1997.

[64] A. Schmeitz and W. Versteden, "Structure and Parameterization of MF-Swift, a Magic Formula-based Rigid Ring Tire Model," *Tire Science and Technology*, pp. 142–164, 2009.

[65] TNO Automotive, "MF-Tool 6.1 Users Manual," 2010.

[66] TNO Automotive, "Measurement requirements and TYDEX file generation for MF-Tyre/MF-Swift 6.1," 2008.

[67] SAE J2717, "Tests to Define Tire Size (Geometry), Mass, and Inertias," *SAE Standard*, 2006.

[68] P. Lugner and M. Plöchl, "Specifications of the test procedures," *Vehicle System Dynamics*, vol. 45, pp. 21–28, Jan. 2007.

[69] H. Dorfi and R. Wheeler, "Vibration modes of radial tires: application to non-rolling and rolling events," *SAE Technical Paper*, no. 724, 2005.

[70] SAE J2704, "Tire Normal Force/Deflection and Gross Footprint Dimension Test," *SAE Standard*, 2010.

[71] ISO 18164:2005, "Passenger car, truck, bus and motorcycle tyres – Methods of measuring rolling resistance," 2005.

[72] N. Balaramakrishna and R. K. Kumar, "A study on the estimation of SWIFT model parameters by finite element analysis," *Proceedings of the Institution of Mechanical Engineers, Part D: Journal of Automobile Engineering*, vol. 223, pp. 1283–1300, Oct. 2009.

[73] A. Tuononen, L. Hartikainen, F. Petry, and S. Westermann, "Parameterization of in-plane rigid ring tire model from instrumented vehicle measurements," in *11th International Symposium on Advanced Vehicle Control*, 2012.

[74] SAE J2730, "Dynamic Cleat Test with Perpendicular and Inclined Cleats," *SAE Standard*, 2006.

[75] SAE J2909, "Light Vehicle Dry Stopping Distance," *SAE Standard*, 2010.

[76] G. E. Elkins, P. Schmalzer, T. Thompson, and A. Simpson, "Long-Term Pavement Performance Information Management System Pavement Performance Database User Reference Guide," *McLean: Federal Highway Administration*, 2003.

[77] TNO Automotive, "MF-Tyre/MF-Swift 6.1.2.1 Help Manual," 2012.

[78] F. Mancosu, R. Sangalli, F. Cheli, G. Ciarlariello, and F. Braghin, "A Mathematical-Physical 3D Tire Model for Handling/Comfort Optimization on a Vehicle: Comparison with Experimental Results," *Tire Science and Technology*, vol. 28, pp. 210–232, Oct. 2000.